공학박사 학위논문

Investigation on a single molecule analysis through a solid-state nanopore and its application for DNA sensor

2012년 6월

서울대학교 대학원

재료공학부

이 민 현

Investigation on a single molecule analysis through a solid-state nanopore and its application for DNA sensor

지도 교수 김기범

이 논문을 공학박사 학위논문으로 제출함

2012 년 6 월

서울대학교 대학원

재료공학부

이 민 현

이민현의 공학박사 학위논문을 인준함

2012년 6월

위 원 장	안 철 희	(인)
부위원장	김 기 범	(인)
위 원	남 기 태	(인)
위 원	정 봉 현	(인)
위 원	김 영 록	(인)

Investigation on a single molecule analysis through a solid-state nanopore and its application for DNA sensor

A DISSERTATION SUBMITTED TO
DEPARTMENT OF MATERIALS SCIENCE AND ENGINEERING
SEOUL NATIONAL UNIVERSITY

FOR THE DEGREE OF
DOCTOR OF PHILOSOPHY

Min-Hyun Lee

June 2012

Abstract

The nanopore system become one of major technologies in the 3rd generation of DNA sequencing methods in order to perform the cost effective and time effective readout. This dissertation especially focuses on the solid-state nanopore system which has several advantages; 1. It has better mechanical endurance than lipid bilayer in protein nanopore system. 2. The size of nanopore in the system can be controlled during the fabrication. 3. It is connected to an external electric circuit, which can read electrical signal and control single molecular motion, and so on. However, the solid-state nanopore has some disadvantages as follows; 1. The DNA translocation speed of the solid-state nanopore is too fast (~100,000 nt/sec) compare to that of the protein nanopore (~100 nt/sec). 2. The thickness of silicon nitride membrane is at least 20 nm, therefore, a few tens of nucleotides always exist in the nanopore at once. 3. The range of ionic current noise is from a few tens of pA RMS to few hundred of pA RMS in the solid-state nanopore. Note that the ionic current noise in the protein nanopore is around sub-10 pA RMS. The difference between each nucleotide type has only few pA, thus, the solid-state nanopore cannot distinguish the nucleotide types. Also, other issues on the solid-state nanopore are the uniformity / reproducibility / stability of the nanopore size and shape, the interaction problem between organic materials

(DNA) and inorganic materials (silicon nitride), the surface charge effect of composition materials of nanopore devices, and so on. Among these issues, this dissertation describes the origin of high ionic current noise of Si substrate based solid-state nanopore and proposes a new fabrication method of insulated substrate based solid-state nanopore device to reduce ionic current noise.

First, we measured leakage current in silicon substrate based nanopore membrane device immersed in an aqua environment, which typically shows the current level of few nA. This current level is compared with the measured current density (400 nA/cm^2 at 1 V) from the pristine Si wafer (p-type, $10^{16}/cm^3$ B doping) indicating that the exposed Si surface in a nanopore membrane device acts as an electrochemical reaction site. The leakage current is drastically reduced from > 10 nA to < 100 pA at 1 V by the deposition of a dielectric layer on the Si substrate based nanopore membrane device. We also noted that the root-mean-square (RMS) noise of the ionic current is also reduced from 38 pA to 28 pA in correlation with the reduction of leakage current. It indicates that electrochemical reaction of silicon provides one of the major noise sources.

Next, we proposed that the main reason of high ionic current noise comes from the silicon substrate. Therefore, the insulated substrate based solid-state nanopore is expected to have lower ionic current noise. We

introduced a fishing method in order to transfer the silicon nitride membrane on the insulating substrate which has a micropore. The ionic current noise of this novel typed solid-state nanopore device is under 10 pA RMS ionic and the lowest value is around 5 pA RMS. These results are due to the reduced charges passing through the substrate and the lower membrane capacitance. Also, the 5 nm thick silicon nitride membrane is used to transfer and to form nanopores so the effective thickness of nanopore is about 2 nm. Finally, we demonstrated the distinguishment of the nucleotide types (A, T, C, G) by using 1.3 nm diameter and 5 nm thick solid-state nanopore on insulating substrate with one of homopolymer (40 nt ssDNA).

In the last part, both analytical and numerical solutions are obtained in order to understand the potential distribution inside the nanopore and nanochannel with respect to the surface charge density and electrolyte concentration. It is shown that the Debye screening length where the potential drops to 1/e of the surface potential is not enough to describe the change of the ionic conductance in cylindrical cavity geometry. Here, we introduced the concept of the relative ionic conductance – the ratio of ionic conductance as compared to that in zero surface potential – to assess the effect of surface charge on the overall ionic conductance variation. The relative ionic conductance was numerically calculated with various parameters; radius, surface potential, and electrolyte strength. Calculated relative ionic

conductance was enhanced by the increased surface charge and this effect was more improved at low electrolyte strength and small radius nanopore. Also, the high surface charge effect leaded the linearity of ionic conductance with radius. The calculated relative ionic conductance was fitted by using an empirical equation and the result was also compared with the experimental values in different membrane materials.

Key words: Nanopore, solid-state nanopore, ionic field effect transistor, DNA sensing, dielectric substrate, noise reduction method, DNA sequencing

Student number: 2006-20864

Table of contents

List of tables

CHAPTER 1

CHAPTER 3

List of figures

CHAPTER 1

CHAPTER 3

CHAPTER 4

CHAPTER 1.

Introduction

1.1. DNA & DNA sequencing

1.1.1. Properties of DNA (deoxyribonucleic acid)

As well known, the deoxyribonucleic acid (DNA) is a key molecule containing the genetic information which used in the development and functioning of all known living organism. Basically, the unit (informally, bases) of DNA consist of two parts; one is backbone which composed of phosphate groups and sugars (deoxyribose) by ester bond, and another is nucleotide which consisted with one of four types of molecules – adenine (A), thymine (T), cytosine (C), and Guanine (G). Also, each base has one negative charge resulted from phosphate groups. In living cell, DNA generally exists as double strand state (called as dsDNA) for its stability, and it is depolymerized to single strand state (called as ssDNA) to do functional activities (replication to dsDNA and transcription to RNA). For dsDNA formation, two strand of ssDNA which have different direction (3', sugar end, and 5', phosphate group end) were attached to each other by complementary base pairing. The complementary base pairing was occurred between purines (fused five- and six-membered heterocyclic compounds, A, and G) and pyrimidines (six-membered rings, T, and C) by formed hydrogen bonds. The complementary base pairing only occurred in A-T, and C-G pair limited by number of hydrogen bonds in each nucleotide.[1,2]

The physical structure of ssDNA is 1.2 nm width and 0.33 nm length at one bases with fully stretched status. Also, dsDNA has 2.2~2.6 nm width and 0.33 nm length at one bases.[1,2]

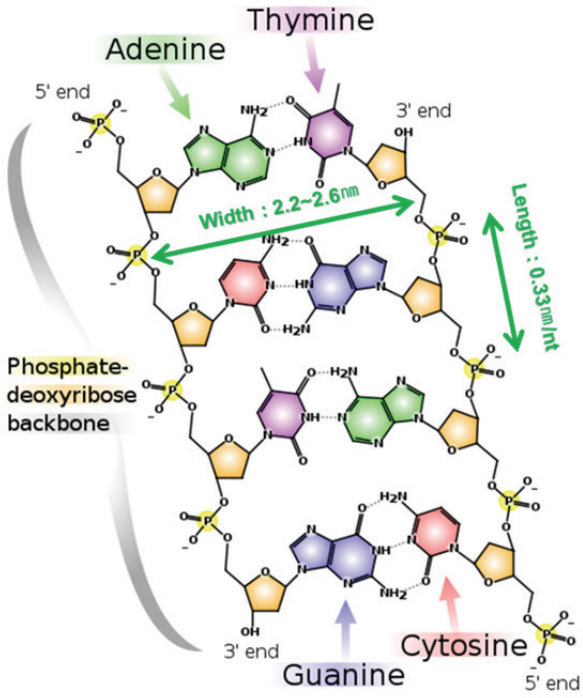

Figure 1-1. Structure of dsDNA. Each ssDNA was consisted of phosphate-deoxyribose backbone and one of four nucleotides (A, T, C, and G). The physical sized of bases is 0.33 nm length and 2.2~2.6 nm for dsDNA, and 0.33 nm for ssDNA. Adopted from Wikipedia[2].

1.1.2. 1st generation technology for DNA sequencing

Decoded in the sequence of nucleotides of a DNA strand has the potential to revolutionize the practice of medicine. Using genomic information can improve the detection of infections and general diagnosis, as well as the prevention and treatment of disease. For example, the personal genetic information can give information for possibilities of genetic disease and congenital malformation of embryo. Furthermore, the genetic information helps decrypt of RNA and protein expression in central dogma system.

The DNA sequencing was firstly obtained in 1971 by using two dimensional chromatography for 12 base pairs DNA[3]. However, this method was not powerful enough to determine complete gene sequences, but just useful for 10-20 bp analysis.

In 1973, A. M. Maxam and W. Gilbert at Harvard Univ. reported the sequence of 24 bps DNA using 'chemical degradation' method[4,5]. Chemical degradation sequencing method was consisted of four chemical treatments (as shown in Figure 1-2) that preferentially break the glycosideic bond at adenine (A), at guanines (G), at cytosines (C), and cytosines and thymines equally (C + T). Using this method, the ssDNA easily created some DNA fragments of various lengths and these fragments had the information of

DNA sequence converted to length. The key issues of the chemical degradation sequencing method is to control the reaction rate to backbone scissoring only once per one DNA strand. The cleavage DNA fragments were read by electrophoresis.

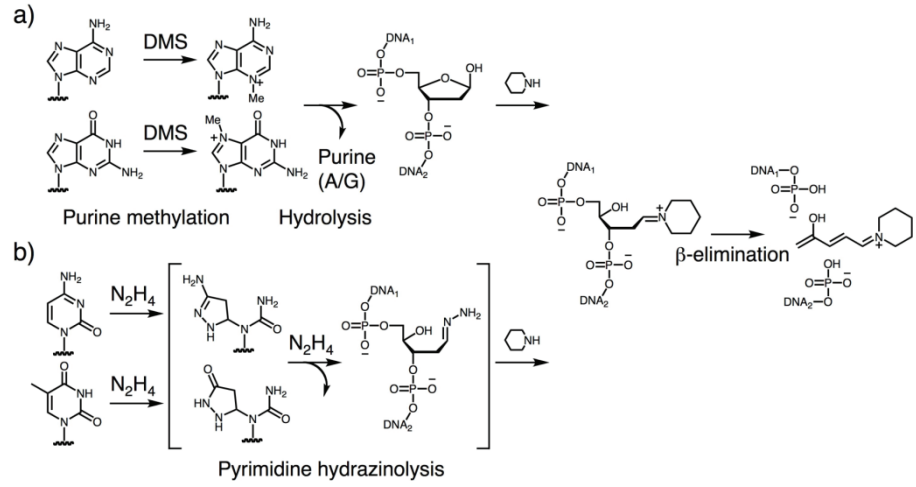

Cleavage Position	Cleavage conditions	Backbone scission
G > A	1) 0.5% DMS 20 °C 15 m; 2) 90 °C 15 m (pH 7)	Piperidine (0.5 M) 90 °C 30 m
A > G	1) 0.5% DMS 20 °C 15 m; 2) 0.1 M HCl, 0 °C 2 h	
C + T	18 M N_2H_4 20 °C 15 m	(for all reactions)
C	18 M N_2H_4 and 2 M NaCl 20 °C 20 m	

Figure 1-2. 1st generation DNA sequencing method based on chemical degradation process. **a)** Purine nucleotides can be cleaved by hydrolysis reaction using DMS. **b)** Pyrimidine nucleotides can be selectively released by the hydrazinolysis reaction. The bottom table summarizes the conditions of chemical degradation process for each chemical treatment.

The first successful method to DNA sequencing was in 1975 by Sanger, and it was called as ‘plus and minus’ method[6-8]. Now, this method was called as ‘Sanger method’ and it has completely dominated DNA sequencing technology over the past 30 years. The key technologies of Sanger method are consisted of ‘termination reaction’ and ‘gel electrophoresis’ as seen in Figure 1-3. Termination reaction was to use chain-terminating nucleotide (dideoxynucelotide, ddNTP) rather than subsets of four natural deoxynucelotide (dNTP) to cause base-specific termination during DNA synthesis. Following the termination reaction, different length of DNAs was achieved with four dNTP and single type ddNTP. Consequently, DNA sequence was converged to length of DNA according to four independent pipelines. The DNA length was extracted by using gel electrophoresis, subsequently, DNA sequence could be read.

However, Sanger method has many limitations for wide spreading in clinical area. The gel electrophoresis method required extremely high number of DNA molecules which have same length. Thus, synthesized DNA should be followed the replication process. Also, termination reaction shows a low yield for long DNA strand, because ddNTP termination reaction was occurred by random and stochastic operation. Thus, existence probability of long DNA through termination reaction was extremely low. To solve these issues, PCR (polymerase chain reaction) method and capillary electrophoresis was

invented, but the limitations are still tough to overcome. As a result, Sanger method has very low throughput for DNA sequencing, and the read length is too low (lower than 100 bp), and the cost is 1 kbp/$.

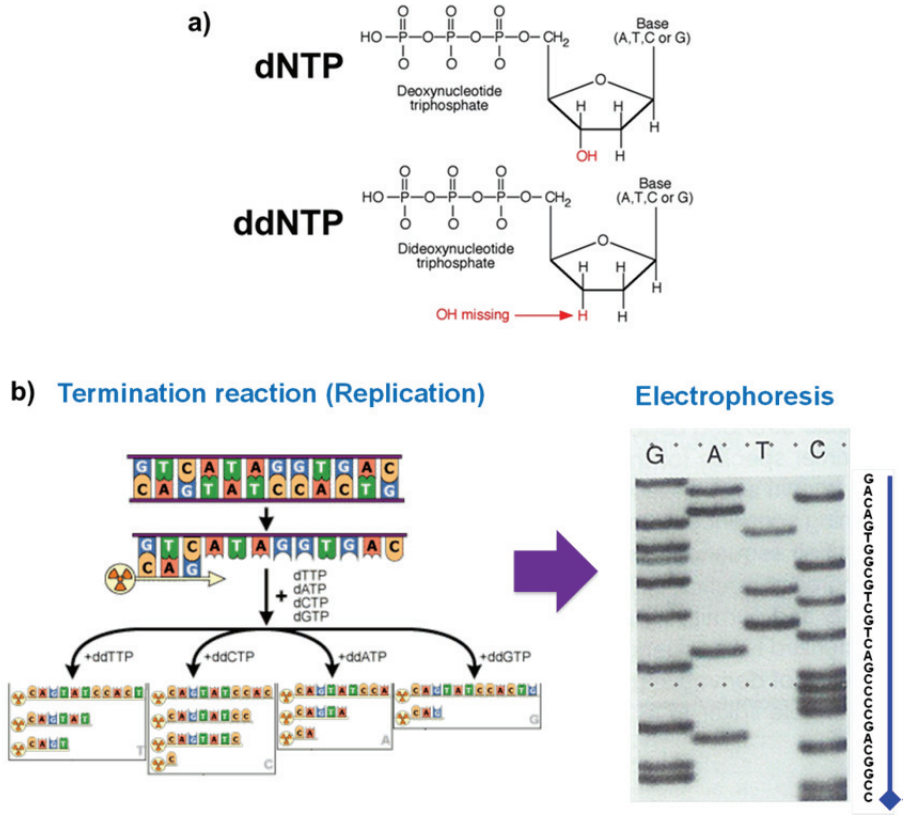

Figure 1-3. 1st generation DNA sequencing method based on termination reaction and gel electrophoresis. **a)** Molecular structure of deoxynucleotide (dNTP) and dideoxynucleotide (ddNTP). dNTP has capability to continuous replication and ddNTP has restricted the replication of DNA. **b)** By using dNTP and ddNTP, the different length of DNA was formed through replication (termination reaction), and the different of length of replicated DNA was analyzed by gel electrophoresis.

The Sanger method has experienced thremendous improvements over the past 30 years in DNA sequencing area. The technological improvements has induces in the efficiency in terms of cost and throughput more than five orders of magnitudes[9,10].

In original publication by Sanger, ddNTP / dNTP ratio was empirically determined to be approximately 100:1 to obtain the optimal distribution of terminate DNA fragments. Such large excess of ddNTP was required by the slower synthesis rate of ddNTP by Pol.I (DNA polymerase) than dNTP about ~3000 times[11]. This feature induces a cost limitation (ddNTP was the most expensive material in Sanger method.) and a speed limitation (ddNTP synthesis was also the most time consuming process).

To solve these problems, many biologists involved to find other DNA polymerase or mutation form of Pol. I. To the candidate DNA polymerase, T7 DNA polymerase and *Taq* (*Thermus aquaticus*) DNA polymerase were intensively studied[11-13]. They found that T7 DNA polymerase retarded ddNTP synthesis than dNTP synthesis only by 3 times11, while comparatively Pol. I DNA polymerase and *Taq* DNA polymerase did same process by 3000 times[12] and 600 times[13], respectively (summarized in Figure 1-4a). The selectivity of dNTP / ddNTP was enhanced or degraded by point-mutation of DNA polymerase at Y526 (tyrosine at 526). Y526 has single OH: at T7 DNA polymerase, whereas the corresponding positions are F762 (phenylalanine)

for Pol. I DNA polymerase and F667 for *Taq* DNA polymerase and do not have the OH: functional group. The phenolic OH of the tyrosine or the 3'-OH of the incoming dNTP should be required to held Mg(II) in place (Figure 1-4c). However, the condition with ddNTP and phenylalanine in DNA polymerase cannot held Mg(II) in place, then the DNA synthesis to be retarded. When the Y526 amino acid changed to phenylalanine (Y526F), T7DNA polymerase shows the high selectivity between ddNTP and dNTP. Also, F762Y at Pol. I. DNA polymerase and F667Y at *Taq* DNA polymerase loose the selectivity of them (Figure 1-4a,b).

a)

Genotype		Rate ratio of dNTP/ddNTP incorporation				
		G	A	T	C	Overall
T7 DNA polymerase	WT	3.2	3.3	2.8	3.7	3.0
	Y526F	6,400	7,300	8,400	11,400	8,000
Taq DNA polymerase	WT	140	720	1,100	250	600
	F762Y	0.56	0.72	0.54	0.75	0.6
E. coli DNA polymerase I	WT	1,400	4,700	4,500	2,600	3,000
	F667Y	0.45	0.59	0.56	0.32	0.5

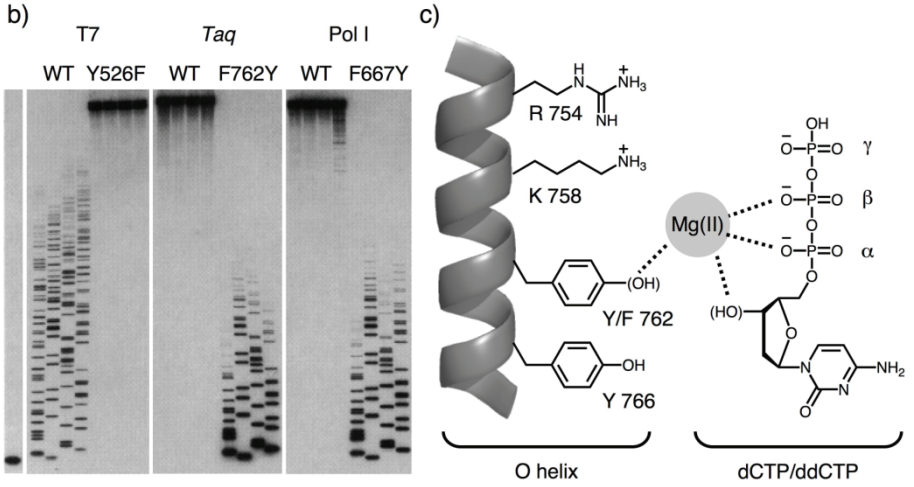

Figure 1-4. The selectivity of dNTP / ddNTP for DNA polymerase and its molecular mechanism. **a)** Summarized table of the ratio of dNTP / ddNTP for wild-type (WT) and mutation form of T7 DNA polymerase, *Taq* DNA polymerase, and Pol. I DNA polymerase. **b)** The gel electrophoresis images of each DNA polymerases with dNTP : ddNTP = 6 : 1 condition. **c)** Cartoon for the reaction mechanism of DNA polymerase[11-13].

Other undesirable features of Pol. I DNA polymerase as far as its use in DNA sequencing is proofreading activity. Proofreading means the 3' to 5' exonuclease activity, that a nucleotide was detaches instead of attached at the 3' end. This proofreading function is useful for DNA replication through DNA polymerase, but, it could make the data complicated to analysis, as result of random length of the synthesis ssDNA. The proofreading reaction of Pol. I DNA polymerase can be limited by amino acid mutation[14]. For instance, WT Pol. I DNA polymerase has 1.07×10^4 U/mg as polymerase activity and 1 A. U. as exonuclease activity. Whereas, D355A/E357A and D424A mutation in Pol. I DNA polymerase shows almost same polymerase activity (0.93×10^4 U/mg for D355A/E357A, 1.11×10^4 U/mg for D424A) and degraded exonuclease activity with 5 order magnitude (1.3×10^{-5} A. U. for D355A/E357A, 1.4×10^{-5} A. U. for D424A)[14]. Also, T7 DNA polymerase mutants are established with same strategy[15].

Another limitation of original Sanger method was depended on the gel electrophoresis to determine the weight (length) of the synthesis DNA fragments. Also, a set of four chain termination reaction should be carried out in separate experiments for each ddNTP type. In 1986, L. M. Smith *et al.* developed a set of four fluorescent dyes for each nucleotide[16]. Four fluorescent dyes can be independently detected in a one sample, so that the four chain termination reaction can be pooled together and determine the

length in a same gel electrophoresis. Advantages of fluorescent dyes in Sanger DNA sequencing method are enabling real time sequencing as well as reducing the time consuming process and a safety issues.

1.1.3. 2nd generation technology for DNA sequencing

To overcome the limitation of 1st generation DNA sequencing technology, 2nd generation DNA sequencing method was introduced. Nearly all of the 2nd generation DNA sequencing method based on 'Sequencing by Synthesis (SBS)' technology. As one of the example, Figure 1-5 shows the SBS method (called as Solexa technology) of Illumina Corporation[17]. The target DNAs were localized typical substrate which has pre-attached bundle of primer for PCR process. The attached target DNAs were amplification by using PCR method at fixed position (called as 'Bridge amplification'). As a result, the cluster was formed which has same DNA sequence. Finally, the DNA sequence was readout using fluorescence detection through synthesis process with dye-assisted dNTP by using polymerase or ligase.

Using these techniques, the throughput of DNA sequencing was improved and the read length exceeded 100 bp. Also, parallelize reading of different DNAs was possible in a substrate. However, 2nd generation DNA sequencing method has some limitation; it still used an amplification process and an optical detection. Position of DNA cluster could not controlled, thus all of substrate have to read by optic system. And the read length stays in under 1000 bp.

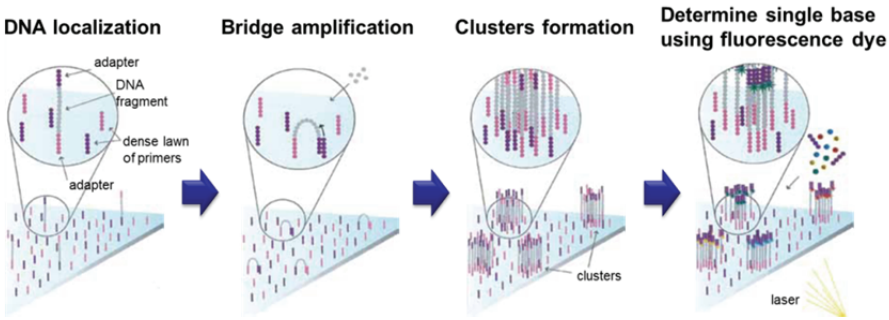

Figure 1-5. One of examples of 2nd generation DNA sequencing methods. DNA was localized in a typical substrate, and it formed cluster which had same sequence by amplification method (such as PCR). DNA sequencing was operated by fluorescence optical detection during each base synthesis[17].

In addition, some reacted material from DNA synthesis can be used to DNA sequencing. During the DNA synthesis by DNA polymerase, a pyrophosphate (PP_i) and a proton (H^+) are produced and liberated in solution. These two kinds of products can be detected by using Roche 454 Platform (454 Life Sciences Inc.)[18,19] for PP_i and Ion Torrent (Ion Torrent Systems Inc., Figure 1-6)[20,21] for H^+, therefore we can monitoring the hybridization of ssDNA. Using these tools, DNA sequence can be read when DNA polymerase and only one of the four dNTPs are added in the hybridization step in each cycle. After then, all reagents are washed out, and the different one of the four dNTPs are added. From this reaction, DNA sequencing is operated with direct and real time without electrophoresis process.

Using these techniques, the throughput of DNA sequencing was improved and the read length exceeded 100 bp. Also, parallelize reading of different DNAs was possible in a substrate. However, 2nd generation DNA sequencing method has some limitation; it still used an amplification process and an optical detection. Position of DNA cluster could not controlled, thus all of substrate have to read by optic system. And the read length stays in under 1000 bp.

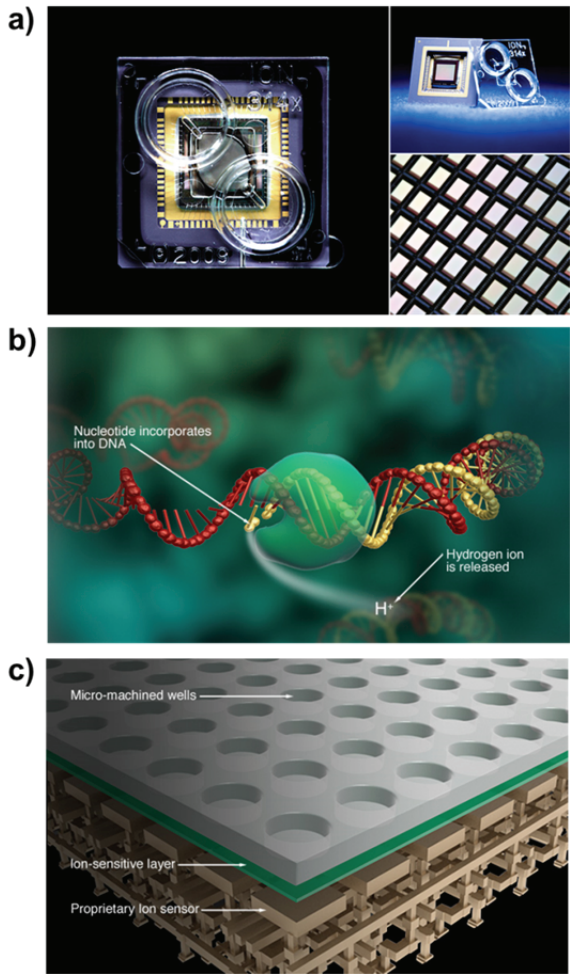

Figure 1-6. Ion Torrent DNA sequencing platform. **a)** Image of Ion Torrent device which world 1st Si based DNA sequencing tool. **b)** Single proton was released during DNA hybridization by DNA polymerase and dNTP. **c)** Released protons were detected by Si based pH detector and DNA bundle were located in micro-machined well[20,21].

1.1.4. 3rd generation technology for DNA sequencing

2nd generation DNA sequencing methods were basically based on SBS technology, DNA immobilization in substrate, and DNA amplification to DNA bundle formation. In these series of reaction, the most time and cost consuming work is the DNA amplification using PCR process. Therefore, 3rd generation DNA sequencing technology based on the single molecule detection by optical and electrical measurement. One of them is SMRT (Single Molecule Real-Time sequencing) by Pacific Biosciences Inc.[22-24]. SMRT technology is based on the single fluorescence dye detection method using zero-mode waveguide. During DNA synthesis with fluorescence dye attached dNTP, single fluorescence dye cannot be detected by influence of background fluorescence signal from other molecule. However, zero-mode waveguide with 50 nm diameter nano well provided 1000 magnitude enhanced signal without background fluorescence (Figure 1-7a). Using this phenomena, SMRT technology immobilizes DNA polymerase at zero-mode wave guide nanowell which fabricated with massive array for parallel detection (Figure 1-7b), and the released fluorescence dyes are detected when DNA hybridization (Figure 1-7c).

Also, the nanopore DNA sequencing technology based on single molecule based technology and the nucleotide type is distinguished electrically and optically.

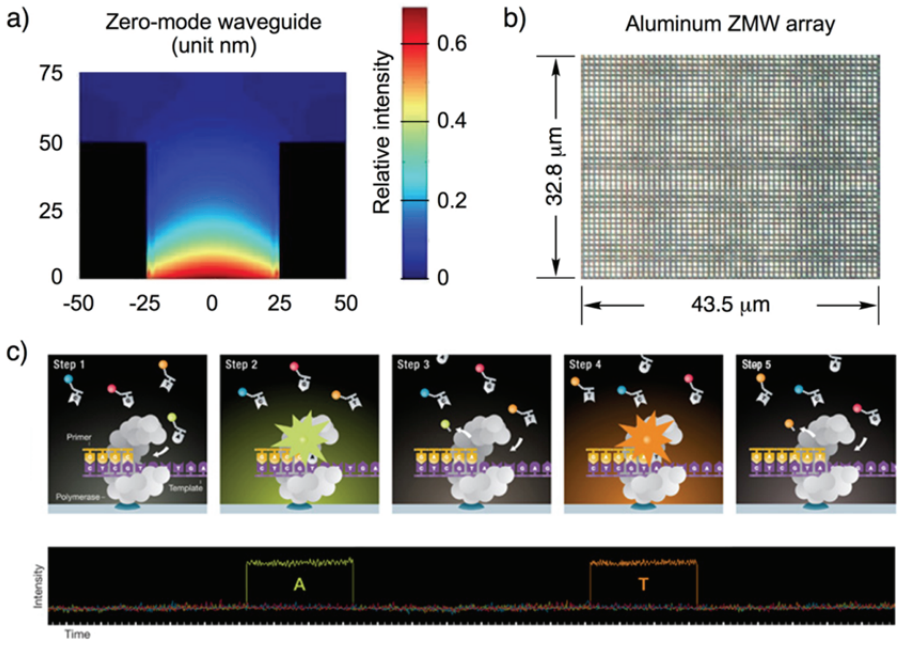

Figure 1-7. SMRT DNA sequencing technology by Pacific Biosciences Inc. **a)** Schematic image of the calculated detection volume of 50 nm diameter nano well (zero-mode waveguide). This dramatic reduction in the detection volume provides the need 1000 times improvement in rejection of background fluorescence. **b)** To massive parallel readout of DNA sequence, zero-mode waveguide array containing millions of wells was fabrication on the aluminum based substrate. **c)** DNA polymerase is immobilized in bottom of nano well. When fluorescence dNTP and DNA incorporated to DNA polymerase, fluorescence dye is released and detected by optical system[22-24].

1.1.5. Growth of DNA sequencing and single molecule sequencing

The DNA sequencing rapidly innovated for prerequisite to personalized genomic medicine as well as new approaches in biology, evolution and the environment. Figure 1-8 shows the growth of DNA sequencing technologies as view of cost and speed[25-27]. 1st generation DNA sequencing methods based on Sanger method was invented at 1995, and improved by shot-gun method in 2000, and by capillary electrophoresis in 2005. 2nd generation DNA sequencing method based on sequencing by synthesis was started in 2008 by using polymerase and upgraded by using ligase in 2009. However, the speed and cost still need to improve for personal DNA sequencing. The target of DNA sequencing for personal genetic medicine is cheaper than 10^8 bp/$ and faster than 10^7 bp/sec. Still, DNA sequencing technologies are intensively studied and these technology are summarized in Table 1-1.

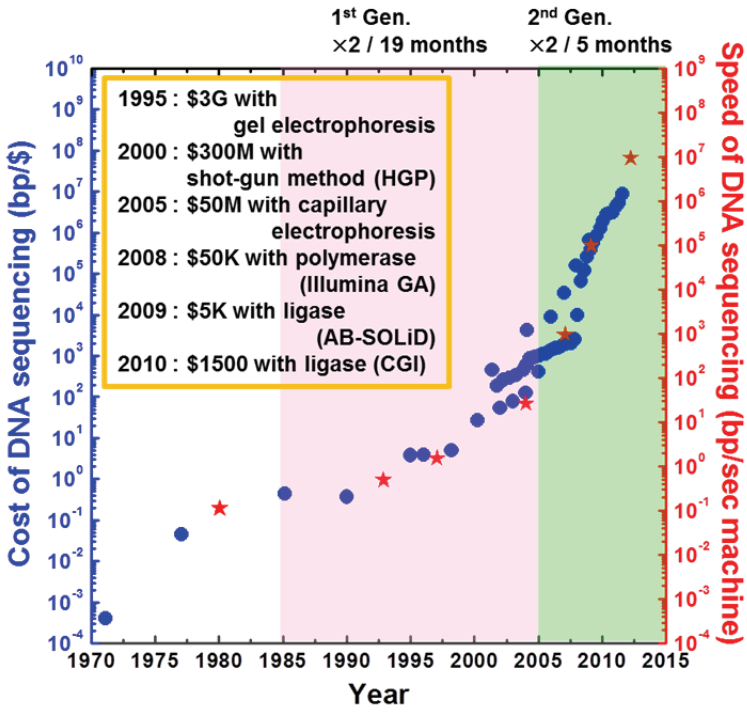

Figure 1-8. Growth of DNA sequencing technology as view of cost and speed. Adopted from Ref. 25-27. 1st generation DNA sequencing methods based on Sanger method was invented at 1995, and improved by shot-gun method in 2000, and by capillary electrophoresis in 2005. 2nd generation DNA sequencing method based on sequencing by synthesis was started in 2008 by using polymerase and upgraded by using ligase in 2009.

Illumina-GA	**SbP**	Fluorescent read-length > 100 bp
Roche-454	**SbP**	Long reads > 0.4 kbp
Ion Torrent	**SbP**	**$50K/bp, small device**
Helicos	**SbP-sm**	High parallelism & quantitation
Polonator	**SbL/P**	**Open source**, $170K device, 100Mb haplotypes
AB-SOLiD	**SbL**	Longest ligation reads
CGI	**SbL**	**$2000/bp**, rolony grid, 100Kb haplotypes
Intelligent Bio	**SbP**	Hexagonal grid
Pacific Bio	**SbP-sm**	Long reads (> 2.0kbp)
Halcyon	**EM-sm**	**Long reads (> Mbp), $100/bp**
GnuBio	**SbP**	Droplets
Bionanomatrix	**SbP-sm**	Fluorescent mapping
Bisigen	**SbP-sm**	Polymerase <> dNTP FRET
GE Global	**SbP-sm**	
Light Speed	**SbL**	16x higher density, > 10x speed
Genizon BioSci	**SbH**	In situ sequencing
ZS Genetics	**EM-sm**	Iodine labels
Nabsys	**Pore-SbH-sm**	Small device
Oxford Nanopore	**Pore-protein-sm**	Small device
Electronic Biosci	**Pore-Protein-sm**	
IBM	**Pore-Si-sm**	Small device

Table 1-1. Recent technology for DNA sequencing at 2012. Top side technologies (red) have already commercialized and middle side technologies (blue) have commercialized plan. Bottom side technologies are still studied in laboratory level. SbP : Sequencing by Polymerase, SbL : Sequencing by Ligase, EM : Electron Microscopy, SbH : Sequencing by Hybridization, Pore : Nanopore based, Pore-protein : Protein nanopore based, sm : single molecule detection technology.

1.2. Nanopore technologies

1.2.1. Concept of nanopore sequencing

An alternative approach for sequencing DNA involves direct examination of the DNA structure and sequence by threading through a biological or synthetic (solid-state) nanopore[28]. The idea of nanopore sequencing was first proposed in 1989 by D. Deamer of the University of California[29] and the patent was introduced in 1995 by D. Deamer, D. Branton, and J. J. Kasianowicz[30]. The nanopore sequencing technology involves a very thin membrane (under few tens of nanometer thickness) that contains nanopores of sub-10 nm diameter. This membrane located between two chambers (cis- and trans-chamber) with electrolyte as shown in Figure 1-9. Without single molecule, the ion species (K^+ and Cl^- ion with KCL electrolyte) was flowed through the nanopore by applied bias that applied by Ag/AgCl electrode at chambers. Also, the single molecule which has charge in itself was dragged into the nanopore by applied bias. When the single molecule was passed through the nanopore, the ion species was blocked by the volume of single molecule, and then the ion current was dropped (so called blockade current). The blockade current has two information; the dwell time and the blockade current level could be discriminated into the

length and the cross-sectional area of single molecule, respectively.

This idea was firstly experimented in 1996 by D. Deamer, D. Branton, and J. J. Kasianowicz[31]. The first experiment proposed that the DNA sensing was possible using a nanopore device which consisted by lipid bilayer membrane and α-hemolysin protein nanopore (33-kD, 293-amino acid). Bacteria *Staphylococcus aurus* secrets the α-hemolysin protein which spontaneously inserts itself in a lipid bilayer membrane generating a pore of 1.4 nm diameter[32]. By the similar diameter with ssDNA, protein nanopore would be expected to accommodate single-stranded DNA (ssDNA) sensing and sequencing. The nanopore based DNA sequencing methods do not need the amplification and labeling process as it is the native label-free and single molecule DNA sequencing technology. In addition, electrical readout concept will provide us the higher speed and massive parallelization than optical readout. Also, the nanopore technology is no apparent theoretical upper limit at read length. As a result, the nanopore technology can reduced the cost and the consumed time for DNA sequencing.

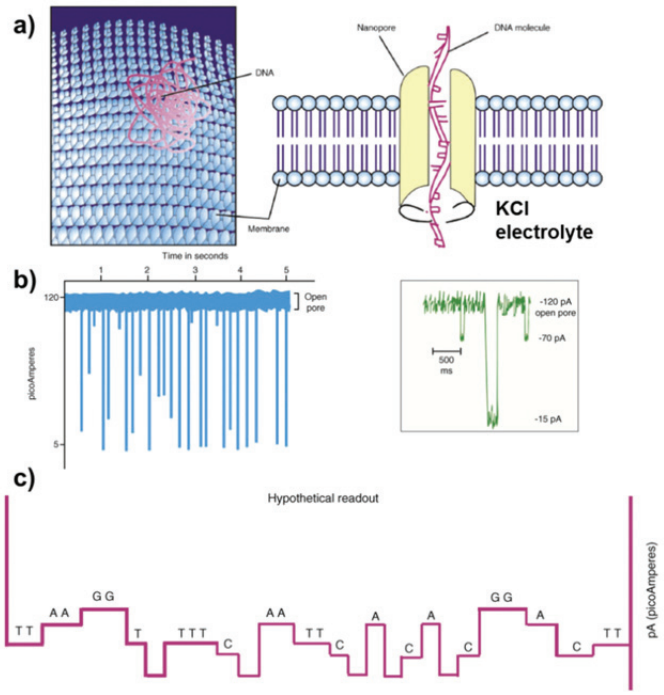

Figure 1-9. Concepts of nanopores sequencing technologies. **a)** Schematic image of nanopore structure based on protein nanopore with transporting DNA. The nanopore located on lipid bilayer membrane which separated an ionic solution into two chambers. **b)** Electrical signal of nanopore device with DNA translocation. Open pore current was derived by applied bias and electrolyte strength. When a DNA molecule passes the nanopore, DNA blocked the ionic movement. Then, ionic current was dropped into typical value related to translocate molecular size and the dwell time depended on the length of molecule. **c)** Ideal signal of DNA sequencing result by using nanopore sequencer. Adopted from Ref. 28

1.2.2. Type and fabrication method of nanopores

Commonly used nanopores can be cast into two categories, biological (protein) nanopore and solid-state (synthetic) nanopore. The α-hemolysin (Figure 1-10a) is the most noted among the former type[31,33-41]. While it remains the most common biological nanopore in experiments, the channel is too long for single nucleotide reading. Therefore, many scientists tried to form the narrowest sensing zone by mutation[38] or another molecule insertion[35]. Recently, MspA form *Mycobacterium semgmatis* (Figure 1-10a) was engineered and intensively used for sensing and discrimination among different DNA bases[42-45]. In contrast to α-hemolysin, MspA has conical structure which is more effective DNA sequencing by thinner sensing zone from sharp inner constriction.

Protein nanopore device are generally fabrication on lipid bilayer membrane which located across microsize orifice in Teflon chamber. After then, the buffers in both chamber (cis- and trans-) are exchanged to 1 M KCl electrolyte. When 1 ug/ml concentrated α-hemolysin addition in cis chamber, the single channel is formation within 5 minutes. To prevent further channel formation, the buffer at cis chamber is flushed by fresh buffer.

These protein nanopore has many advantages; 1. The nanopore diameter and structure are highly uniform and reproducible. 2. The nanopore

size of narrowest region is well matched to ssDNA, therefore it is suitable for the ssDNA detection and sequencing. 3. The surface charge of nanopore wall can be easily modified by protein mutation. It serves a key method to modulate the translocation frequency and speed of ssDNA. However, the predetermine nanopore diameter limited the application of protein nanopore to ssDNA excepting other single molecule, such as protein and nano particle. Moreover, the lipid bilayer membrane as supporting material of protein nanopore lack of the mechanical robust, that the life time is few minutes to several hours.

In the past decade, advancements in nanotechnology have enabled scientists to make sub-10 nm sized nano structure with high precision and enough throughputs (Figure 1-10b). Firstly, the focused ion beam was used to fabricate sub-10 nm sized nanopore on silicon nitride or silicon oxide membrane (Figure 1-11a)[46]. The ion beam sculpturing equipment was composed the ion beam generator and feedback system to the ion beam turn off when single ion was detected at opposite side of nanopore. This technique supplies a enough size of nanopore and a controllability, but, but it has limitation on the complex of equipment and uncommonness.

On the other hand, it is well known phenomena that the sample has damaged during TEM observation with high accelerating voltage (tens of kV ~ hundreds of kV). In 2003, the possibility of nanopore fabrication using

this phenomena was reported (Figure 1-11b)[47] and it is usually used in nanopore area[48-61], Currently. The nanopore fabrication mechanism are still complex to understanding, but, it is accepting that the high energy electron induces a direct atomic displacement like as sputtering mechanism[80].

However, the nanopore fabrication method still not matched to product and commercialize. Because, the nanopore fabrication using TEM has lack of uniformity on nanopore size and structure, well designed process condition, and reproducibility of process. Therefore, some people used the CMOS compatible technology, which has well used in Si based electronic device fabrication, to form the nanopore. Electron beam lithography provides us nanometer size controllability, but, the throughput is too low to product electronic device. However, in the nanopore device, the treated area is small enough to secure the producibility[62]. To the nanopore fabrication by CMOS compatible way, the nanoholes were patterned on e-beam resist (PMMA, ZEP, and so on). After then, the nanohole patterns were transferred to target membrane by reactive ion etching (RIE). From this technique, the number of nanopore and the size of nanopore can be easily controlled (Figure 1-12). Subsequently, the nanopore size also modulated by deposition other materials using atomic layer deposition (ALD).

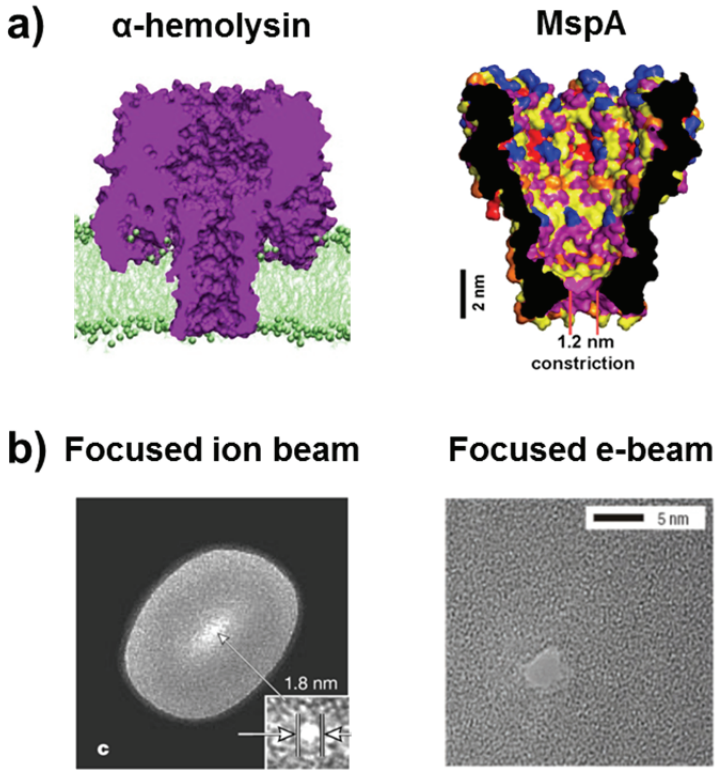

Figure 1-10. Variation of nanopore type. **a)** Type of protein nanopore, α-hemolysin[31] and MspA[42]. **b)** Solid-state nanopore fabricated on SiO_2 or Si_3N_4 membrane by focused ion beam[46] and focused electron beam[47] in transmission electron microscopy (TEM).

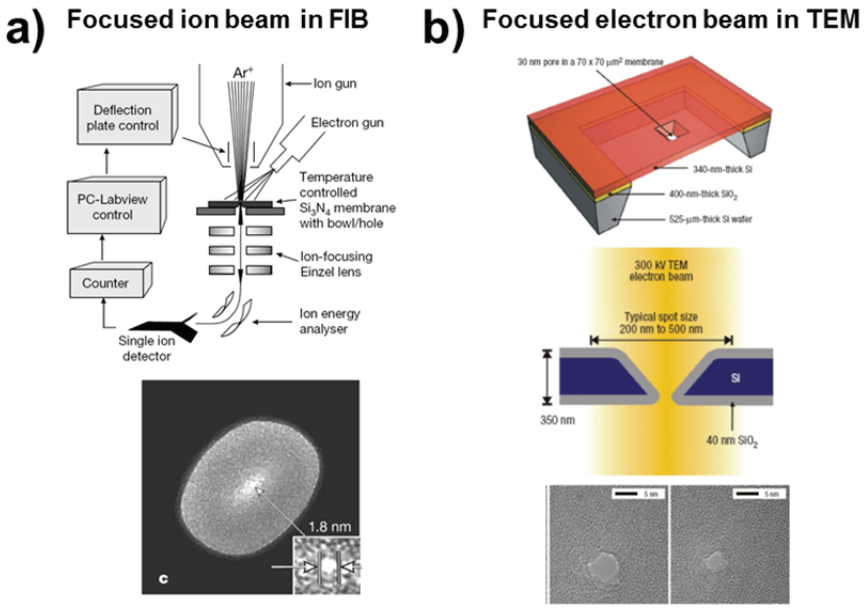

Figure 1-11. Fabrication method for solid-state nanopore by using focused ion beam and focused electron beam. **a)** An ion beam sculpting equipment was built by custom design to feedback control by single ion detection through the nanopore, when nanopore formed[46]. **b)** A few nanometer sized nanopore fabrication method by focused electron beam in TEM, and this method is generally used in solid-stat nanopore fabrication[47].

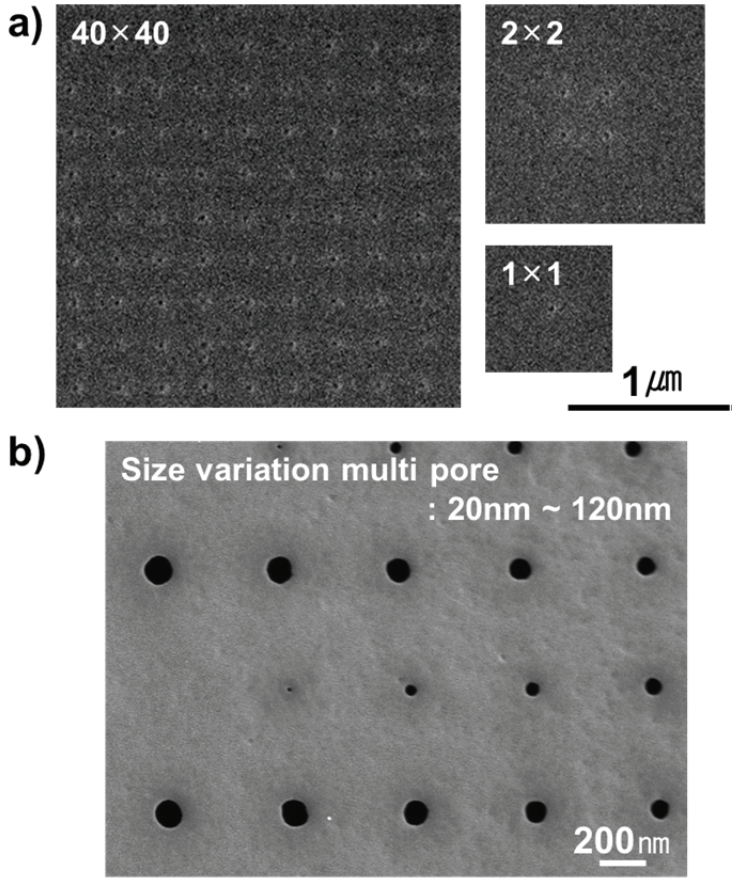

Figure 1-12. Electron beam lithography and reactive ion etching (RIE) process for the solid-state nanopore fabrication. **a)** Electron beam lithography result on PMMA positive resist as a function of number of nanopore. Used e-beam lithography tool has 100 kV accelerating voltage and 500 pA emission current (JBX-6300FS). **b)** Nanopore formation on silicon nitride membrane by e-beam lithography and RIE with diameter variation. The smallest size of nanopore is about 20 nm.

Nevertheless, the solid-state nanopore has fundamental limitation to the DNA sequencing. It is a longer nanopore length (thicker membrane) than the length of single nucleotide. Generally, most of solid-state nanopore researcher used 20 nm thick silicon nitride membrane, it means that the ~60 nucleotides of ssDNA are always located in the nanopore when the ssDNA transports. To overcome this issue, 10 nm thick silicon nitride membrane also used[55], but, the limitation still remained.

However, the game is fully changed by development of graphene nanopore[63-66]. The graphene is a monolayer graphite film and its thickness 0.34 nm. It means that the only single nucleotide positioned in mono layered graphene nanopore. It is reported in 2008, the graphene could be easily sculpted using electron beam in TEM. Afterwards, the graphene nanopores were eventually reported in three independent groups at the same time[64-66] (Figure 1-13a-c). In addition, the thickness of graphene was measured at cracked area, and the thickness of graphene confirmed as 0.34 nm / layer. And the graphene nanopore was perforated using 200 kV TEM (Figure 1-13d) from this work.

Graphene nanopore has many attractive points such as 0.34 nm thickness, expectation of conductive change by nucleotide type, high surface charge density, and so on. However, it still has many limitation to the sub-2 nm sized nanopore fabrication and the stability during measurement.

Nonetheless, one of critical issues is that the electric field should be dominated by the nanopore diameter not the length at 1.5 nm diameter and 0.34 nm length nanopore, thus, the single nucleotide resolution of graphene nanopore would be carefully studied from now on.

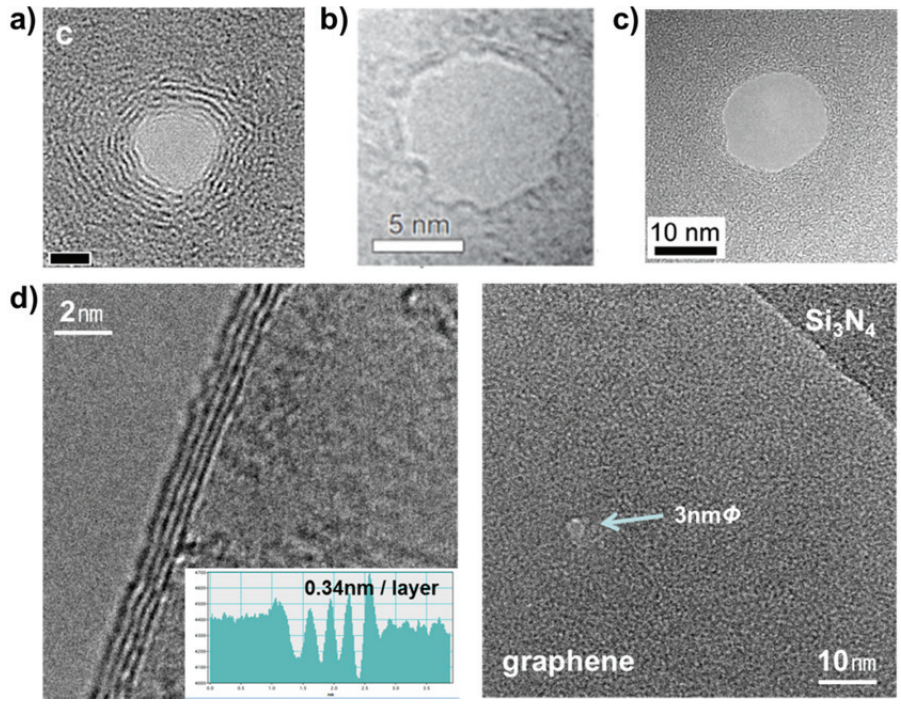

Figure 1-13. Graphene nanopore. **a)** First reported graphene nanopore[63], and it was used as nanopore sensor for DNA detection[64]. **a, b, c)** The graphene nanopore devices as a DNA sensor were reported by independent group at a same time (64, 65, 66) **d)** Observation of graphene membrane in cracked area. The graphene membrane has 0.34 nm thickness. Fabricated graphene nanopore with 3 nm diameter (in this works)

One of other limitation of solid-state nanopore is the higher ionic current noise than the ionic current noise of protein nanopore. Figure 1-14 shows the ionic current signal of the protein nanopore (Figure 1-14a) and the solid-state nanopore (Figure 1-14b). The amplitude of ionic current has meaning that the ionic current noise from thermal energy, external electrical circuit, and so on. The most of the protein nanopores show the sub 10 pA RMS ionic current noise, but, the ionic current noise of solid-state nanopores has range from tens of pA RMS to hundreds of pA RMS. As a result, the solid-state nanopore cannot tried to the DNA sequencing, due to sub-10 pA difference between nucleotide types.

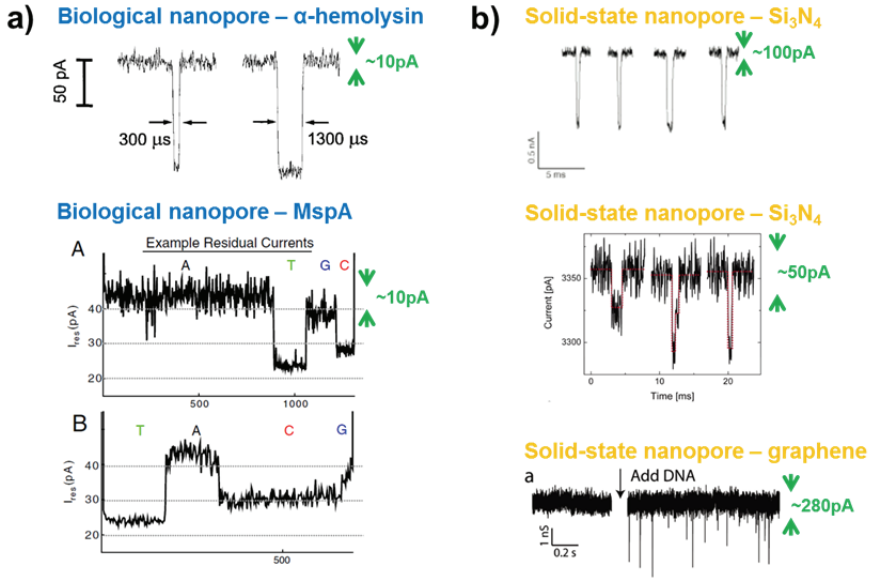

Figure 1-14. Comparison of ionic current noise between biological nanopore and solid-state nanopore. **a)** Ionic current noise of biological nanopore, α-hemolysin[31] and MspA[43]. **b)** Ionic current noise of solid-state nanopore, silicon nitride membrane[49,68] and graphene membrane[66].

The front line of nanopore structure is the hybrid nanopore. The hybrid nanopores are composed of the biological nanopore and the solid-state nanopore, hence, the both advantage can be used in hybrid nanopore device. Basically, the protein nanopore is inserted in the solid-state nanopore, in order to have a mechanical robust and uniform and fixed size nanopore. The protein nanopore was inserted into the solid-state nanopore by the electrical dragging force between the attacked DNA at protein nanopore and external bias (Figure 1-15). Also, the DNA origami has interesting point that its nanopore shape and size can be easily designed, thus, it will be useful not only DNA sequencing and detection but also other biomolecule detection (Figure 1-16).

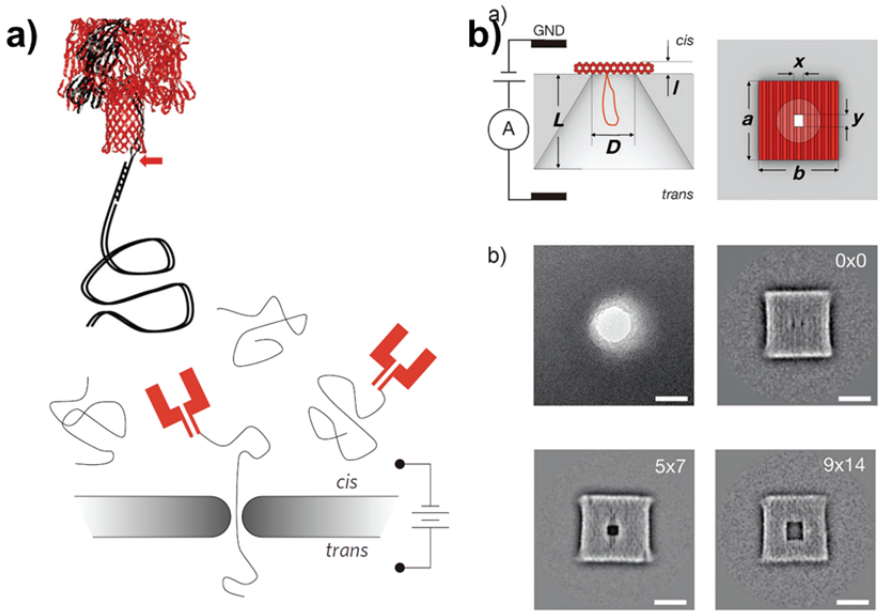

Figure 1-15. Hybrid nanopore formed by the biological nanopore attaching on the solid-state nanopore. **a)** Combine of α-hemolysin and silicon nitride nanopore. To insertion of α-hemolysin, α-hemolysin was modified by dsDNA attaching[72]. **b)** Combine of DNA origami and silicon nitride nanopore. Also, DNA origami has dsDNA strand for insertion to the solid-state nanopore[73].

1.2.3. Current status and obstacles for DNA sequencing using nanopores

DNA sequencing using nanopore is tried by using only protein nanopore and results from protein nanopore. Before the DNA sequencing, protein nanopores were assessed the possibility of nucleotide discrimination[33,74,43,44]. First result of nucleotide discrimination[33] used the α-hemolysin and longer (~kbp) ssDNA homopolymer. As a results A, C, T can be distinguished and the blockade current has two level in one nucleotide according to the direction of the ssDNA. In sequence, the nucleotide discriminations were tried with immobilized ssDNA by using hairpin duplex[43] or biotin / avidin adhesion[44,74]. Using immobilized technique, the blockade current levels of each nucleotide type (A, T, C, G) were determined, furthermore, the sensing area and length resolution (~ 3 nt) are also determined for the α-hemolysin[74] and MspA[44].

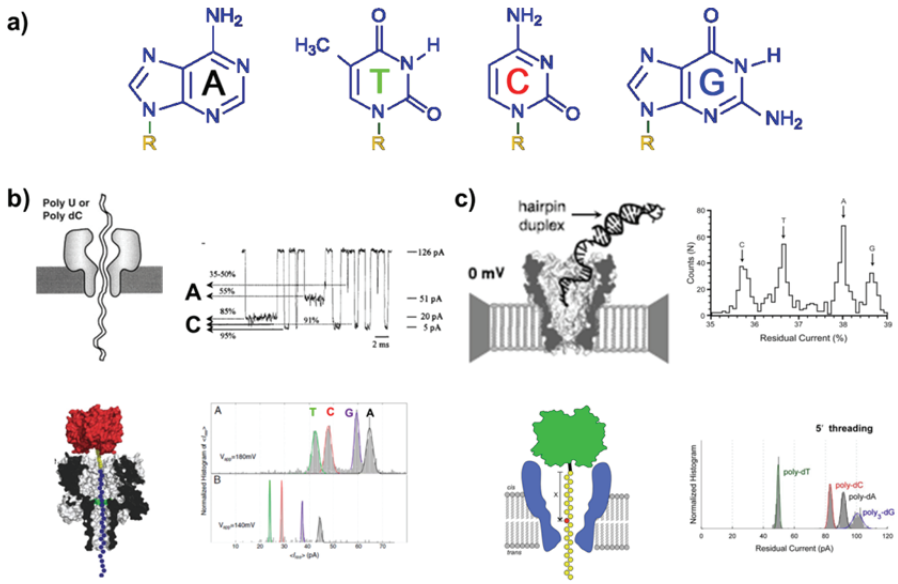

Figure 1-16. Structure of each nucleotide type (A, T, C, G) and the report of homopolymer distinguishment using protein nanopore. **a)** Structure of four nucleotides, adenine, thymine, cytosine, guanine. **b)** Discrimination of nucleotide type through α-hemolysin by enough long homopolymer[33] and immobilized ssDNA using biotin-avidin bond[74]. **c)** Discrimination of nucleotide type through MspA by immobilized ssDNA using hairpin duplex[43] and biotin-avidin interaction[44].

The first possible technique to DNA sequencing using nanopore was proposed in 2009. It was used the cyclodextrin decorated α-hemolysin and exonuclease enzyme. At the pristine α-hemolysin, ssDNA and single dNTP were passed too fast to detect and distinguish the type. The cyclodextrin provide a longer translocation time of dNTP to α-hemolysin. In addition, exonuclease decomposed the ssDNA to dNTP in cis chamber, then, we can detect the translocation of the decomposed dNTP. Actually, this report didn't describe the complete DNA sequencing, but, if the exonuclease sticks the top of the α-hemolysin, this technique can be used for DNA sequencing.

Specifically, the DNA sequencing using nanopore device is possible in 2012 by using phi29 DNA polymerase with α-hemolysin[41] and MspA[45]. Phi29 DNA polymerase has two different properties; exonuclease property at 3' to 5' and synthesis (polymerase property) at 5' to 3' direction. As a result, using phi29 DNA polymerase as molecular motor, the ssDNA can be moved step by step in the nanopore, therefore, the DNA sequence successfully achieved. However, this DNA sequencing technique still has lack of the determination of multiple same nucleotide in a row, the precision of DNA sequencing, and so on.

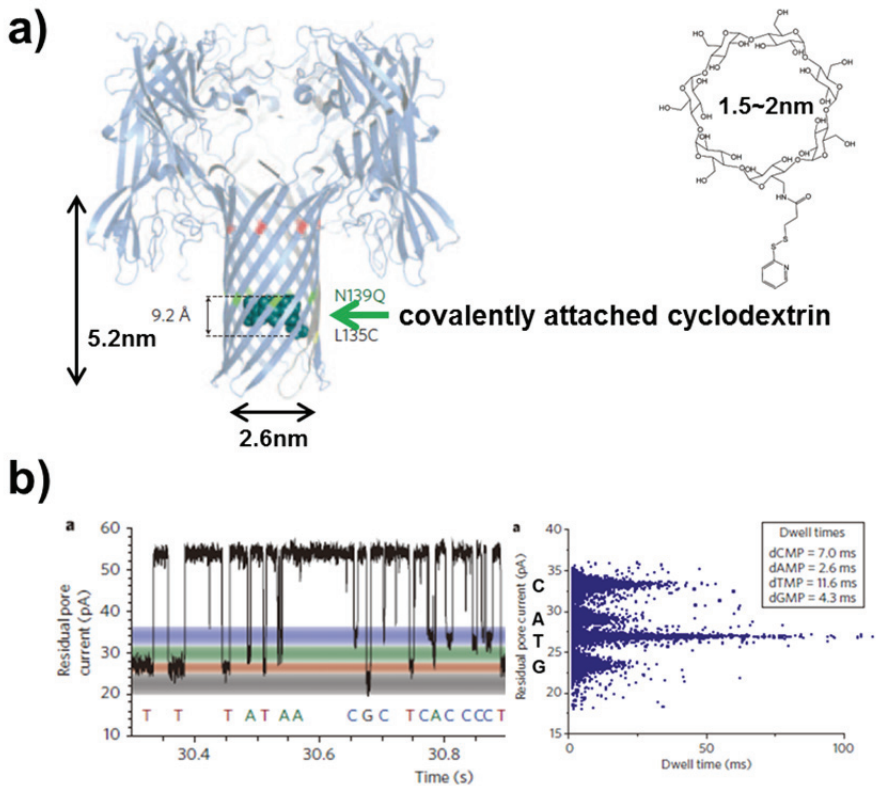

Figure 1-17. First DNA sequencing result by using α-hemolysin which has single nucleotide resolution and exonuclease. **a)** Biological engineered protein nanopore based on α-hemolysin and cyclodextrin. Cyclodextrin provide a smaller sensing area and a longer reading time to determine a nucleotide type. **b)** The reported results of A, T, C, G discrimination. A, T, C, G are clearly separated in blockade current distribution[35].

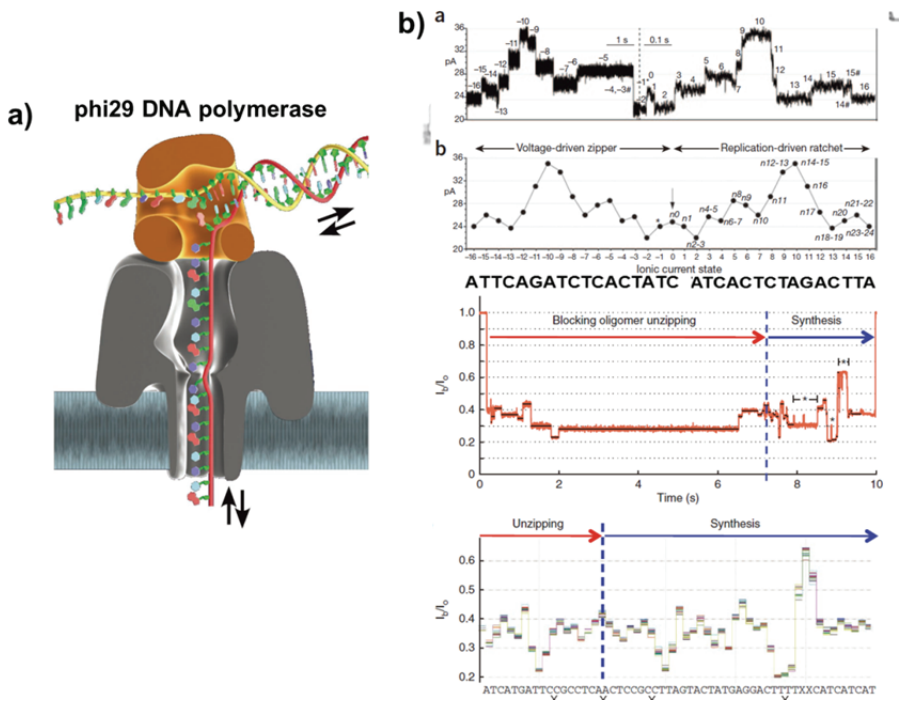

Figure 1-18. Nanopore DNA sequencing method using phi29 DNA polymerase with α-hemolysin and MspA. **a)** Schematic diagram of incorporation structure of DNA, phi29 DNA polymerase, and α-hemolysin. **b)** DNA sequencing results using phi29 DNA polymerase with α-hemolysin[41] and MspA[45]. The signals are separated two parts; one is unzipping process by exonuclease property of phi29 DNA polymerase and another is synthesis process by polymerization through phi 29 DNA polymerase.

On the other side, the solid-state nanopore has more complex problem to DNA sequencing. One of the most important issues is the higher ionic current noise than required the value, < 10 pA RMS (Figure 1-14). Other issue is the faster translocation speed of DNA through the solid-state nanopore. Comparison to the protein nanopore (100 nt/sec), the DNA translocation speed is 100,000 nt/ sec in the solid-state nanopore. It means that the solid-state nanopore cannot serve us the enough time to determine the nucleotide type. Because only hundreds of ions are transporting when a single nucleotide translocates in solid-state nanopore. To reduce the speed of DNA translocation, many idea (Figure 1-19) was tried, but, it was still not enough.

In the other hands, various measurement technology are applied to nanopore system[75-79]. One of the successful methods is a tunneling measurement using transvers embedded electrode in nanopore[75,76]. Tunneling current is the most sensitive technique in electrical measurement, thus, it can be used to DNA sequencing in nanopore. Other method is optical readout by using nanopore as wave guide. And another interested technology is the DNA sequencing using mass spectroscopy which one of the most sensitive spectroscopy. In this case, the nanopore acted as a aperture for the ssDNA injection.

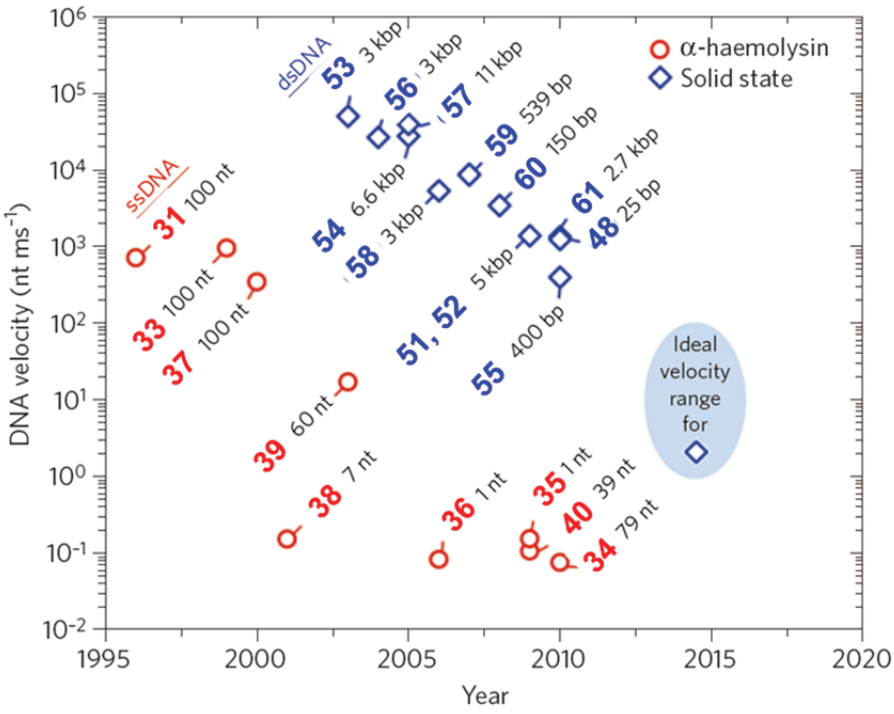

Figure 1-19. Speed of DNA translocation through nanopore device. Red circle remarks the reported value from α-hemolysin and blue diamond remarks the reported value from solid-state nanopore. The speed control methods could be categorized; using hairpin or local structure of ssDNA[33,34,38,40], viscosity control of electrolyte[37,58], lowered applied bias[39,48,54], asymmetric salt gradient[55], restricted structure of nanopore[35,36,61], and charge of surface materials[51,52,56,57,59,60].

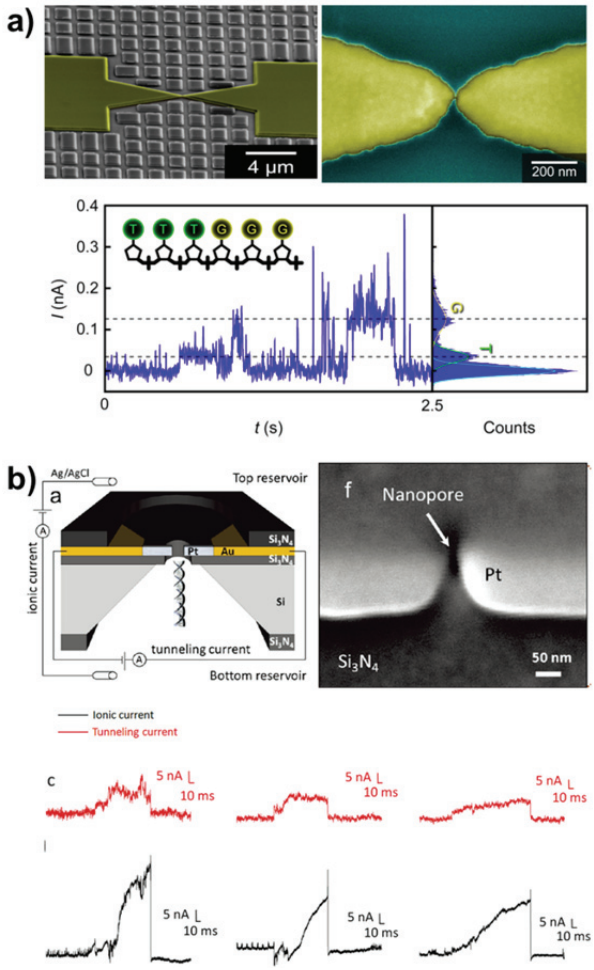

Figure 1-20. DNA sequencing using a tunneling electrode embedded nanopore device. **a)** Au electrode fabrication with nanopore structure and the discrimination of TTTGGG ssDNA[75]. **b)** Pt tunneling electrode with nanopore structure by using focused ion beam. And the correlation between the ionic current through the nanopore and the tunneling current through the tunneling electrode[76].

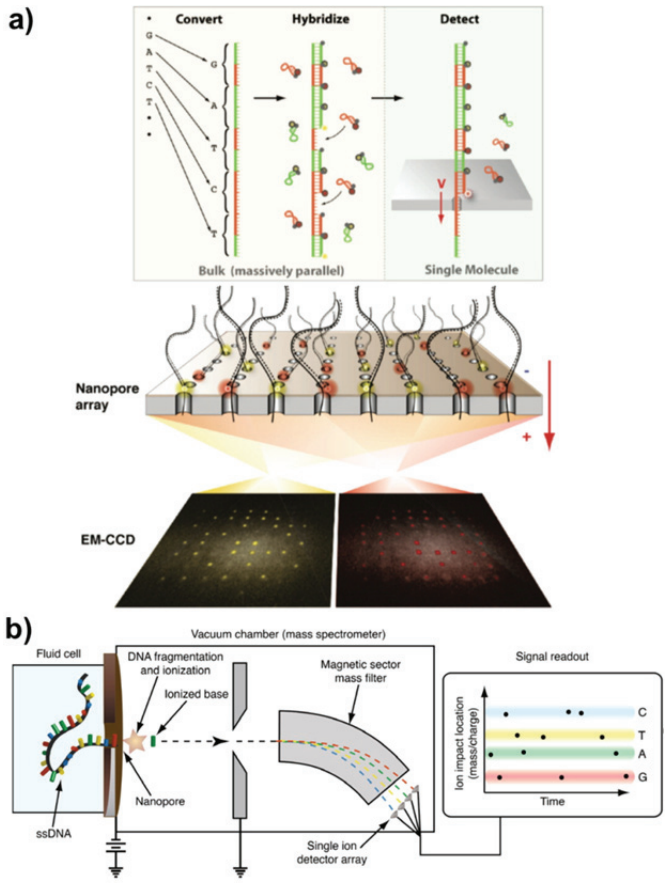

Figure 1-21. Candidate DNA sequencing method using nanopore excepting the electrical readout (blockade current and tunneling current). **a)** Optical readout using multiple nanopore array and unzipping of dsDNA which has fluorescence dye[78]. **b)** Single nucleotide detection and determination by using mass spectroscopy. Nanopore is used to scissoring a single nucleotide from ssDNA strand[79].

1.2.4. Overview of nanopore technologies

In Figure 1-11, the limitations and issues of nanopore technology in each area are summarized. The considered parts are sectioned with fabrication methods, measurement technologies, analysis algorithms, target molecules, and simulation approaches. In fabrication methods, the biological nanopores require the biological engineering such as mutation techniques and the improved mechanical stability for increasing lift-time. The solid-state nanopore should secure the reproducibility and stability of pore size and structure. Also, optimized structure for DNA sequencing should be studied. In addition, hybrid nanopore device can be acquired the advantages of biological and solid-state nanopore. However, it required the permanent attaching technique between solid-state nanopore and protein nanopore. And, more intensive study will be needed.

For the measurement technology, the control techniques of single molecule movement are key issues in nanopore application. For these purposes, many method have tried such as surface charge modification, optical tweezer, control the applied bias, viscosity of electrolyte, using enzyme, and so on. The reading method is usually used by measurement of blockade current, but the tunneling current measurement and optical detection also tried to massive parallel reading. Also, noise minimizing to

distinguish the nucleotide type and bandwidth increasing over 1 MHz should be required for improvement of time resolution and current resolution.

Thus far, the DNA is intensively studied in nanopore area for DNA sequencing and DNA sensing. Recently, RNA is focused as target molecule of nanopore technology, because the RNA is key factor of gene expression. Furthermore, using the advantage of nanopore method; the small volume of target molecule could be detected without amplification process, the protein is highly attractive target for the nanopore technology. Also, other molecules should be analyzed by nanopore.

On the other hand, the analysis technique and the simulation technique related to nanopore are intensively studied by algorithm development. These improvement will help to realize of DNA sequencing by nanopore device.

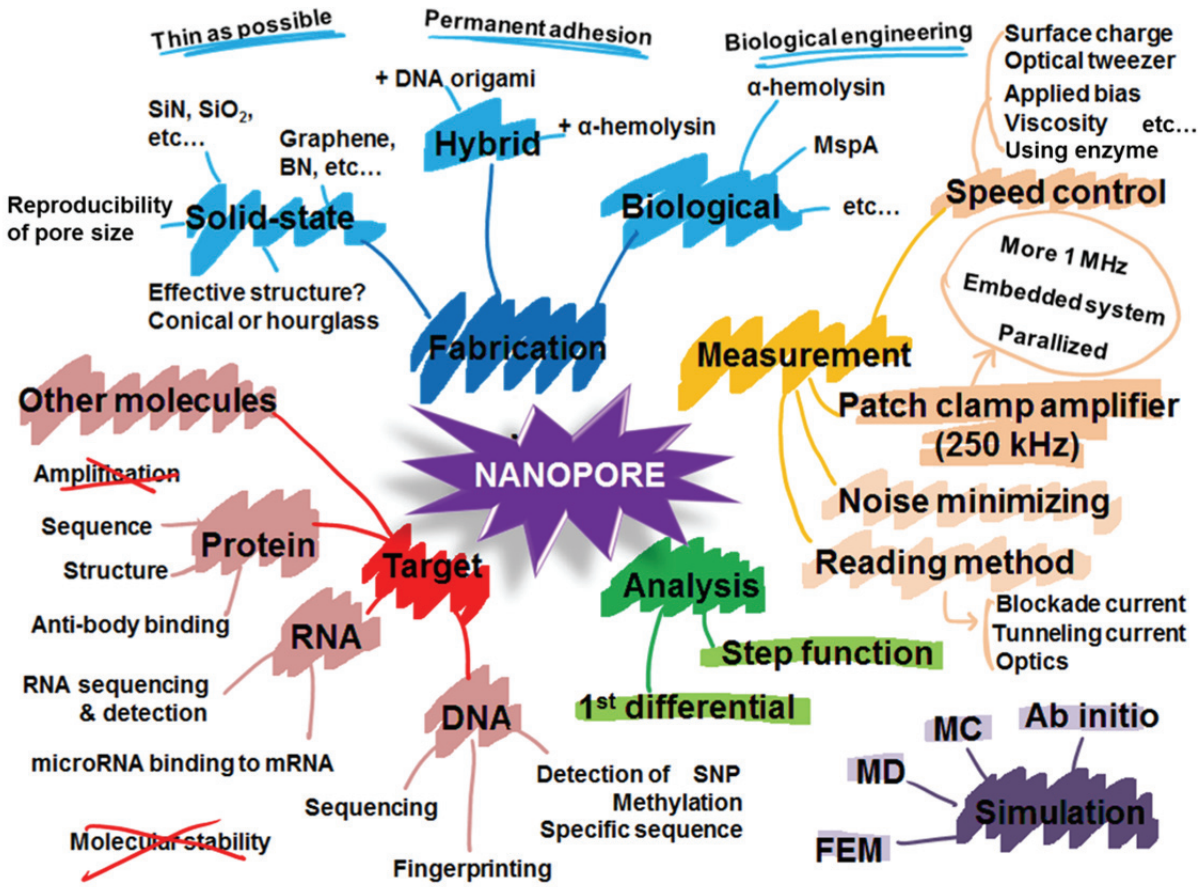

Figure 1-22. Overview of nanopore technologies categorized with fabrication, measurement, target molecules, analysis, and simulation.

1.3. Outline of dissertation

This dissertation describes the research results about the ionic current noise issues of the solid-state nanopore device.

Chapter 1 provides a general review on the DNA and DNA sequencing technologies. In addition, the nanopore technologies as one of the candidate of 3rd generation DNA sequencing method are described.

In chapter 2, the leakage current and its origin of Si substrate based solid-state nanopore are studied as one of candidate factor of high ionic current noise of Si substrate based solid-state nanopore device. Also, the dielectric passivation methods are proposed as the reduction method of ionic current noise as well as leakage current.

In chapter 3, we propose a novel type and fabrication method for the sub-10 pA RMS noise solid-state nanopore based on the insulating substrate. Moreover, the nucleotide type discrimination is presented by using 1.3 nm diameter and 5 nm thick nanopore.

In chapter 4, the surface charge effect on the ionic conductance of nanopore is studied by analytically and experimentally. For the analytically studied, the electrical potential distribution and the charge distribution are simulated by MATLAB and COMSOL and converted to ionic conductance. Furthermore, this effect is comparison with experimental result with different composed material of nanopore device.

Finally, in chapter 5, we summarize the origin and the reduction method of ionic current noise of solid-state nanopore and the first discrimination of each nucleotide type using insulating substrate based solid-state nanopore. Also, the surface charge effect in the nanopore device shows the advantage of high surface charge materials as nanopore structure with their preliminary result and challenging research topics.

References

[1] W. K. Purves, S. Sadava, G. H. Orians, H. C Hellerr, Life: The Science of Biology, 7ed, Sinauer Associates, 2003

[2] http://en.wikipedia.org/wiki/DNA, 10Jun. 2012

[3] R. Wu, E. Taylor, 1971, *J. Mol. Biol.* **57**, 491

[4] W. Gilbert, A. M. Maxam, 1973 *Proc. Natl. Acad. Sci. U. S. A.* **70**, 3581

[5] A. M. Maxam, W. Gilbert, 1977, *Proc. Natl. Acad. Sci. U. S. A.* **74**, 560

[6] F. Sanger, A. R. Coulson, 1975, *J. Mol. Biol.* **94**, 441

[7] F. Sanger, 1975, *Proc. R. Soc. Lond. B. Biol. Sci.* **191**, 317

[8] F. Sanger, S. Nicklen, A. R. Coulson, 1977, *Proc. Natl. Acad. U. S. A.* **74**, 5463

[9] J. Shendure, R. D. Mitra, C. Varma, G. M. Church, 2004, *Nat. Rev. Genet.* **5**, 335

[10] M. L. Metzker, 2005, *Genome Res.* **15**, 1767

[11] S. Tabor, C. C. Richardson, 1995, *Proc. Natl. Acad. Sci. U. S. A.* **92**, 6339

[12] M. R. Atkinson, M. P. Deutscher, A. Kornberg, A. F. Russell, J. G. Moffatt, 1969, *Biochemistry* **8**, 4897

[13] M .A. Innis, K. B. Myambo, D. H. Gelfand, M. A. Brow, M. A., 1988, *Proc. Natl. Acad. Sci. U. S. A.* **85**, 9436

[14] V. Derbyshire, P. S. Freemont, M. R. Sanderson, L. Beese, J. M. Friedman, C. M. Joyce, T. A. Steitz, 1988, *Science* **240**, 199

[15] S. Tabor, C. C. Richardson, 1989, *J. Biol. Chem.* **264**, 6447

[16] L. M. Smith, J. Z. Sanders, R. J. Kaiser, P. Hughes, C. Dodd, C. R. Connell, C. Heiner, S. B. Kent, L. E. Hood, 1986, *Nature* **321**, 674

[17] http://www.illumina.com/technology/solexa_technology.ilmn, 10Jun. 2012

[18] M. Ronaghi, S. Karamohamed, B. Pettersson, M. Uhlen, P. Nyren, 1996, *Anal. Biochem.* **242**, 84

[19] P. Nyren, 1987, *Anal. Biochem.* **167**, 235

[20] http://www.iontorrent.com, 10Jun. 2012

[21] N. Pourmand, M. Karhanek, H. H. J. Persson, C. D. Webb, T. H. Lee, A. Zahradnikova, R. W. Davis, 2006, *Proc, Natl. Acad. Sci. U. S. A.* **103**, 6466

[22] J. Korlach, P. J. Marks, R. L. Cicero, J. J. Gray, D. L. Murphy, D. B. Roitman, T. T. Pham, G. A. Otto, M. Foquet, S. W. Turner, 2008, *Proc. Natl. Acad. Sci. U. S. A.* **105**, 1176

[23] J. Eid, *et al.*, 2009, Science **323**, 133

[24] http://www.pacificbiosciences.com/products/smrt-technology, 10Jun. 2012

[25] http://www.genome.gov/sequencingcosts, 10Jun. 2012

[26] E.Y. Chan *et al.*, 2005, *Mutat. Res.* **573**, 13

[27] http://genome.wellcome.ac.uk, 10Jun. 2012

[28] P. K. Gupta, 2008, *Trends in Biotechhnol.* **25**, 602

[29] E. Pennisi, 2012, *Science* **336**, 534

[30] G. Church, D. W. Deamer, D. Branton, R. Baldarelli, J. Kasianowicz, *U.S. Patent* 5,795,782, 17Mar. 1995

[31] J. J. Kasianowicz, E. Brandin, D. Branton, D. W. Deamer, 1996, *Proc. Natl. Acad. Sci. U. S. A.* **93**, 13770

[32] L. Song, M. R. Hobaugh, C. Shustak, S. Cheley, H. Bayley, J. E. Gouaux, 1996, *Science* **274**, 1859

[33] M. Akeson, D. Branton, J. J. Kasianowicz, E. Brandin, D. W. Deamer, 1999, *Biophys. J.* **77**, 3227

[34] F. Olasagasti *et al.,* 2010, *Nature Nanotech.* **5**, 798

[35] J. Clarke *et al.*, 2009, *Nature Nanotech.* **4**, 265

[36] Y. Astier, O. Braha, H. Bayley, 2006, *J. Am. Chem. Soc.* **128**, 1705

[37] A. Meller, L. Nivon, E. Brandin, J. golovchenko, D. Branton, 2000*, Proc. Natl. Acad. Sci. U. S. A.* **97**, 1079

[38] S. Howorka,, S. Cheley, H. Bayley, 2001, *Nature Biotechnol.* **19**, 636

[39] M. Bates, M. Burns, A. Meller, 2003, *Biophys. J.* **84**, 2366

[40] V. Borsenberger, N. Mitchell, S. Howorka, 2009, *J. Am .Chem. Soc.* **131**, 7530

[41] G. M. Cherf, K. R. Lieberman, H. Rashid, C. E. Lam, K. Karplus, M. Akeson, 2012, *Nature Biotechnol.* **30**, 344

[42] T. Z. Butler, M. Pavlenok, I. M. Derrington, M. Niederweis,, J. H. Gundlach, 2008, *Proc. Natl. Acad. Sci. U. S. A.* **105**, 20647

[43]I. M. Derrington, T. Z. Butler, M. D. Collins, E. Manrao, M. Pavlenok, M. Niederweis, J. H. Gundlach, 2010, *Proc. Natl. Acad. Sci. U. S. A.* **107**, 16060

[44] E. A. Manrao, I. M. Derrington, M. Pavlenok, M. Niederweis, J. H. Gundlach, 2011, *PLoS ONE* **6**, e25723

[45] E. A. Manrao, I. M. Derrington, A. H. Laszlo, K. W. Langford, M. K. Hopper, N Gillgren, M. Pavlenok, M. Nirderweis, J. H. Gundlach, 2012, *Nature Biotechnol.* **30**, 349

[46] J. Li, *et al.*, 2001, *Nature* **412**, 166

[47] A. J. Storm, J. H. Chen, X. S. Ling, H. W. Zandbergen, C. Dekker, 2003, *Nature Meter.* **2**, 537

[48] M. Wanunu, *et al.*, 2010, *Nature Nanotechnol.* **5**, 807

[49] R. M. M. Smeets, *et al.*, 2006, *Nano Lett.* **6**, 89

[50] M. J. Kim, M. Wanunu, D. C. Bell, A. Meller, 2006, *Adv. Mater.* **18**, 3149

[51] B. M. Venkatesan, *et al.*, 2009, *Adv. Mater.* **21**, 2771

[52] B. M. Venkatesan, A. B. Shahm J. M. Zuo, R. Bashir, 2010, *Adv. Funct. Mater.* **20**, 1266

[53] J. Li, M. Gershow, D. Stein, E. Brandin, J. A. Golovchenko, 2003, *Nature Meter.* **2**, 611

[54] A. J. Storm, *et al.*, 2005, *Nano Lett.* **5**, 1193

[55] M. Wanunu, W. Morrison, Y. Rabin, A. Y. Grosberg, A. Meller, 2010, *Nature Nanotechnol.* **5**, 160

[56] P. Chen, *et al.*, 2004, *Nano Lett.* **4**, 2293

[57] A. J. Storm, J. H. Chen, H. W. Zandbergen, C. Dekker, 2005, *Phys. Rev. E* **71**, 051903

[58] D. Fologea, J. Uplinger, B. Thomas, D. S. McNabb, J. Li, 2005, *Nano Lett.* **5**, 1734

[59] Y. R. Kim, *et al.*, 2007, *Biosensors Bioelectron.* **22**, 2926

[60] M. Wanunu, J. Sutin, B. McNally, A. Chow, A. Meller, 2008, *Biophys, J.* **95**, 4716

[61] Z. Chen, *et al.*, 2010, *Nature Mater.* **9**, 667

[62] S. W. Nam, M. J. Rooks, K.-B. Kim, S. M. Rossnagel, 2009, *Nano Lett.* **9**, 2044

[63] M. D. Fischbein, M. Drndic, 2008, *Appl. Phys. Lett.* **93**, 113107

[64] C. A. Merchant, *et al.*, 2010, *Nano Lett.* **10** 2915

[65] G. Garaj, *et al.*, *Nature* **467**, 190

[66] G. F. Schneider, *et al.*, *Nano Lett.* **10**, 3163

[67] G. M. Skinner, M. van den Hout, O. broekmans, C. Dekker, N. H. Dekker, 2009, *Nano Lett.* **9**, 2953

[68] A. Singer, *et al.*, 2010, *Nano Lett.* **10**, 738

[69] R. M. M. Smeets, S. W. Kowalczyk, A. R. Hall, N. H. Dekker, C. Dekker, 2009, *Nano Lett.* **22**, 454121

[70] S. W. Kowalczyk, A. R. Hall, C. Dekker, 2010, *Nano Lett.* **10**, 324

[71] S. W. Kowalczyk, *et al.*, 2011, *Nature Nanotechnol.* **6**, 433

[72] A. R. Hall, *et al.*, 2010, *Nature Nanotechnol.* **5**, 874

[73] R. Wei, V. Gatterdam, R. Wieneke, T. Rampe, U. Rant, 2012, *Nature Nanotechnol.* **7**, 257

[74] D. Stoddart, *et al.*, 2009, *Proc. Natl. Acad. Sci. U. S. A.* **106**, 7702

[75] A. P. Ivanov, E. Instuli, C. M. McGilvery, G. Baldwin, D. W. McComb, T. Albrecht, J. B. Edel, 2011, *Nano Lett.* **11**, 279

[76] M. Tsutsui, S. Rahong, Y. Iizumi, T. Okiazaki, M. Taniguchi, T. Kawai, 2011, *Scientific Reports* **1**, 46

[77] G. V. Soni, *et al.*,2010, *Rev. Sci. Instrum.* **81**, 014301

[78] B. McNally, *et al.*, 2010, *Nano Lett.* **10**, 2237

[79] M. Wanunu, 2012, *Phys. Life Rev.* **9**, 125

[80] H.-M. Kim, M.-H. Lee, K.-B. Kim, 2011, *Nanotechnol.* **22**, 275303

CHAPTER 2.

Leakage Current in a Si Based Nanopore Structure and Its Influence on Noise Characteristics

2.1. Introduction

Solid-state nanopore structure has been actively investigated for the manipulation and detection of biomolecules in aqueous solutions, such as DNA, RNA, and proteins as well as ions and charged nanoparticles[1-5]. Most notably, this structure has been suggested as a basic tool for a rapid detection of DNA molecule and, ultimately, for the rapid sequencing of its bases without the time-consuming polymerase chain reaction (PCR) intermediate process[1-3]. While the solid-state nanopore structure has certain advantages compared with the biological protein nanopore, such as α-hemolysin or MspA, in the aspect of its long-term stability and capability to be integrated in an integrated circuit for the electrical manipulation and detection[4-8], there still remain several fundamental barriers precluding the use of this structure as a rapid DNA sequencer. These fundamental barriers include the relatively higher translocation speed and the longer channel length of the solid-state nanopore structures[3,9,10].

Another notable phenomenon observed in a solid-state nanopore structure is its higher noise level in measured ionic current as compared to that in protein nanopores[11-14]. The noise level measured from a biological protein nanopore inserted in a lipid bilayer is typically in the 10 pA RMS. On

the contrary, in a solid-state structure, the measured noise level approaches typically a few hundred pA. This higher noise level has been one of the major limitations to realizing a single base-level detection of DNA since the expected ion current signal, still arguably, for the base-level detection would be in the level of tens of pA. For instance, successful base-level detection was reported recently in a biological nanopore structure with the noise level of 10 pA RMS[15,16].

Indeed, various attempts have been made to identify the origin of this high level of noise in a solid-state nanopore structure and to reduce it[11,12]. In general, two types of noise signal are reported from the current power spectral density; one is Johnson noise, which appears at high frequency, and the other is Flicker noise, which appears at low frequency. Johnson noise, appearing at high frequency, is understood to be the result of thermal fluctuation of charged particles; while the Flicker noise appearing at low frequency can be explained by the generation and recombination reaction of charged particles via the impurities in the conductive channel[11-14]. It appears that there is not that much difference in the Johnson noise between the biological and solid-state nanopore[11]. For instance, Smeets *et al.* stated that it is closely related with the measurement system[13]. However, much difference exists in the Flicker noise, indicating that there is another source of noise in

the solid-state nanopore that is different from the biological nanopore structure. Although the exact source of noise was not revealed, few reports claimed that the Flicker noise in the solid-state nanopore structure can be drastically reduced either by depositing an Al_2O_3 insulating layer by atomic layer deposition (ALD)[12] or by coating a layer of polydimethylsiloxane (PDMS) on top of the membrane[11]. Using this method, the noise power spectrum density at 1 Hz was reported to be reduced by 100~1,000 times.

2.2. Experimental details

A Si-based nanopore structure was fabricated on a free-standing silicon nitride membrane deposited on double-side polished Si substrate with a thickness of 500 μm and ~10^{16}/cm^3 B-doping. For the Si_3N_4 membrane, low-stress silicon nitride with a thickness of 20 nm was deposited by low pressure chemical vapor deposition (LPCVD) on both sides of a Si wafer (27 Å/min at 825 °C, 30 sccm SiH_2Cl_2, 5 sccm NH_3, and 150 mTorr). Additionally, a 300 nm thickness of silicon nitride was deposited by plasma enhanced chemical vapor deposition (PECVD) on the back side of the Si substrate as a potassium hydroxide (KOH) etch mask (100 Å/min at 300 °C, 800 sccm 5% SiH_4/N_2, 10 sccm NH_3, 1200 sccm N_2, 580 mTorr, and 20 W 13.56 MHz / 187 kHz RF plasma with 6:1 ratio, sequentially). The back side nitride layer was patterned by photolithography and reactive ion etched with 10 mm by 10 mm square dies. Wet etching by KOH was performed to create a silicon nitride membrane with 50 μm × 50 μm size. This structure is used as a base sample for the Si based nanopore device.

In order to form a dielectric layer, we used a dry oxidation, ALD, and PECVD, respectively. Dry oxidation was done in a furnace with 5.0 slpm N_2 and 0.5 slpm O_2 at 900 °C and the thickness of the SiO_2 was determined by

Nanospec. Al_2O_3 was deposited by ALD with 1.2Å/cycle growth rate with a sequence of trimethyl aluminum (TMA) 1 sec., N_2 purging 5 sec., H_2O 1 sec., and N_2 purging 5 sec. at 200 °C. PECVD SiO_2 was deposited with a 30 nm/min growth rate by 160 sccm 5% SiH_4/N_2, 1500 sccm N_2O, 240 sccm N_2, at 550 mTorr condition with 187 kHz RF plasma, at 300 °C. Nanopores were perforated using focused electron beam in a 200 kV transmission electron microscope (TEM, JEOL 2010F).

In order to measure the ionic current though the nanopore, we used Ag/AgCl electrode in both cis- and trans-chamber at 1M KCl solution. The contact area between Si based nanopore and electrolyte is about 5 mm^2 in both chambers. The ionic current was measured using either a parameter analyzer (Agilent 4156C) or the patch clamp amplifier (Axopatch 200B), or both for certain samples.

2.3. Results and Discussion

2.3.1. Electrical behavior of Si based nanopore and its leakage current

After the fabrication of Si-based nanopore membrane samples, we have measured ion current through the nanopore utilizing two different types of measurement systems; one using a parameter analyzer and the other one using a patch clamp amplifier. The former one measures static (absolute) current and is commonly used to assess silicon based electronic devices. In contrast, the patch clamp analyzer measures the relative (differential) current and is commonly used to measure ionic current through the nanopore to monitor the translocation of DNA as well as other biomolecule translocation because of its higher bandwidth.

While it is not common to measure the ionic current by utilizing these two different systems in the same nanopore structure and thus has never been reported so far, as far as we are aware of, our measurement shows a drastic difference in the current-voltage (I-V) characteristics as is shown in Figure 2-1a. The conductance at 1 V with each measurement shows a similar value (~15 nS), but the I-V curve obtained from the parameter analyzer (solid line in Figure 2-1a) shows a hysteresis curve which does not go through the zero

point. On the contrary, the data from the patch clamp amplifier (dashed line in Figure 2-1a) goes through the zero point and does not show a hysteresis behavior. This difference is understood considering the characteristics of patch clamp amplifier measurement in which the current is controlled to go through zero point using the pipette offset adjustment. Consequently, the current at 0 V is not measured in the patch clamp amplifier system.

In order to understand the non-zero current level at 0 V bias and the appearance of the hysteresis curve in the parameter analyzer measurement, we hypothesize that electrochemical reactions are occurring from the solid state device which resulted in steady-state current generation through the Ag/AgCl electrodes. In order to confirm this hypothesis, we have measured the current from the device without nanopore perforation (Figure 2-1b). As expected, a few pA current is measured from the patch clamp amplifier. However, parameter analyzer shows that a constant level of current is flowing through the device. This result clearly shows that electrochemical reactions are occurring through the solid-state device.

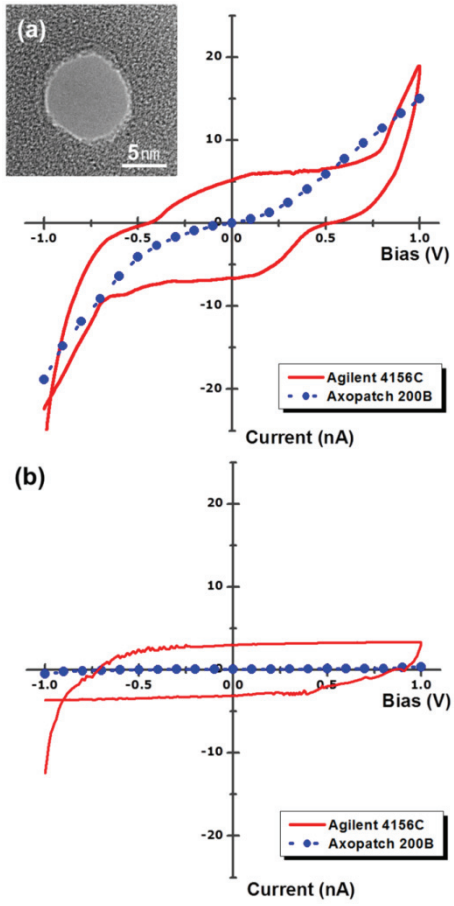

Figure 2-1. a) Current-voltage (I-V) characteristics of nanopore with 10 nm diameter and, **b)** I-V characteristic of membrane structure without nanopore at 1M KCl. The red solid line represents the I-V curve from Agilent 4156C system and the blue dash line is obtained from Axopatch 200B. (Inset) A TEM image of the nanopore in the Si_3N_4 membrane with 20 nm thickness is shown.

2.3.2. Electrochemical reaction of Si substrate and reduction method

In general, it is known that a protective surface layer of SiO_2 is rapidly formed when the Si surface is exposed in a water environment. However, this SiO_2 layer is also known to dissolve as several aqueous forms under the applied electrical potential[17]. Moreover, it is known that both oxidation and reduction reaction occurs at the exposed Si surface and causes ionic leakage current[18]. The standard electrochemical potential of Si is -0.857 V, thus, Si can be easily oxidized in water environment and passivated by the formation of a stable oxide film on the surface. However, the native SiO_2 covered Si surface is also known to react under applied bias with the following reactions[18].

$$\begin{aligned} Si + 2H_2O &= SiO_2 + 4H^+ + 4e^- \\ SiO_2 + H_2O &= H_2SiO_3\left(\text{soluble}\right) \\ Si + 3H_2O &= H_2SiO_3\left(\text{soluble}\right) + 4H^+ + 4e^- \end{aligned}$$

In order to confirm the electrochemical reaction of the exposed Si surface, we measured the current which flows through the bare Si wafer with a carbon plate as a counter electrode in pH 7 water (Figure 2-2a). Current measurement as a function of time was used to study electrochemical reaction through Si substrate. Here, bare Si substrate was cleaned with

diluted hydrofluoric (HF) to remove native SiO_2. The electrochemical current through native Si substrate shows about 400 nA/cm^2 at 1 V bias even up to 10 minutes. Obviously, this result shows that current is flown by an electrochemical reaction of the Si in an electrical field.

To reduce this current level, dielectric layers of thermal SiO_2, PECVD SiO_2, and ALD Al_2O_3, respectively, were deposited on the bare Si wafer and the current density was measured at 1 V (Figure 2-2b). The result clearly shows that all dielectric layers with a thickness over 10 nm effectively reduce the current level down to 50nA/cm^2. Again, this result shows that an electrochemical reaction occurs at an exposed Si surface, and that this reaction is somewhat prevented by the deposition of dielectric layer.

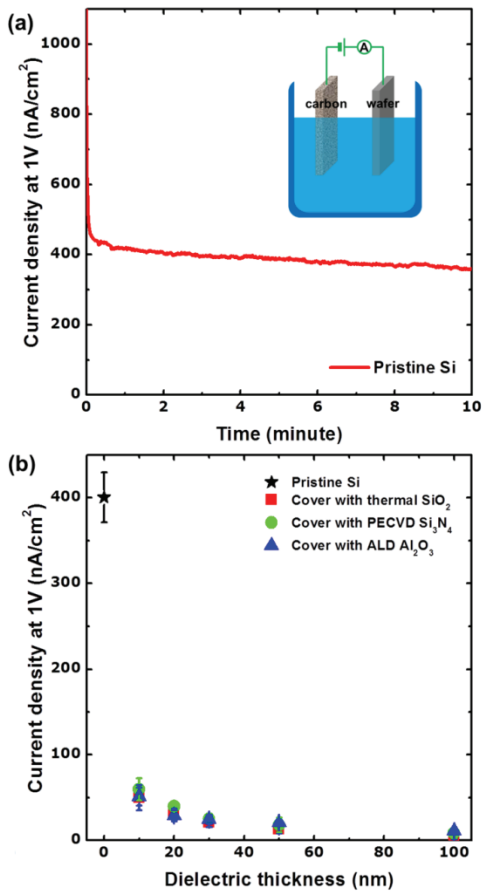

Figure 2-2. a) Electrochemical reaction current density at 1 V bias as a function of time on a bare Si wafer treated by diluted HF dipping for native SiO_2 etching. **b)** Electrochemical reaction current density at 1 V bias with various dielectric layers on a Si wafer. The red square, green circle, and blue triangle represent the Si silicon wafer covered on both side by thermal SiO_2, PECVD SiO_2, and ALD Al_2O_3, respectively. (Inset) A schematic diagram illustrates the measurement of the electrochemical reaction of the Si wafer.

2.3.3. Reduction of leakage current of Si based nanopore

Once we understood that the exposed Si substrate acts as a source of leakage current, and that it could be reduced by coating a dielectric layer, we have measured the leakage current from the various nanopore membrane structures, with and without dielectric coating, as is shown in Figure 2-3. Here, the leakage current is measured by using parameter analyzer on the samples without nanopore perforation. First, the Si-based nanopore structure with a 20 nm thickness of Si_3N_4 layer shows a leakage current level of 5 nA at 1 V. Apparently, current flows through a thin top nitride layer (exposed to the top cis-chamber) to the exposed Si layer (exposed to the bottom trans-chamber). A leakage current is decreased by coating the exposed Si layer with thermal oxide. However, one needs more than 50 nm thickness of oxide layer to reduce the leakage current below 100 pA level. The necessity of relatively thick thermal oxide layer to reduce the leakage current level strongly indicates that the quality of 20 nm thickness of Si_3N_4 layer is not good enough to prevent electrochemical reaction which is occurring at the top surface. It should be remembered that the interface area between Si_3N_4 and Si on the top surface of a membrane structure is much larger than the exposed Si area at the back side.

From the results in Figure 2-2b, we have learned that the leakage

current in the Si-based nanopore device can be decreased by the deposition of dielectric layer on the exposed Si surface. First, thermal oxidation is an effective way to coat the dielectric SiO_2 layer on an exposed Si surface. Thermal oxidation preserved the active membrane thickness because the oxidation only occurs at the exposed Si surface. Namely, the top Si_3N_4 layer is not thermally oxidized as is schematically shown in Figure 2-3b. The leakage current reduced to 100 pA with 50 nm thickness of thermal SiO_2, and finally to tens of pA with over 60 nm thickness of thermal SiO_2. We also prepared samples with PECVD SiO_2 deposited on the top side and ALD Al_2O_3 deposited on both sides of the sample as shown in Figure 2-3c, d, respectively. An ~20-nm-thick PECVD SiO_2 and ALD Al_2O_3 show the ~100 pA leakage current at 1 V, which is a comparable value to 50 nm thermal SiO_2. Dielectric coating on both sides by ALD Al_2O_3 shows the lowest leakage current at an overall range of dielectric thickness. However, it should be noted that the deposition of the dielectric layer on top of the nitride membrane will eventually increase the overall thickness of the membrane layer, which is detrimental in resolving each bases during the DNA translocation. Extending the observation, it is important that any exposed Si layer formed during the fabrication of the membrane structure should be passivated by a good quality of dielectric layer and the nitride membrane layer should also be a highly insulating one.

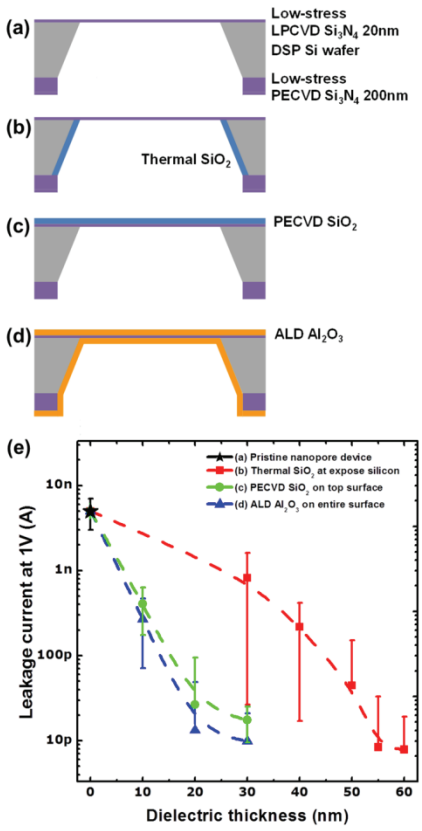

Figure 2-3. **a)** Schematics of the pristine nanopore device. The pristine device used a LPCVD Si_3N_4 membrane with 20 nm thickness and a PECVD 200-nm-thick Si_3N_4 hard mask on the back side. **b-d)** The schematics of the pristine device covered with dielectric layer of **b)** thermal SiO_2 grown at 900 °C, **c)** PECVD SiO_2 deposited on the top side, and **d)** ALD Al_2O_3 deposited on the entire surface. **e)** The leakage current at 1V with several types of pristine nanopore devices. Each curve corresponds to the device type of **a-d**.

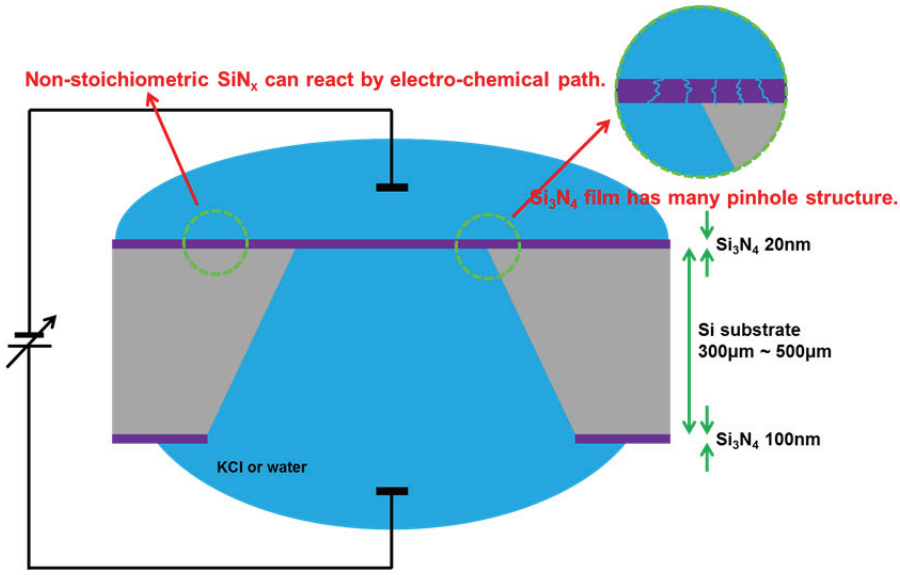

Figure 2-4. Expected mechanism of leakage current from Si based solid-state nanopore device. The pristine nanopore device has only 20 nm thick Si_3N_4 membrane. We expected that it has many pin-hole structures during KOH etching process or the chemical reaction could be occurred by its un-stoichiometric property.

2.3.4. Effect on an ionic current noise from reduced leakage current

The noise characteristic of nanopore devices has also been investigated in relation to the leakage current characteristic. In order to investigate it, we fabricated 10 nm diameter nanopore using focused electron beam on the structures shown in Figure 2-3a-d and the ionic current was monitored using a patch clamp amplifier. As an illustration, Figure 2-5a shows the recorded ionic current at 0 V bias through the 10-nm-diameter nanopore with the increase of thermal SiO_2 thickness from 0 nm to 60 nm. To evaluate the noise properties, we used an amplitude and RMS noise of ionic current. The amplitude of ionic current was achieved from the maximum value of the measured data and the RMS noise of ionic current was calculated from the recorded ionic current. The nanopore device on the 20 nm thickness of Si_3N_4 membrane showed that the amplitude and RMS noise of the ionic current is ~100 pA and ~36 pA, respectively. The noise continuously decreases with the increase of the dielectric layer thickness and reached up to ~75 pA amplitude and ~27 pA RMS. Figure 2-5b summarizes the RMS noise of ionic current in the devices shown in

Figure 2-3a-d as a function of dielectric layer thickness. The RMS noise of the ionic current showed a similar trend to the leakage current shown in Figure 2-3e. This result clearly indicates that there is a close correlation between the leakage current and the noise level.

Figure 2-5c shows the power spectrum analysis of the noise characteristics of the devices. This result shows that the frequency independence noise (mainly, Johnson noise) of our nanopore devices has almost the same values at high frequency regime (> 1 kHz) which is known to be associated with the capacitance of the whole measurement system circuit[11,13]. In order to check the effect of capacitance, we have calculated the total capacitance of the bare Si substrate and the samples with different dielectric coating in Table 1. Except the case of PDMS coated nanopore where the thickness of PDMS layer is close to 10 μm, dielectric coated nanopore had almost the identical capacitance value. Therefore, the effect of dielectric coating is minimal in reducing the Johnson noise which appears at high frequency.

On the contrary, it is noted that the low frequency noise of our pristine nanopores and a dielectric coated nanopore reveals that, even though the amplitude of the Flicker noise varies from pore to pore, the low frequency noise was generally decreased as the leakage current level is decreased. The

low frequency noise with $1/f^n$ characteristic has been well observed[11-13,20] and characterized[13,14] in nanopore structures. While the exact origin of $1/f^n$ noise is still unknown in nanopores, it was generally described by the charge fluctuation[12,19] either from the number[21] or mobility[22] of the conducting charge. It can be hypothesize that the existence of a leakage current path raised the unexpected charge conductance by electrochemical reaction.

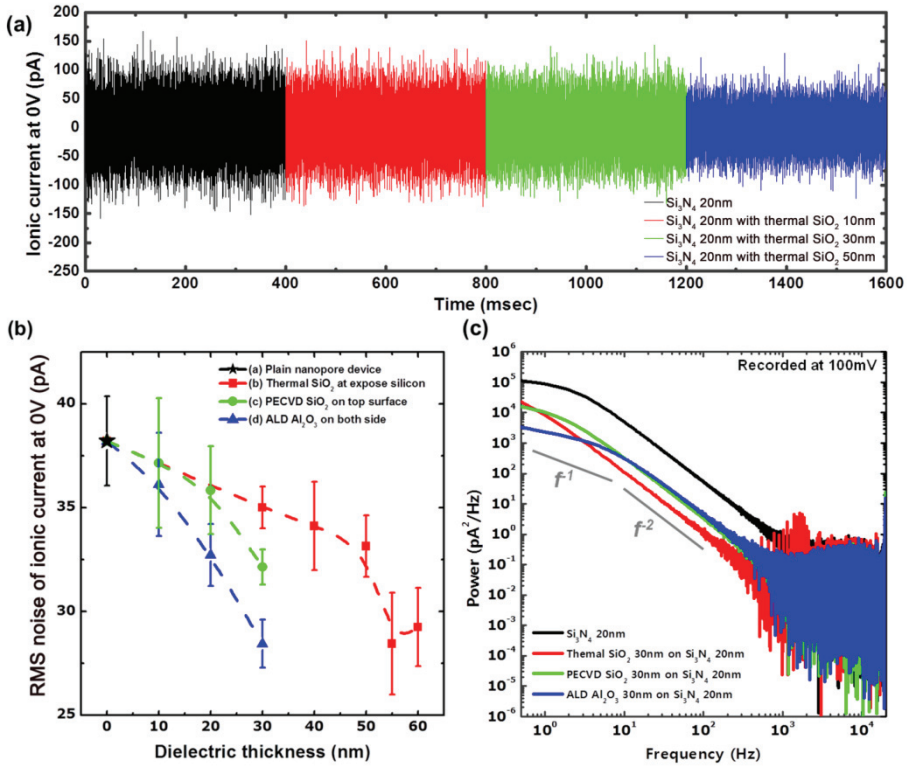

Figure 2-5. **a)** Ionic current as a function of time on thermal SiO_2 covered nanopore device with thickness variation. The black, red, green, and blue line represent the thermal SiO_2 thickness at 0 nm, 10 nm, 30 nm, and 50 nm, respectively. **b)** RMS noise of ionic current with different dielectric materials and thicknesses. **c)** Current power spectral densities of dielectric covered nanopore device at 100 mV bias with the thermal SiO_2 30 nm, PECVD SiO_2 30 nm, ALD Al_2O_3 30 nm, which are represented as a red, green, and blue line, respectively. All ionic current was measured with 10 kHz low-pass Bessel filter.

2.4. Summary and Conclusions

In conclusion, by measuring the ionic leakage current using a parameter analyzer, we find that there is a high level of leakage current in the Si-based solid-state nanopore structure. This ionic leakage current is not commonly measured in patch clamp amplifier. Through a judicious experimental plan, we identified that this leakage current occurs as a result of the electrochemical reaction at the water/Si interfaces. Furthermore, we identified that this high leakage current level is closely related with the low frequency noise level in an ionic current. By depositing a thin dielectric layer, we can eliminate the source of leakage current, and therefore, can reduce the low frequency noise level.

References

[1] J. J. Kasianowicz, E. Brandin, D. Branton, D. W. Deamer, 1996, *Proc. Natl. Acad. Sci. U. S. A.* **93**, 13770

[2] D. Branton, D. W. Deamer, A. Marziali, H. Bayley, S. A. Benner, T. Butler, M. Di Ventra, S. Garaj, A. Hibbs, X. H. Huang, *et al.* 2008, *Nat. Biotechnol.* **26**, 1146

[3] B. M. Venkatesan, R. Bashir, 2011, *Nat. Nanotechnol.* **6**, 615

[4] A. J. Storm, J. H. Chen, X. S. Ling, H. W. Zandbergen, C. Dekker, 2003, *Nat. Mater.* **2**, 537

[5] J. Li, D. Stein, C. McMullan, D. Branton, M. J. Aziz, J. Golovchenko, 2001, *Nature*, **412**, 166

[6] S. Polonsky, S. Rossnagel, G. Stolovitzky, 2007, *Appl. Phys. Lett.* **91**, 153103

[7] S.-W. Nam, M. J. Rooks, K.-B. Kim, S. M. Rossnagel, 2009, *Nano Lett.* **9**, 2044

[8] M. Tsutsui, M. Taniguchi, K. Yokota, T. Kawai, 2010, *Nat. Nanotechnol.*

5, 286

[9] A. J. Storm, C. Storm, J. H. Chen, H. Zandbergen, J. F. Joanny, C. Dekker, 2005, *Nano Lett.* **5**, 1193

[10] M. Wanunu, T. Dadosh, V. Ray, J. M. Jin, L. McReynolds, M. Drndic, 2010, *Nat. Nanotechnol.* **5**, 807

[11] T.-C. Vincent, T. Dhruti, W. Matthew, N. J. Nahid, M. Andre, 2008, *Nanotechnol.* **18**, 305505

[12] P. Chen, T. Mitsui, D. B. Farmer, D. B. J. Golovchenko, R. G. Gordon, D. Branton, 2004, *Nano Lett.* 4, 1333

[13] R. M. M. Smeets, U. F. Keyser, N. H. Dekker, C. Dekker, 2008, *Proc. Natl. Acad. Sci. U. S. A.* **105**, 417

[14] R. M. M. Smeets, N. H. Dekker, C. Dekker, 2009, *Nanotechnol.* **20**, 2095501

[15] J. Clarke, H. C. Wu, L. Jayasinghe, A. Patel, S. Reid, S. H. Bayley, 2009, *Nat. Nanotechnol.* **4**, 265

[16] I. M. Derrington, T. Z. Butler, M. D. Collins, E. Manrao, M. Pavlenok, M. Niederweis, J. H. Gundlach, 2010, *Proc. Natl. Acad. Sci. U. S. A.* **107**,

16060

[17] Y.-J. Oh, D. Bottenus, C. F. Ivory, S. M. Han, 2009, *Lab on a Chip* **9**, 1609

[18] X. G. Zhang, Electrochemistry of Silicon and its Oxide. 2001, Kluwer Academic Publishers: New York

[19] F. Hooge, 1994, *IEEE Transactions on Electron Devices,* **41**, 1926

[20] Z. Siwy, A. Fulinski, 2002, *Phys. Rev. Lett.* **89**, 158101

[21] A. L. McWhorter, 1/f noise and related surface effects in Germanium. 1955, Ph.D. dissertation, MIT, Cambridge, MA

[22] F. Hooge, 1969, *Phys. Lett. A* **29**, 139

CHAPTER 3.

Single molecule transport through a dielectric substrate based solid-state nanopore

3.1. Introduction

Nanofluidic systems have attracted considerable interest for applications ranging from detection and analysis of single molecules including proteins, RNA, DNA, nano particle, and ion[1-3]. Nanopore platforms, one of the nanofluidic systems, have recently focused on single molecule analysis from a Coulter counter[4,5] and a structure examination to the DNA sequencing[6-11]. Most of DNA sequencing reports using nanopore system was rely on the biological nanopore based on α-hemolysin[6-8] and MspA[9-11]. The reason to make DNA sequencing possible still doesn't understand, but, the single nucleotide was distinguished by using a difference of blockade current in 100~200 mV bias with few pA resolution, shown in Table 3-1. However, the order of the nucleotides in each report was complicated by type of protein nanopore and direction of ssDNA. Nevertheless, DNA sequencing is almost realized in the protein nanopore with some restriction; a high error rate and a lifetime of device from mechanical stability.

In contrast, a solid-state nanopore also intensively studied for single molecule sensing as well as DNA sequencing with a robust characteristic of silicon nitride membrane[12-14]. However, the solid-state nanopore has many hurdles to the DNA sequencing; slowdown of translocation speed,

minimization of ionic current noise, uniformity of nanopore diameter with 1~1.5 nm, and minimization of a sensing zone thickness[3]. In these objectives, here are many progresses; sub-10 nm thickness Si_3N_4 membrane[15] and graphene nanopore[16-18] for minimization of sensing zone, dielectric (Al_2O_3[19], SiO_2[20], and so on) passivation and PDMS coating[21] for the minimization of ionic current noise.

However, the noise level of ionic current through the solid-state nanopore is still higher than one of the biological nanopore and a required noise level, < 10 pA RMS. In this work, we propose a novel structure and its fabrication method for an ultra-low-noise solid-state nanopore based on dielectric substrate. Decreasing the noise of ionic current provided the signal-to-noise ratio of biomolecules, while the identical structure and measurement system of nanopore. Furthermore, sub-2 nm diameter nanopore in 5 nm thickness Si_3N_4 membrane facilitate the detection of ssDNA with tens of based pairs, as well as the discrimination of type of nucleotide of homo nucleic acids. When ssDNA was translocated through the low-noise solid-state nanopore, homopolymer strands of adenine, cytosine, thymine, and guanine each produced a distinct, and current blockade could be distinguished in individual experiments. We also demonstrate the directly comparing the blockage currents of poly A, poly T, poly C, and poly G ssDNA, simultaneously in a same pore.

Type	$\Delta I_{block}(A)$ (pS)	$\Delta I_{block}(T)$ (pS)	$\Delta I_{block}(C)$ (pS)	$\Delta I_{block}(G)$ (pS)	I_{open} (pS)	Bias (mV)	Rank of ΔI_{block}	Min. ΔI (pS)	Ref.
α-hemolysin	778	805	790		958	120	T>C>A	12	5' lead [6]
	806	799	778		958	120	A>T>C	7	3' lead [6]
	805	808	814	802	1019	160	C>T>A>G	3	5' lead in WT [7]
	639	645	656	627	1050	160	C>T>A>G	6	5' lead in MT [7]
	139	144	111	167	300	180	G>T>A>C	5	single nt. [8]
MspA	1442	1573	1537	1476	1806	180	T>C>G>A	34	5' lead [9]
	1490	1627	1593	1534	1801	140	T>C>G>A	34	5' lead [9]
	1345	1500	1612	1606	1822	180	C>G>T>A	6	5' lead [10]
	1314	1546	1360	1263	1822	180	T>C>A>G	46	3' lead [10]
	367	489	385	428	611	180	T>G>C>A	18	5' lead [11]

Table 3-1. Blockade Conductance of each nucleotide through a protein nanopore. Blockade conductance of each nucleotide through an α-hemolysin and MspA protein nanopore and open conductance of nanopore with given (optimal) bias. Order of blockade conductance like those shown each blockade conductance had variety of each measurements and the required resolution to distinguish each nucleotide was bout few-tens of pS.

3.2. Experimental details

Dielectric substrate based nanopore were fabrication on 10 mm x 10 mm dielectric substrate. Especially, for the fabrication of SiO_2-related substrate (300-um-thick Pyrex substrate and 200-um-thick quartz substrate), 200-nm-thick a-Si was deposited on both side of Pyrex or quartz substrate by LPCVD, which was used as masking layer through the HF wet etching. Photo lithography was used to write an opening area. For the asymmetric micropore fabrication, 5 um x 5 um to 2 um x 2 um square entrance on top side was formed by 49 wt.% HF wet etching (5 min for Pyrex substrate, 20 min for quartz substrate) with photo lithography and a-Si RIE using SF_6 gas. Then, a protective film was coated on top side for the mechanical endurance and protection during followed HF wet etching. A 100 um x 100 um sized entrance was formed on bottom side using same method. Wet etching was operated to connect bottom chamber to top chamber, ~45 min for Pyrex substrate and ~100 min for quartz substrate. Finally, fabricated micropore had asymmetric hourglass shape and 50 um diameter circular membrane with 5 um x 5 um to 2 um x 2 um opening area on top side. After micropore fabrication, the protective layer was stripped out.

An active membrane was deposited on other substrate, we used a 500-

nm-thick Ni / 500-um-thick Si substrate in this work. Si_3N_4 layer was deposited with different thickness (5 nm, 10 nm, and 20 nm) on this substrate by using PECVD (13.56 MHz plasma with 1200 sccm N_2, 800 sccm 5% SiH_4/N_2, 10 sccm NH_3 at 580 mTorr, 60 watt, 300 ^oC). The transfer process began with spin coated PMMA (A 6, MicroChem) resist at 2500 rpm for 45 sec, making PMMA/Si_3N_4/Ni/Si structure. Ni film was dissolved in $FeCl_3$ solution in 30 min, and then PMMA/Si_3N_4 free standing membrane floated on solution. The membrane was carefully cleaned in D.I. water several times, we fish out the membrane onto the dielectric substrate which had a micropore. We let the sample dry at room temperature until the membrane was flat on the surface of dielectric substrate. Then finally dissolve the PMMA with acetone.

A nanopore were perforated and analyzed in a JEOL 2010F TEM with modified TEM holder. For adjustment of the pore shape and size, an electron beam current was controlled from 1 nA to 8 nA and a reduction method by using un-focused electron beam was used[27].

All nanopores was immersed into EtOH in several minutes before measurement, and all experiments were carried out using solution of 1 M KCl, 1 mM EDTA, 10 mM Tris-HCl with pH 8. The nanopore chip was installed between two buffered electrolytes with custom jig fabricated by using PDMS. In each electrolyte, Ag/AgCl electrodes equipped and

connected to patch clamp amplifier system. Ionic current, measured using an Axopatch 200B amplifier, was digitized at 250 kHz with 10 kHz 6-pole Bessel filter. For homopolymer nucleic acid analysis, we used poly A_{40}, poly T_{40}, poly C_{40}, and poly G_{40}, which purified by PAGE method and were stored at -20 ^{o}C until immediately before use. For experiments, 1 nM homopolymer in electrolyte was used at the *cis* chamber.

Data was collected by Clampex (MDS Analytical Tech.) and analyzed with Matlab (Mathworks). Translocation of DNA was first identified using current thresholds over than noise level with a base line correction. For each DNA strand type, data was taken on 1.3 nm diameter and 5 nm thick nanopore. The mean current values and standard deviation reported herein were determined by the peak value and the standard deviation of a Gaussian fitted to the histogram of mean residual currents for all experiments.

3.3. Results and Discussion

3.3.1. Noise characterization of dielectric substrate based nanopore and its origin

Figure 3-1a shows a schematic diagram of fabrication process. A micropore in SiO_2 substrate (Pyrex or quartz) was formed by photo lithography and HF wet etching process with asymmetric open area and etching time. Asymmetrical micropore was effective to make smaller membrane size and open area on top side that supplied the mechanical stability to a transferred membrane. The fabricated micropore in SiO_2 substrate was shown in Figure 3-1b and its size was 5 μm x 5 μm to 2 μm x 2 μm. The transferred membrane was formed on a sacrificial metal film at another substrate and detached by metal wet etching. After than the transferred to SiO_2 substrate by fishing method[22]. For the stability of transferred membrane, we used 300 nm thick PMMA as protective layer and it was etched out after transferring by using acetone. Si_3N_4 20 nm thick was firstly transferred to SiO_2 substrate and it was shown in Figure 3-1c. Figure 3-1d shows that the nanopore drilled by focused electron beam in transmission electron microscope (TEM) and its size has ~ 1.5 nm diameter.

Finally, the fabricated nanopore device had sub-10 nm diameter

nanopore with thickness variation (5 nm, 10 nm, and 20 nm) on 1cm x 1cm sized dielectric substrate. To electrical characterize the low-noise solid-state nanopore, the nanopore device was located on the PDMS jig. Electrolyte solution (1 M KCl, 1 mM EDTA, 10 mM Tris-HCl with pH 8.0) was added above and below the nanopore device, each contacted by a Ag/AgCl electrode, and voltage was applied to drive charged ions as well as biomolecules through the nanopore. Each Ag/AgCl electrode was connected to patch clamp amplifier system (Axopatch 200B, Axon Instrument, Inc.) and data was collected by using ADC (Digidata 1440A, MSD Analytical Technologies) and analyzed using pClamp (Molecular Devices), ClampFit (Molecular Devices), and MATLAB (Mathworks).

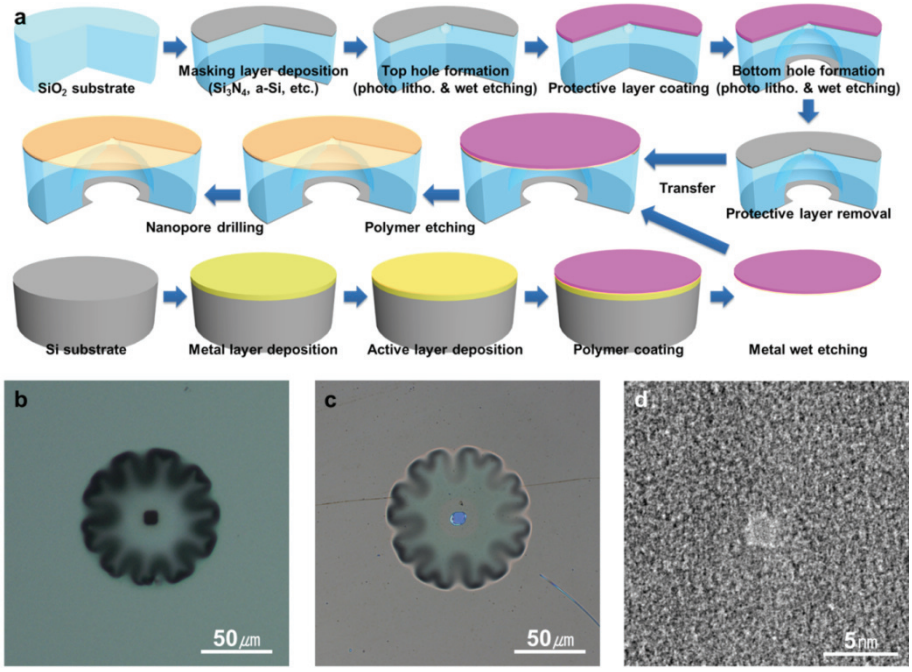

Figure 3-1. Dielectric substrate based nanopore. **a)** Process schematic diagram showing the device consisting of micro sized pore in dielectric substrate and few nm thickness free-standing membrane. The free-standing membrane was transferred to dielectric substrate by fishing method. **b)** Optical microscope image of micro pore in dielectric substrate before the membrane transfer and **c)** after the membrane transfer. **d)** TEM image of a 1.5nm diameter nanopore drilled by a highly focused electron beam in TEM.

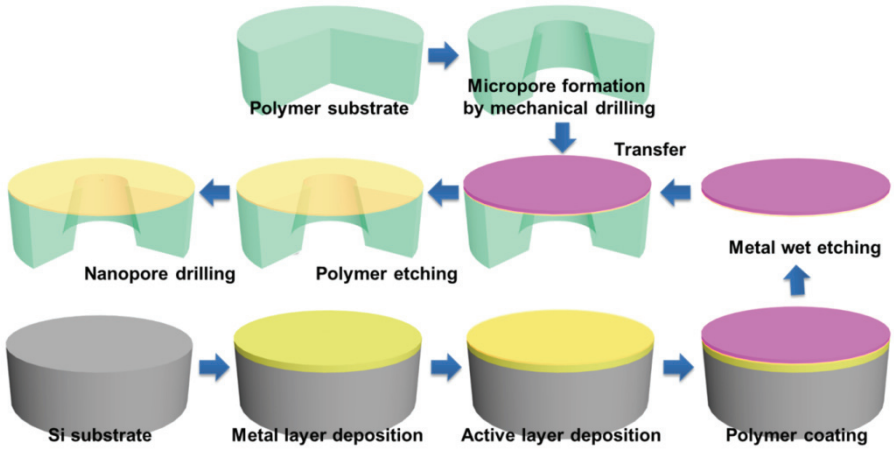

Figure 3-2. Process schematic diagram for the polymer substrate based nanopore. Only difference with SiO_2-related substrate based nanopore was a method for micropore fabrication such as a mechanical drilling (for Teflon, PDMS) or a drilling by using hot filament (for PET, PC). After the micropore drilling, transferring of active membrane and nanopore perforation were same to SiO_2-related substrate based nanopore (using a fishing method for active membrane transferring and a focused electron beam in TEM for nanopore drilling.)

3.3.2. Noise characterization of dielectric substrate based nanopore and its origin

Firstly, the noise characteristic of dielectric substrate based nanopore was studied in 20 nm thick Si_3N_4 membrane comparing with different structure device. The ironical current noise through solid-state nanopores was generally observed to be substantially higher than biological nanopores. Figure 3-3a shows typical current traces, for a Si_3N_4 20 nm on Si 500 μm substrate (red), a Si_3N_4 20 nm on SiO_2 200 nm and Si 500 μm substrate (green), and a Si_3N_4 20 nm on a-Si 200 nm and 200 μm quartz substrate, recorded with sub-10 nm diameter sized nanopore at a 250 kHz sampling rate with using an 10 kHz internal low-pass four-pole Bessel filter. Pristine Si_3N_4 nanopore on Si substrate had ~38 pA RMS ionic current noise. Dielectric material such as SiO_2 was inserted between Si_3N_4 and Si substrate to decrease a ionic current noise, ~ 29 pA RMS. However, this noise level still higher than biological nanopores and such higher noise will be critical for applications such as single-molecule sequencing and force spectroscopy for genotyping.

The two sources of noise when performing current measurement through nanopore dominated; a Johnson noise (or thermal noise or Nyquist noise) associated with a relatively high capacitance of the SiN_x membrane and Si

substrate in high frequency (>100 Hz)[23], and a Flicker noise related to a combination of noise source with $1/f^{\alpha}$ characteristics in low frequency (<100 Hz)[21,24]. The Johnson noise was represented as the thermally excited charge carriers or carrier fluctuation in the equivalent circuit with the nanopore resistor (R_p) and nanopore capacitance (C_p) resulting from the liquid contact to the nanopore chip containing the nanopore. The current power spectral density (S_I) determined by Jonson noise is given as,

$$S_I = |Y|^2 4k_B T Re(1/Y),\ Y = \omega C_p D \qquad \textbf{Equation 3-1.}$$

where, $k_B T$ is represented the thermal energy, Y is admittance of nanopore, ω is the frequency, and D is the dielectric loss constant. Generally, the Johnson noise was decreased with decrement of capacitance of nanopore device. On the other hand, the origin of Flicker noise was not fully understood, but, two different models were proposed in nanopore system, described namely surface trap model (based on surface charge fluctuation) and Hooge's mobility fluctuation model. From the R. M. M. Smeets *et al.* reports[24], it's clear that at higher concentration of KCl, the mobility fluctuation of charged ion was dominated on low frequency noise.

Our dielectric substrate based solid-state nanopore device showed the

sub-10 pA RMS noise in overall device. And the typical value was 5.3 pA RMS with 3.2 nm diameter nanopore which considered as an achievable lowest noise value to date and a comparable value to noise of protein nanopore (seen at Figure 3-3a, b). The noise characteristic of this device with whole frequency was shown in power spectral density plot at Figure 3-3b. It was clear that the noise was reduced as -30 dB than Si substrate based solid-state nanopore at the overall frequency. Quartz based patch pipettes have previously been shown to provide low ionic current noise in single-channel patch clamp measurements[25]. Similar at the nanopore system, the Si substrate could not be provided a gigaohm seal in the electrolyte because of its low resistivity (1~30 Ωcm, B doped). Also, a dielectric substrate based nanopore showed <100 pF capacitance and few hundreds Ω access resistance, which contribute to low access time. These values were a lower capacitance and higher access resistance than Si substrate based nanopore, few nF and ~10 Ω (more detailed in Figure 3-4). As a result, the lowest noise in dielectric substrate based nanopore was achieved by its lower capacitance and a gigaohm seal with its high resistivity (also, the noise characteristic with different 4-pole Bessel filter frequency was shown in Figure 3-5).

Additionally, we tested the other dielectric substrate based solid-state nanopore included as polymer substrate (PET, PDMS, Teflon, PC). Figure 3-3c shows the ionic current noise through Si_3N_4 20 nm thick membrane

dependent on the substrate type without nanopore. Ionic current noise was continuously decreased as thicker dielectric materials deposition on Si substrate, but, the noise still had ~20 pA RMS at 300 nm SiO_2 deposition. From this tendency, sub-10 pA RMS noise in Si substrate based solid-state nanopore was expected with over 500 nm thickness SiO_2 deposition. In different to Si substrate, the dielectric substrate based device shows the sub-10 pA RMS in all materials (power spectrum density was shown in Figure 3-6).

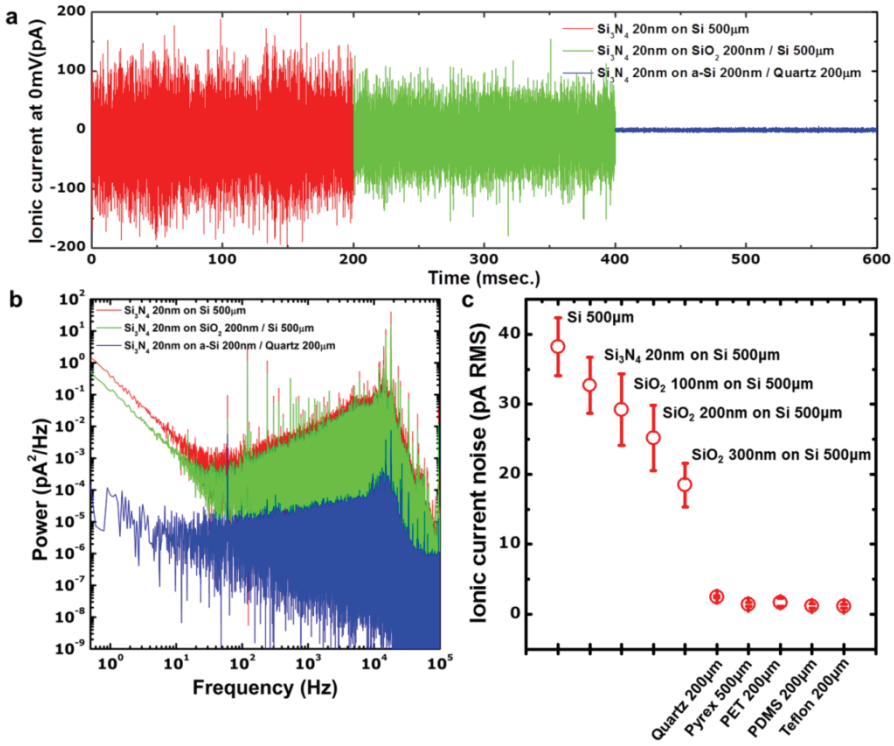

Figure 3-3. Ionic current noise in dielectric based nanopore. **a)** RMS ionic current noise with different structures at 0 mV applied bias; Si_3N_4 20 nm on Si 500 μm (red), Si_3N_4 20 nm on SiO_2 200 nm / Si 500 μm (green), and Si_3N_4 20 nm on a-Si 200 nm / quartz 200 μm (blue). **b)** Power spectrum of different structures from **a**. **c)** RMS ionic current noise through Si_3N_4 20 nm on various substrates without nanopore. Micro pore was fabricated by KOH etching in Si based substrate, by HF etching in SiO_2 based substrate (Pyrex, quartz, described in Figure 3-1), and by mechanical drilling in polymer based substrate (PET, PDMS, Teflon, more detailed in Figure 3-2).

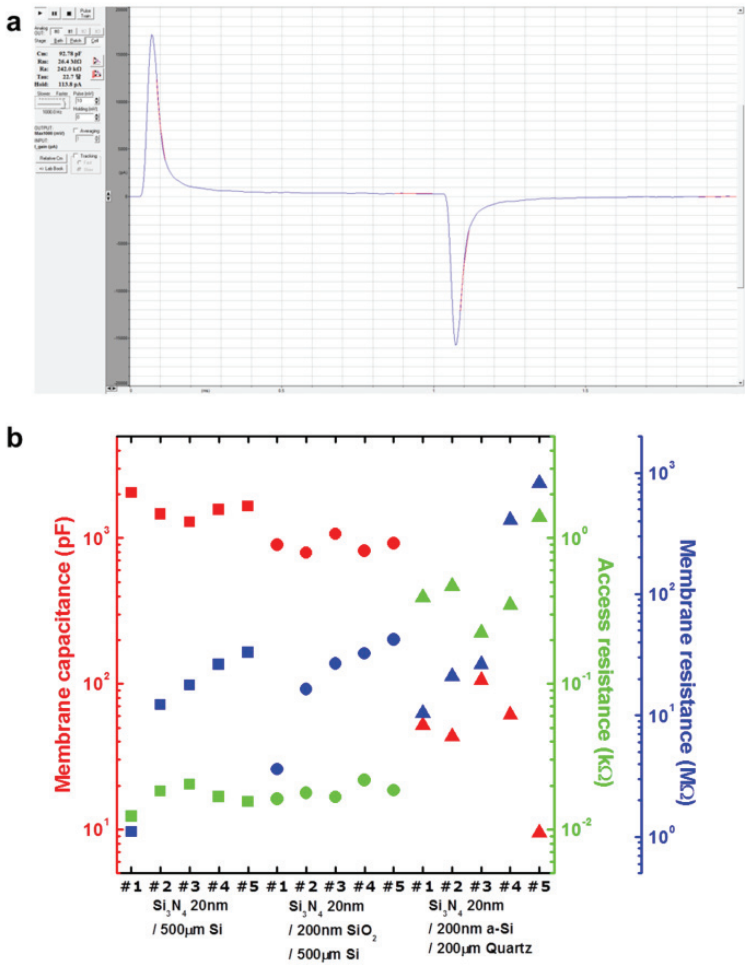

Figure 3-4. Relationship between membrane capacitance and nanopore resistance. **a)** Measurement methods for membrane capacitance and nanopore resistance by using "Membrane Test" mode in Clampex program (MDS Analytical Tech.) for Axopatch 200B. **b)** Membrane capacitance (red), access resistance (green), and membrane resistance (blue) as a function of device

type, Si_3N_4 20 nm on 500 μm Si substrate (square), Si_3N_4 20 nm on 200 nm SiO_2 / 500 μm Si substrate (circle), Si_3N_4 20 nm on 200 nm a-Si / 500 μm Si substrate (triangle). The nanopore conductance related to membrane resistance. And the access resistance was contributed from resistance from electrolyte and electrode. The RC time constant was calculated by multiply membrane capacitance by access resistance. Dielectric substrate based solid-state nanopore shows the lower membrane capacitance and higher access resistance. However, the decrement of membrane capacitance was higher than the increment of access resistance, therefore the RC time constant slightly decreased in dielectric substrate based solid-state nanopore. Also, the decreasing of membrane capacitance had effect on the lowering of ionic current noise.

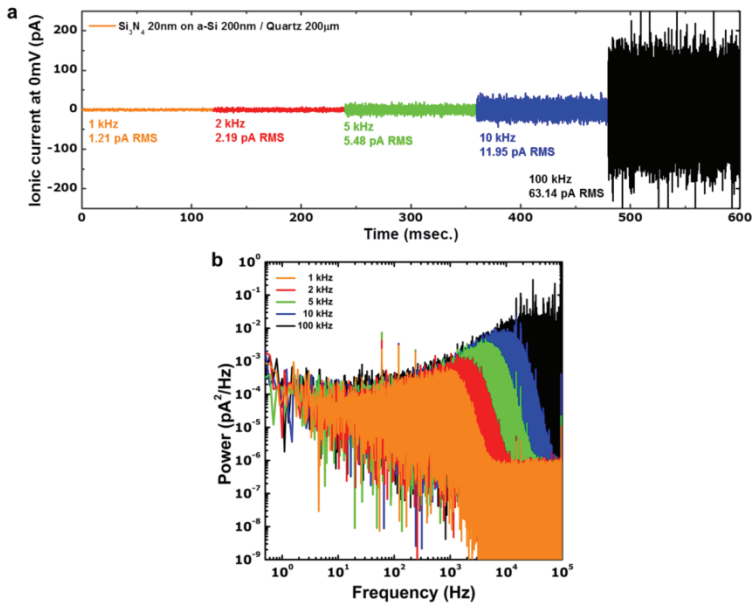

Figure 3-5. Ionic current noise as a function of 6-pole Bessel filter mode. **a)** Ionic current versus time trace of variation of 6-pole Bessel filter mode, 1 kHz (orange), 2 kHz (red), 5 kHz (green), 10 kHz (blue), and 100 kHz (black) which hardware filtering in Axopatch 200B. The dielectric substrate based nanopore showed the ~10 pA RMS at 10 kHz filtering, and this value closed or surpassed to the ionic current noise of biological nanopore. Also, this nanopore showed 63.14 pA RMS at 100 kHz filtering, which smaller than Si substrate based nanopore at 10 kHz filtering (~100 pA RMS). **b)** Power spectrum of different 6-pole Bessel filtering, shown in Figure 3-5a. Johnson noise was increased in high frequency (>10 Hz) and it was reached from 10^{-4} pA^2/Hz at 10 Hz to 10^{-2} pA^2/Hz at 10^4 Hz. When the bandwidth exceeded to frequency of 6-pole Bessel filter, the power spectrum stiffly decreased to 10^{-6} pA^2/Hz.

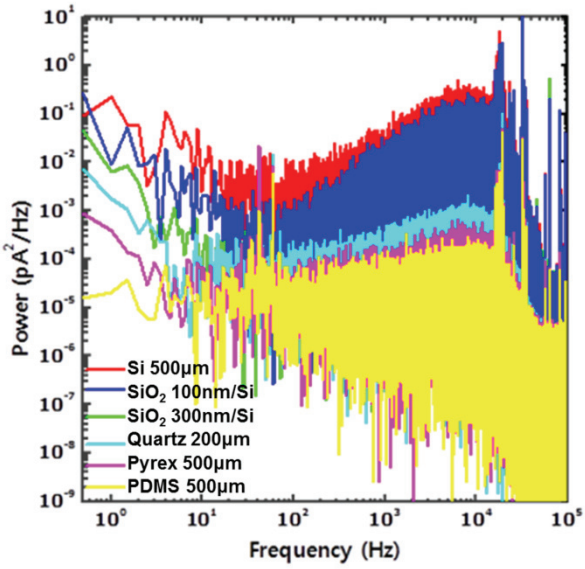

Figure 3-6. Power spectrum of Si_3N_4 20 nm on various substrates. As described in Figure 3-1 and Figure 3-2, the active membrane (Si_3N_4 20-nm-thick) was fabricated by KOH etching in Si substrate based nanopores, HF etching and transferring in SiO_2-related substrate based nanopores, and mechanical drilling and transferring in polymer substrate based nanopore. Si substrate based nanopores were shown higher power spectrum in high frequency (> 10^2 Hz) than others. Also, SiO_2-related nanopores and polymer based nanopores showed the ~10^{-4} pA^2/Hz power spectrum in almost frequency. Other polymer based nanopore (PET, PC, Teflon) was similar power spectrum with results of PDMS.

3.3.3. Electrical properties of Si_3N_4 nanopore on dielectric substrate with varied thickness

Based on ionic noise characteristic study, our devices were confirmed that a dielectric substrate provided a low noise platform and an active membrane (20 nm thick Si_3N_4) performed as ion impermeable layer. To assess an ionic current response of solid-state nanopore based on dielectric substrate, the I-V characteristic was tried and the results was shown in Figure 3-7a with 20-nm-thick Si_3N_4 membrane. Our devices were clearly shown Ohmic behavior even 1.5 nm diameter. Also, the conductance of each nanopore had decreased with electrolyte strength decrease, as shown Figure 3-7b. These results confirmed that our nanopore shape had a hourglass type not a conical shape.

However, 20-nm-thick nanopore has still thicker than protein nanopore, 10-nm-length of α-hemolysin and 8-nm-length of MspA. Therefore, thinner Si_3N_4 membrane transferring was tried. Figure 3-7c shows the conductance as a function of nanopore diameter with different Si_3N_4 membrane thickness, 20 nm (red), 10 nm (green), and 5 nm (blue). 5-nm-thick Si_3N_4 membrane was stable with ~2 μm x 2 μm sized aperture with ion impermeability. The conductance behavior with diameter was well understood in hourglass type with effective thickness and access resistance effect, and was described as

$$C_{nanopore} = C_{KCl}(\frac{4h_{eff}}{\pi d^2} + \frac{1}{d}) \qquad \textbf{Equation 3-2.}$$

where C_{KCl} is the molar conductance of electrolyte, h_{eff} the effective thickness of nanopore, and d the diameter of nanopore[15,26]. Effective thickness was smaller than the thickness of transferred membrane, because of the hourglass shape of nanopore, and the deviate was severe in thicker membrane. This deviation was occurred by nanopore fabrication method, which we used the reduction method after bigger nanopore perforation.

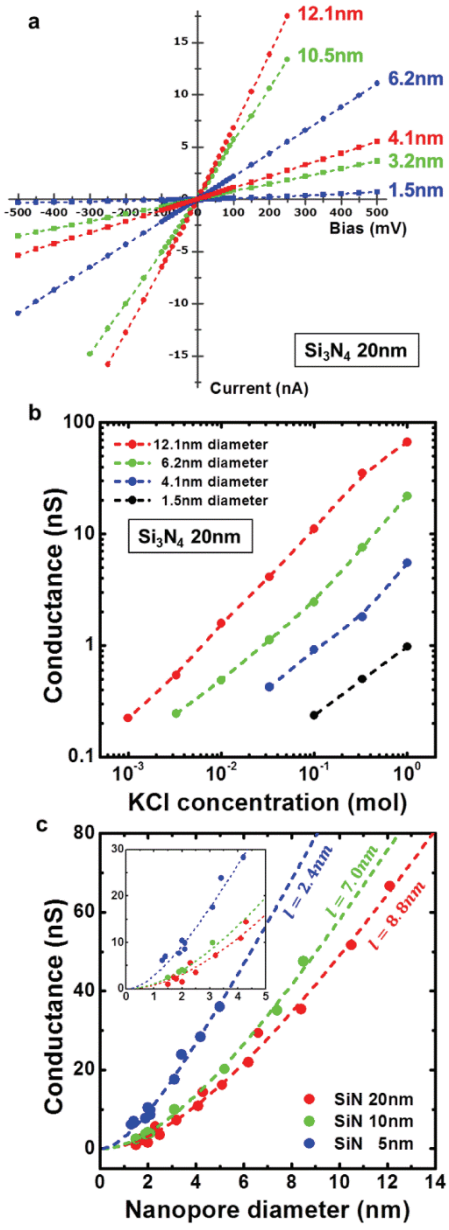

Figure 3-7. Ionic conductance characteristic of dielectric substrate based nanopore. **a)** Measured ionic current as a function of applied bias with

different sized nanopore with 20 nm thick Si_3N_4 membrane. **b)** Measured ionic conductance versus KCl concentration for 12.1 nm diameter nanopore (red), 6.2 nm diameter nanopore (green), 4.1 nm diameter nanopore (blue), and 1.5 nm diameter nanopore (black) with 20 nm thick Si_3N_4 membrane. c**)** Measured ionic conductance versus nanopore diameter with different Si_3N_4 membrane thickness, 20 nm (red), 10 nm (green), and 5 nm (blue). Each dot line and an effective thickness were achieved by fitting with Equation 3-2.

3.3.4. DNA sensing by using dielectric substrate based nanopore

To test a higher signal-to-noise ratio of dielectric substrate based solid-state nanopore, 40 nt ssDNA was used. Figure 3-8a and Figure 3-8b (concatenated plot) shows the ssDNA translocation event with different thickness nanopore at 200 mV and ~2.5 nm diameter. Upon nanopore thickness decreasing, open pore currents increased by electric filed enhancement in nanopore, and blockade current during DNA translocation increased by open pore current incensement. As a results, thinner membrane was provided us an improvement of signal-to-noise ratio, 50~100 ratio at 5-nm-thick nanopore and 250 kHz bandwidth with 10 kHz low-pass Bessel filter.

The DNA translocation data were converted to a blockade current and dwell time in Figure 3-4c. In Figure 3-8c, the dwell time was slightly decreased and blockade current was broadening in thinner nanopore. Slight decrement of dwell time is augmented, because it has to linearly decrease by enhanced electric field in thinner nanopore. This phenomenon was not clearly understood, but was probably a result of the most of electric field was consumed to lead DNA in nanopore and stretch of DNA in nanopore entrance. Broad blockade current in thinner nanopore were previously observed, and a results of the varying transport speeds, interactions and initial structure of each ssDNA molecule before translocation.

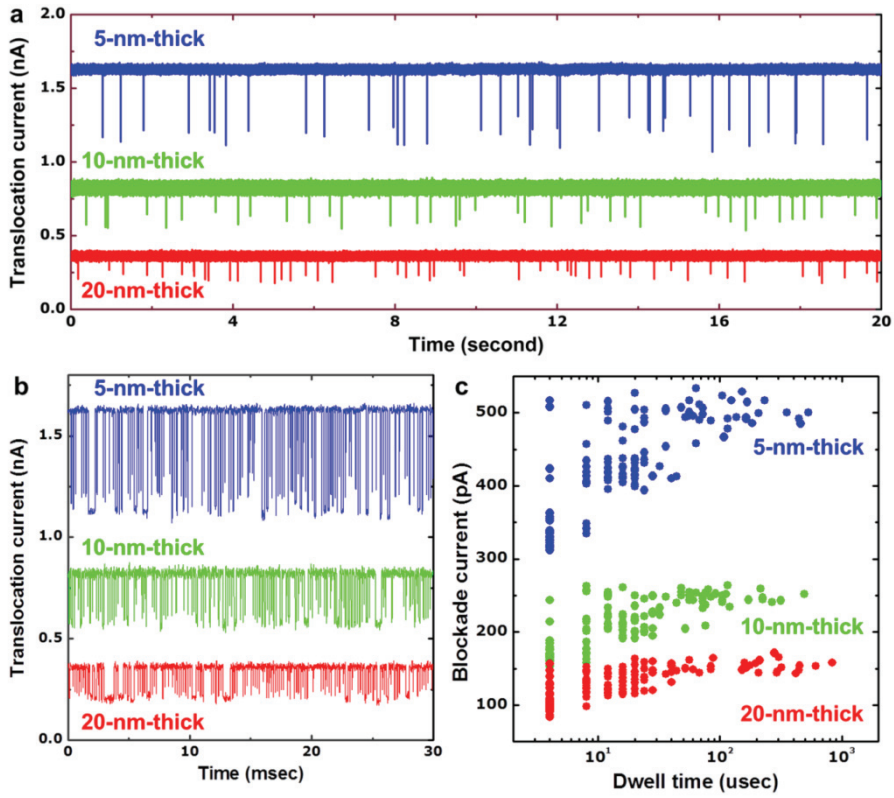

Figure 3-8. Measurement of 40 nt ssDNA using different thickness nanopore. **a)** Ionic conductance as a function of time with 40 nt ssDNA through different thickness nanopore with ~2.5 nm diameter and 200 mV. Translocation signals were enhanced in thinner nanopore and it provided us higher signal-to-noise ratio. **b)** Concatenated sets of translocation events of 40 nt ssDNA. **c)** Distribution of blockade current and dwell time through thickness variety nanopore.

3.3.5. Distingushiment of nucleotide type in dielectric substrate based nanopore

Nevertheless, deviation of blockade current was decreased in small diameter nanopore. Figure 3-9a shows the concentrated event of ssDNA translocation through the 1.5 nm diameter nanopore. The deviation of blockade current was shown, but not extremely in larger nanopore. We used poly A_{40} (black), poly T_{40} (green), poly C_{40} (red), and poly G_{40} (blue) to distinguish each nucleotide type in independent experiment with identical nanopore. In Figure 3-9a, each homopolymer had slightly difference of blockade current.

These results were obviously shown in Figure 3-9b as normalized histogram of residual current. Poly A_{40} and poly T_{40} had definite one Gaussian peak at 688.4 ± 43.1 pA (49.5% I_0) and 631.5 ± 67.6 pA (45.4% I_0), respectively. Poly C_{40} also had marked Gaussian distribution (643.8 ± 85.2 pA, 46.3% I_0) between poly A_{40} and poly T_{40}, but it was seemed to separate two Gaussian peaks, 582.0 ± 59.6 pA (minor peak, 42.9% I_0) and 657.6 ± 49.8 pA (main peak, 47.3% I_0). However, we could not find out the major Gaussian peak for poly G_{40}.

The altered residual current with direction of ssDNA 3’ or 5’ was well known at protein nanopore in previous reports[6,10], which explained the angle the bases in the homopolymer make with the phosphate backbone as possible

reason. In our results, poly A_{40} and poly T_{40} also had two different Gaussian distribution according to its direction, but the peak-to-peak distance possibly too small to distinguish. By contrast, poly C_{40} shows that the two peaks depended on direction of homopolymer. Residual current for poly G_{40} could not be reliably determined in our results, because poly G_{40} was easily formed secondary structure in electrolyte solution[6].

Also, translocation event detection with the combination of homopolymer was tried (Figure 3-10) and the results were similar to the independent experiments. Only poly A_{40} and poly T_{40} were distinguished and poly C_{40} and poly G_{40} was covered by other peaks or had multiple peaks in mixture of homopolymer. Restricted experiment with combination of poly A_{40} and poly T_{40} (Figure 3-11) shows the distinct two Gaussian peak from each homopolymer.

The ionic residual current was lowest (631.5 pA) for poly T_{40}, highest (688.4 pA) for poly A_{40}, and moderate (657.6 pA) for poly C_{40}. These results are qualitatively compared to previous reports with protein nanopores at Table 3-2. Firstly, our nanopore had extremely high open pore conductance (~6.95 nS), and the blockade current also extremely high (3.51 nS for poly A_{40}, 3.80 nS for poly T_{40}, and 3.67 nS for poly C_{40}). One possible explanation for these results is the larger diameter and thinner nanopore structure makes the conductance improvement in open pore state and blockade state. However,

the large sized diameter of nanopore also contributed the standard deviation of residual current. Protein nanopore generally shows low standard deviation as ~10 pA, but our results shows the few-tens of pA. Secondly, the order of blockade current level had T > C > A in our results and it means the most of ssDNA translocation was happened with 5' direction. The reason that only one direction of ssDNA was detected was not understood, but it probably explained with an interaction between ssDNA and surface of nanopore. A MT α-hemolysin[7] and MT MspA[10,11] has C-NH_2 termination and a cyclodextrin decorated α-hemolysin[8] has C–OH termination, therefore they showed the difference order of blockade current for each nucleotide type. Moreover, our Si_3N_4 based solid-state nanopore mainly has Si-N, so the order of blockade current similar to the MT α-hemolysin and MT MspA. It is hard to explain quantitatively, so it should be need to molecular dynamics simulation.

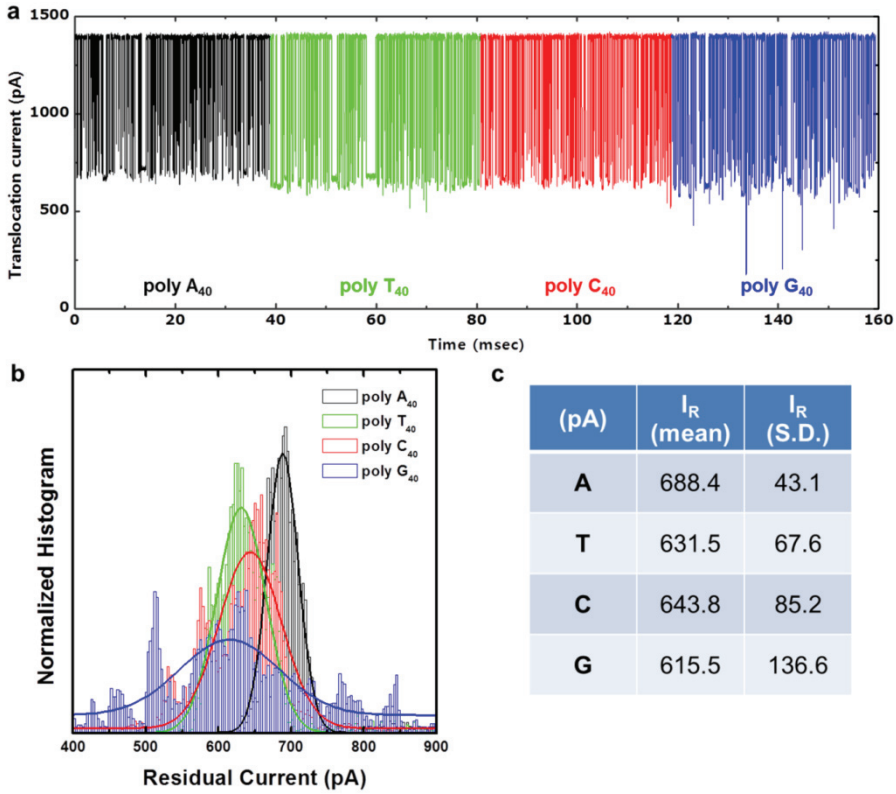

(pA)	I_R (mean)	I_R (S.D.)
A	688.4	43.1
T	631.5	67.6
C	643.8	85.2
G	615.5	136.6

Figure 3-9. Homopolymer distinguishing using 1.5 nm diameter and 5 nm thick nanopore. **a),** Concatenated sets of each homopolymer (poly A_{40}, poly T_{40}, poly C_{40}, and poly G_{40}) translocation events through 1.5 nm diameter and 5 nm thick nanopore with 200 mV. **b),** Normalized histogram of the residual current amplitudes, which show stiff distribution of poly A_{40} and poly T_{40}, and relatively board distribution of poly C_{40} and poly G_{40}. Poly C_{40} and poly G_{40} almost overlapped by other homopolymer. **c)** Mean value and standard deviation of residual current of each homopolymer, which fitted Gaussian distribution from Figure 3-5b.

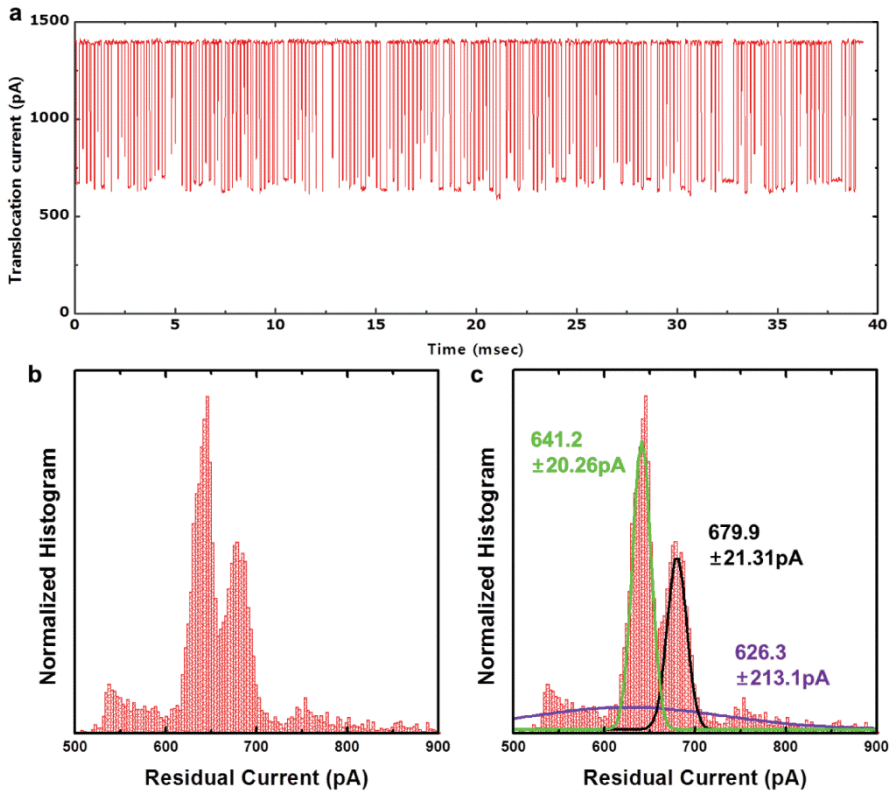

Figure 3-10. Translocation events of mixture of homopolymer. **a)** Concatenated sets of translocation events of mixture of each homopolymer (poly A_{40}, poly T_{40}, poly C_{40}, and poly G_{40}) through 1.5 nm diameter and 5 nm thick nanopore with 200 mV. **b)** Normalized histogram of the residual current amplitudes, which show two peak in 600~700 pA regime which correspond to poly A_{40} and poly T_{40}. Poly C_{40} was expected that almost overlapped with range of poly A_{40} and poly T_{40}. And poly G_{40} was shown in broad range in 500~900 pA. **c,** Fitting results of histogram of residual current.

Poly A_{40} and poly T_{40} had almost same value to the results of single homopolymer translocation events (poly A_{40} : 688.4±43.1 pA, poly T_{40} : 631.5±67.6 pA). The purple curve was expected that consisted from poly C_{40} and poly G_{40}.

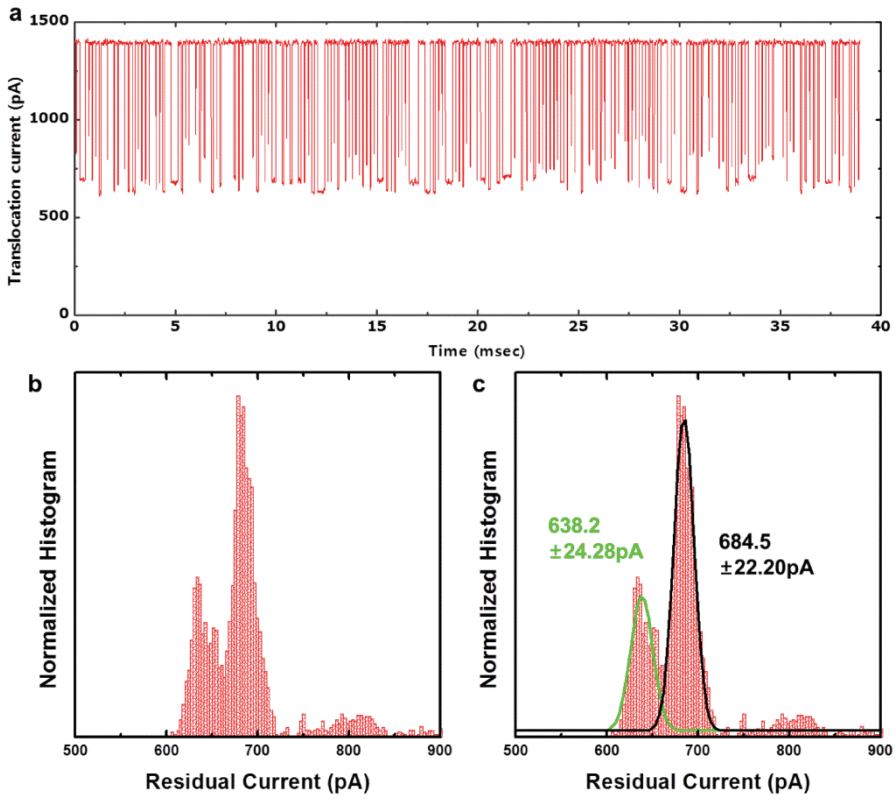

Figure 3-11. Translocation event of mixture of poly A_{40} and poly T_{40}. **a)** Concatenated translocation events of mixture of poly A_{40} and poly T_{40} through 1.5 nm diameter and 5 nm thick nanopore with 200 mV. **b)** Normalized histogram of the residual current amplitudes, which show stiff two Gaussian peaks contributed of poly A_{40} and poly T_{40}. **c,** Fitting results of histogram of residual current of mixture of poly A_{40} and poly T_{40}. It has similar results to single homopolymer translocation events (poly A_{40} : 688.4±43.1 pA, poly T_{40} : 631.5±67.6 pA) and the tow homopolymer was clearly distinguished.

Type	$\Delta I_{block}(A)$ (pS)	$\Delta I_{block}(T)$ (pS)	$\Delta I_{block}(C)$ (pS)	$\Delta I_{block}(G)$ (pS)	I_{open} (pS)	Bias (mV)	Rank of ΔI_{block}	Min. ΔI (pS)	Ref.
α-hemolysin	778	805	790		958	120	T>C>A	12	5' lead [6]
	806	799	778		958	120	A>T>C	7	3' lead [6]
	805	808	814	802	1019	160	C>T>A>G	3	5' lead in WT [7]
	639	645	656	627	1050	160	C>T>A>G	6	5' lead in MT [7]
	139	144	111	167	300	180	G>T>A>C	5	single nt. [8]
MspA	1442	1573	1537	1476	1806	180	T>C>G>A	34	5' lead [10]
	1490	1627	1593	1534	1801	140	T>C>G>A	34	5' lead [10]
	1345	1500	1612	1606	1822	180	C>G>T>A	6	5' lead [11]
	1314	1546	1360	1263	1822	180	T>C>A>G	46	3' lead [11]
	367	489	385	428	611	180	T>G>C>A	18	5' lead [12]
	3510	3800	3670		6950	200	T>C>A	130	This work

Table 3-2. Blockade Conductance of each nucleotide through a nanopore device. Blockade conductance of each nucleotide through an α-hemolysin and MspA protein nanopore and open conductance of nanopore with given (optimal) bias. Order of blockade conductance like those shown each blockade conductance had variety of each measurements and the required resolution to distinguish each nucleotide was few-tens of pS. Also, counter parts of solid-state nanopore was shown in last row which achieved in this work.

3.4. Summary and Conclusions

In conclusion, we have developed a novel structure and a fabrication method to dielectric substrate based solid-state nanopore that can be provide us sub-10 pA RMS ionic current noise comparable to protein nanopore. And it was used to make over 100 signal-to-noise ratio with sub-10 nm thickness membrane. Improved signal-to-noise ratio and thinner membrane was useful to detect a small nucleic acids event 40 nt ssDNA. Furthermore, four type of homopolymer consisted with A40, T40, C40, and G40 were discriminated with 1.5 nm diameter and 5 nm thick dielectric substrate based solid-state nanopore. The nanopore has allowed us to distinguish poly A_{40}, poly T_{40}, and poly C_{40}, roughly. Here some problems for the DNA sequencing were remained that uniform fabrication method for 1~2 nm diameter nanopore, high standard deviation of Gaussian peak of each nucleotide type, and determination of sensing zone in solid-state nanopore. However, the solid-state nanopore will overcome these problems by applying or mimicking of protein nanopore technologies.

References

[1] D. Branton, D. W. Deamer, A. Marziali, H. Bayley, S. A. Benner, T. Butler, M. Di Ventra, S. Garaj, A. Hibbs, X. Huang, *et al.* 2008, *Nat. Biotechnol.* **26**, 1146

[2] A. H. J.Yang, S. D. Moore, B. S. Schmidt, M. Klug, M. Lipson, D. Erickson, 2009, *Nature* **457**, 71

[3] B. M. Venkatesan, R. Bashir, 2011, *Nat. Nanotechnol.* **6**, 615

[4] S. M. Bezrukov, I. Vodyanoy, V. A. Parsegian, 1994, *Nature* **370**, 279

[5] J. J. Kasianowicz, E. Brandin, D. Branton, D. W. Deamer, 1996, *Proc. Natl. Acad. Sci. U. S. A.* **93**, 13770

[6] R. F. Purnell, K. K. Mehta, J. J. Schmidt, 2008, *Nano Lett.* **8**, 3029

[7] D. Stoddart, A. J. Heron, E. Mikhailova, G. Maglia, H. Bayley, 2009. *Proc. Natl. Acad. Sci. U. S. A.* **106**, 7702

[8] J. Clarke. H.-C. Wu, L. Jayasinghe, A. Patel, S. Reid, H. Bayley, 2009, *Nat. Nanotechnol.* **4**, 265

[9] I. M. Derrington, T. Z. Butler, M. D. Collins, E. Manrao, M. Pavlenok, M.

Niederweis, J. H. Gundlach, 2010, *Proc. Natl. Acad. Sci. U. S. A.* **107**, 16060

[10] E. A. Manrao, I. M. Derrington, M. Pavlenok, M. Niederweis, J. H. Gundlach, 2011, *PLoS ONE* **6**, e25723

[11] E. A. Manrao, I. M. Derrington, A. H. Laszlo, K. W. Langford, M. K. Hopper, N. Gillgren, M. Pavlenok, M. Niederweis, J. H. Gundlach, 2012, *Nat. Biotechnol.* **30**, 349

[12] A. J. Storm, J. H. Chen, J. H., X. S. Ling, H. W. Zandbergen, C. Dekker, C. 2003, *Nat. Mater.* **2**, 537

[13] J. Li, D. Stein, C. McMullan, D. Branton, M. J. Aziz, J. A. Golovchenko, 2001, *Nature* **412**, 166

[14] M. J. Kim, M. Wanunu, D. C. Bell, A. Meller, A. 2006, *Adv. Mater.* **18**, 3149

[15] M. Wanunu, T. Dadosh, V. Ray, J. Jin, L. McReynolds, M. Drndic, 2010, *Nat. Nanotechnol.* **5**, 807

[16] S. Garaj, W. Hubbard, A. Reina, J. Kong, D. Branton, J. A. Golovchenko, 2010, *Nature* **467**, 190

[17] C. A. Merchant, K. Healy, M. Wanunu, V. Ray, N. Peterman, J. Bartel, M.

D. Fischbein, K. Venta, Z. Luo, A. T. C. Johson, M. Drndic, 2010, *Nano Lett.* **10**, 2915

[18] G. F. Schneider, S. W. Kowalczyk, V. E. Calado, G. Pandraud, H. W. Zandbergen, M. K. Vandersypen, C. Dekker, 2010, *Nano Lett.* **10**, 3163

[19] P. Chen, J. Gu, E. Brandin, Y.-R. Kim, Q. Wang, D. Branton, 2004, *Nano Lett.* **4**, 2293

[20] J. K. Rosenstein, M. Wanunu, C. A. Merchant, M. Drndic, K. L. Shepard, 2012, *Nat. Methods* **9**, 487

[21] V. Tabard-Cossa, D. Trivedi, M. Wiggin, N. N. Jetha, A. Marziali, 2007, *Nanotechnol.* **18**, 305505

[22] K.-S. Kim, Y. Zhao, H. Jang, S. Y. Lee, J. M. Kim, K. S. Kim, J.-H. Ahn, P. Kim, J.-Y. Choi, B. H. Hong, 2009, *Nature* **457**, 706

[23] R. M. M. Smeets, U. F. Keyser, N. H. Dekker, C. Dekker, 2008, *Proc. Natl. Acad. Sci. U.S.A.* **105**, 417

[24] R. M. M. Smeets, N. H. Dekker, C. Dekker, 2009, *Nanotechnol.* **20**, 095501

[25] R. A. Levis, J. L Rae, 1993, *Biophys. J.* **65**, 1666

[26] S. W. Kowlczyk, A. Y. Grosberg, Y. Rabin, C. Dekker, 2011, *Nanotechnol.* **22**, 315101

[27] H.-M. Kim, M.-H. Lee, K.-B. Kim, 2011, *Nanotechnol.* **22**, 275303

CHAPTER 4.

Effect of Surface Charge and Nanopore Geometry on the Debye Screening Length and the Ionic Conductance

4.1. Introduction

Nanofluidic is an emerging area dealing with the transport of fluidics in nanometer scale geometry, more specifically, the transport of ions and molecules and the transport of nanometer scale particles either charged or not in an aqua environment. Nanofluidic compares with the microfluidic in the aspect that at least one of its channel (or pore) dimension should be in the nanometer scale regime so that the surface charge density of solid material and the resulting Debye screening length (λ_D) significantly affects the overall transport phenomena. Thus, nanofluidic devices have emerged as a promising tool for molecular coulter counter, ionic logical device, and single biomolecule analysis such as DNA, RNA, and proteins[1-4].

In many of the applications of nanofluidic, charged molecules as well as ion species are driven through nanopore or nanochannel by an external bias, and the flow of ion species can be measured by an external current measurement system as an ionic current[5]. Since this ionic current can be modulated either by modifying the types (positive or negative) and density of surface charges[6-8] or by an external gate bias[9], actively. It is utmost important to understand the variation of ionic conductance with respect to the variables

such as the geometry of nanopore and nanochannel, surface charge, external applied gating bias, and electrolyte concentration[10-12].

In nanopore device, the geometry effect on ionic conductance is still on a debate; some researchers reported that it is proportional to the pore diameter (d) while others reported that it is proportional to the square of the diameter (d^2). Ionic conductance should be proportional to the square of the diameter if it is subjected to a simple resistor model[13]. However, Kowalczyk *et al.* and Garaj *et al.* reported that the ionic conductance is proportional to its diameter in Si_3N_4 nanopore[14] and graphene[15], respectively. In particular, Kowalczyk *et al.* explained this phenomenon with the concept of access resistance result from hemispherical resistance at an entrance of nanopore[14]. Also, the ionic conductance has third power proportionality by property of flow rate at conical shape nanopore[16]. Compared to nanopore structure, the access resistance is hard to apply to nanochannel system, because of its longer channel length. However, the carbon and SiO_2 based nanochannel device has shown the abnormal ionic conductance than expected value[17,18]. In those paper, an increased electroosmotic velocity due to excess ion concentration[17] or a larger proton concentration[18] were proposed as the reason of the large ionic conductance.

In many of these reported results, the effect of surface charge on the ionic conductance has been mostly under-estimated. It appears not to be a big issue

since the surface charge density of Si_3N_4 is not large enough (p.z.c. = 6.5 pH)[19]. However, in other materials (graphene, carbon nanotube, a-C, Al_2O_3, SiO_2 and so on)[20,21], surface charge is large enough and should not be neglected when one consider the variation of ionic conductance[22-27].

In this work, we have calculated potential distribution inside of the nanopore and nanochannel having cylindrical geometry based on finite element method (FEM) using MATLAB and confirmed by COMSOL Multiphysics. Simulations were indeed successful in characterizing the surface charge effect on electric potential distribution and ionic conductance with different geometry, radius, surface potential, and electrolyte strength. We also experimentally measured the ionic conductance in nanopore system with different radius, material, and electrolyte strength. Finally, we investigated the possibility of enhancing signal-to-noise ratio using high surface potential materials.

4.2. Experimental details

A one-dimensional Poisson-Boltzmann equation model calculating electrical potential distribution, effective λ_D, charge particle distribution, and the ionic conductance along the radial direction was coded with FEM in MATLAB (Mathworks, Natick, Massachusetts). In all calculation, cell size was defined as 0.1 nm and the error should to minimize under 10^{-4} level. Ionic conductance was calculated by integration of charge particle distribution in a cylindrical geometry, and the error of integration was minimized using adaptive Simpson quadrature based algorithm.

Surface charge altered nanopores were fabricated by 20-nm-thick a-C, Al_2O_3, and Si_3N_4 deposition on 20-nm-thick Si_3N_4 membrane. Overall process was following; the 20-nm-thick low-stress LPCVD Si_3N_4 on both side / 50-nm-thick PECVD SiO_2 on top side / 100-nm-thick low-stress LPCVD Si_3N_4 on both side were deposited sequentially on the double-side polished silicon substrate. Consequently, 20 nm Si_3N_4 / 50 nm SiO_2 / 100 nm Si_3N_4 films were formed at top side and 120 nm Si_3N_4 film was formed at bottom side of substrate. The back side of substrate was patterned by photo lithography and reactive ion etching to define the opening area during KOH (potassium hydroxide) etching. KOH etching was performed from the back

side to the front side films, creating 50 μm by 50 μm sized membrane. The altered surface charged materials were deposition by e-gun evaporate (a-C), atomic layer deposition (Al_2O_3) and PECVD (Si_3N_4).

Finally, the nanopore with 5, 10, 15 nm diameter were perforated using focused electron beam in 200 kV transmission electron microscope (TEM, JEOL 2010F) in bi-layer structured membrane (modified surface charge material / Si_3N_4). The chips were wetted in the ethanol, and the ethanol was substitute by deionized water. For the electrical measurement, the chip was mounted on a silicone elastomer based jig, and Ag/AgCl electrodes were introduced in a both chamber. The electrical signal was recorded by using Axon patch 200B with 250 kHz and 10 kHz low-pass Bessel filter.

4.3. Results and Discussion

4.3.1. Potential distribution inside of the nanopore and nanochannel geometry

In order to understand the ionic conductance in nanofluidics, it is important to calculate the exact potential distribution inside of the nanopore and nanochannel geometry. While the potential distribution on flat surface has been solved and is generally known as a function of λ_D, the exact potential distribution inside of the nanopore and nanochannel geometry has not been solved analytically. In here, we first calculated electrical potential distribution for the flat surface, spherical surface, cylindrical surface and cylindrical cavity (nanopore, nanochannel) using FEM simulation coded with MATLAB based on Poisson-Boltzmann equation. Poisson-Boltzmann equation was written as following equation for the universal geometry and z-axis symmetry.[28,29]

$$\left(\frac{d}{dr}+\frac{\chi}{r}\right)\frac{d\psi(r)}{dr}=-\frac{1}{\varepsilon_0\varepsilon}\rho(r)$$
$$=\frac{2enz}{\varepsilon_0\varepsilon}\sinh\left(\frac{ze}{kT}\psi(r)\right) \qquad \textbf{Equation 4-1.}$$

In the above equation, r is the radius direction, χ is the geometry factor (0 for flat, 1 for cylindrical, and 2 for spherical geometry), ψ is the potential function, ε_0 is permittivity of vacuum, ε is relative permittivity of the fluid, e is the charge of electron, n is the far-field concentration of ion species, z is the valence of ions. The boundary condition is defined as

$$\psi\left(r_{nanopore}\right)=\psi_{surface},\quad \left.\frac{d\psi(r)}{dr}\right|_{r=0}=0 \quad \text{for the cylindrical cavity,}$$

$$\psi(0)=\psi_{surface},\quad \left.\frac{d\psi(r)}{dr}\right|_{r\to\infty}=0,\quad \left.\psi(r)\right|_{r\to\infty}=0 \quad \text{for the other geometry,}$$

Equation 4-2.

$\psi_{surface}$ is the surface potential. The analytical solution was obtained only for the flat surface geometry with hyperbolic tangent form with λ_D.

$$\tanh\left(\frac{ze\psi(r)}{4kT}\right)=\tanh\left(\frac{ze\psi_{surface}}{4kT}\right)\exp\left(-\frac{r}{\lambda_D}\right)$$

Debye screening length, $\lambda_D=\sqrt{\dfrac{\varepsilon_0\varepsilon kT}{2e^2nz^2}}$

Equation 4-3.

For the other geometry, analytical solution is not obtained as a simple form. It can only be obtained at the low potential (tens of mV) assumption, where the Poisson-Boltzmann equation can be expressed as follow,

$$\left(\frac{d}{dr}+\frac{\chi}{r}\right)\frac{d\psi(r)}{dr}=\frac{\psi(r)}{{\lambda_D}^2} \qquad \textbf{Equation 4-4.}$$

And the analytical solution is obtained for cylindrical cavity with low potential assumption.

$$\psi(r)=\psi_{surface}\frac{\sinh\left(r/\lambda_D\right)}{\sinh\left(r_{nanopore}/\lambda_D\right)}\frac{r_{nanopore}}{r} \qquad \textbf{Equation 4-5.}$$

In addition, we also obtained the numerical solution with FEM (or FDM, finite difference method) using MATLAB for the general case without assumption.

4.3.2. Calculation of electric distribution and determination of effect Debye screening length

Figure 4-1a,b show the potential distribution inside of the cylindrical cavity for (blue line) analytical solution based on low potential assumption, (green line) numerical solution obtained for cylindrical cavity geometry, and (red line) analytical solution for flat geometry at different electrolyte concentration (Figure 4-1a: 1M and 100 mM KCl, Figure 4-1b: 10 mM and 1 mM KCl). The radius of nanopore is set at 5 nm. It appears that there is not that much difference in the potential distribution function at 1 M KCl concentration. However, in the lower electrolyte concentration, the analytical solution with low potential assumption has over-estimated and the analytical solution from flat surface has under-estimated than the exact (numerical) solution. Under-estimation of flat surface based calculation is caused by the concave structure of nanopore and the over-estimation of low-potential approximation is caused by the reduction of hyperbolic sine to linear form. The discrepancy is more drastic at the lower electrolyte concentration as is shown in Figure 4-1b. Also, the discrepancy is more enhanced in the smaller radius nanopore (Figure 4-1c) and at higher surface potential (Figure 4-1d).

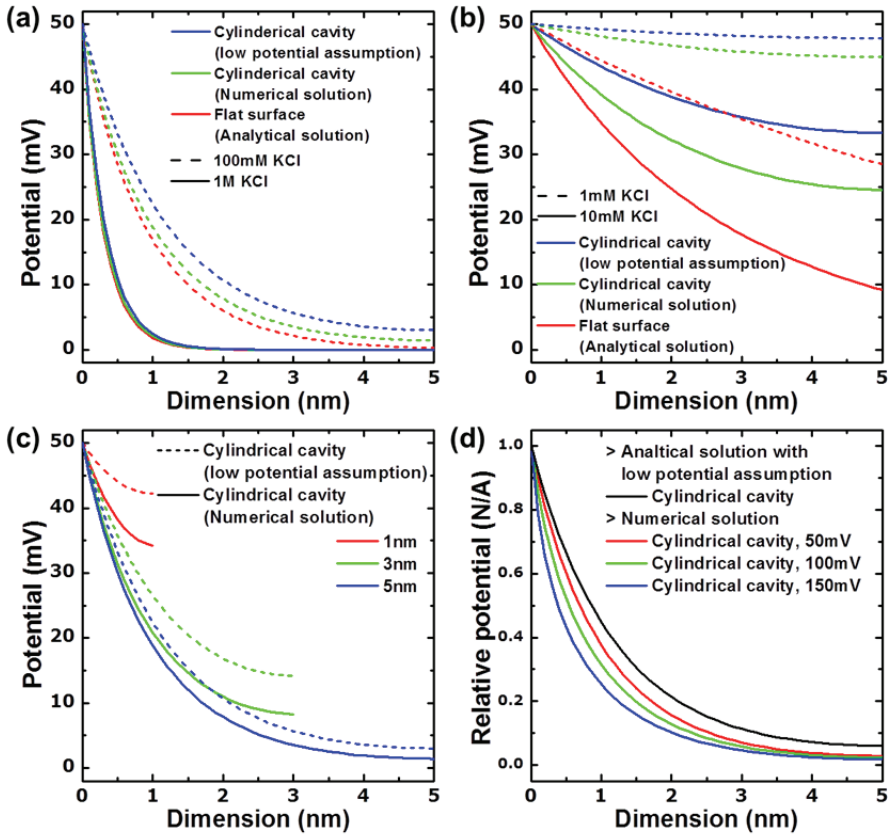

Figure 4-1. Electrical potential distribution in different electrolyte strength (a, b), different radius (c) and different surface potential (d). In (a, b), blue line was calculated from analytical solution of cylindrical cavity model with low potential assumption. Also, green and red line represented the numerical solution results at cylindrical cavity and at flat surface, respectively. (a, b) show the electrical potential distribution at 1 M (solid line in a), 100 mM

(dashed line in a), 10 mM (solid line in b) and 1 mM (dashed line in b) KCl with 5 nm radius nanopore and 50 mV surface potential. **c)** Electrical potential distribution with 1 nm (red line), 3 nm (green line) and 5 nm (blue line) with 100 mM KCl and 50 mV surface potential. Solid line and dashed line were calculated from numerical solution and analytical solution with low potential assumption. **d)** Electrical potential distribution with 5 nm radius nanopore, 100 mM KCl and different surface potential (analytical solution with low potential assumption : black line, 50 mV : red line, 100 mV : green line, 150 mV : blue line).

It should be noted that one generally employs the concept of λ_D shown in Equation 4-5. This equation is derived based on Debye-Huckel approximation from the flat surface geometry at the assumption of low potential. Since the potential distribution is significantly affected by the geometry of surface (flat versus nanopore) as is shown in Figure 4-1, we have extracted the effective λ_D in nanopore geometry from the potential distribution and is shown in Figure 4-2a. The effective λ_D in flat surface (black solid line) was well matched to analytical expression of Equation 4-5 (cyan dashed line) with 50 mV surface potential (low potential condition). The effective λ_D in nanopore was slightly larger than λ_D of flat surface in smaller nanopore and lower electrolyte strength. Figure 4-2b shows the effective λ_D at 10 nm radius nanopore with different surface potential and electrolyte strength. This result clearly shows that the effective λ_D is becoming smaller as the surface potential is being increased. And this variation is becoming larger at low electrolyte concentration. Namely, the λ_D varies with the surface potential which cannot be deduced from the Debye-Huckel approximation. On the other hand, the effective λ_D can be calculated using analytical solution in flat geometry shown in Figure 4-3 and Equation 4-6. The variation of effective λ_D with respect to the surface potential and the size of nanopore are more clearly seen in Figure 4-2c-d at 1 M and 0.1 M KCl concentrations, respectively (more detailed in Figure 4-4).

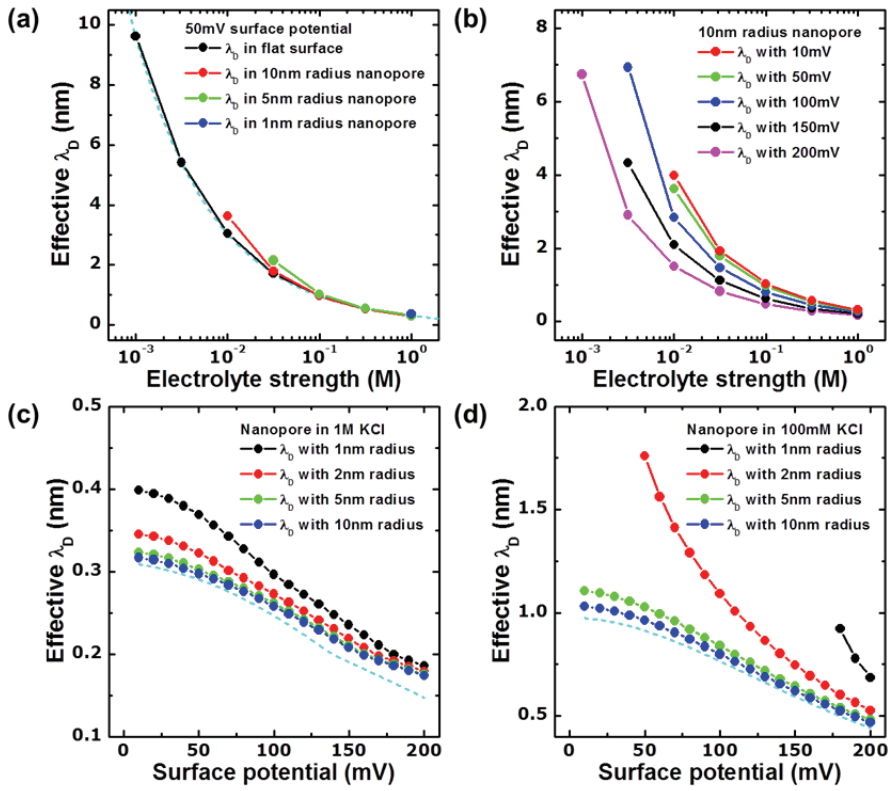

Figure 4-2. Effective λ_D as a function of electrolyte strength (a, b) and surface potential (c, d). Effective λ_D was defined as the position for the 1/e ratio of surface potential. Unmarked data has meaning that the potential doesn't approach the 1/e ratio of surface potential even center of nanopore at given condition. And the cyan dot line was represented the equation based effective λ_D. **a)** Black line was effective λ_D calculated from flat surface. Other lines are extracted from calculated electrical potential distribution in

nanopore with different radius; red line is 10 nm, green line is 5 nm and blue line is 1 nm radius. **b)** Effective λ_D as considered with different surface potential in 10 nm radius nanopore. **c, d)** Effective λ_D as a function of surface potential in different radius; black line is 1 nm, red line is 2 nm, green line is 5 nm and blue line is 10 nm with c) 1 M KCl d) and 100 mM KCl conditions. Cyan dashed line was represented the effective in λ_D flat surface.

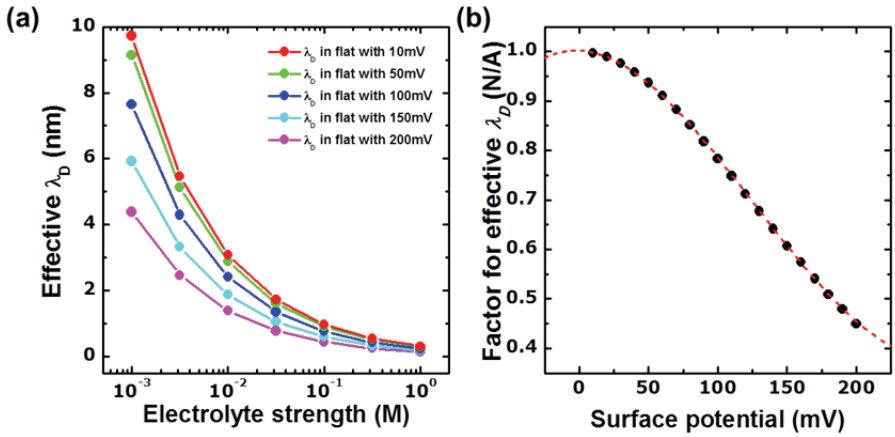

Figure 4-3. **a)** Effective λ_D as a function of electrolyte strength in flat surface with different surface potential. Effective λ_D was changed by surface potential against calculated λ_D from Equation 4-5. Effective λ_D was also calculated analytically, in Equation 4-6. **b)** Factor for effective λ_D (effective λ_D / calculated λ_D) as a function of surface potential. Factor for effective λ_D was calculated from a) and, also acquired as natural logarithm term from Equation 4-6. Red dashed line was fitting line with 3th order polynomial. $y = 1.0018 - 0.12424x - 27.612x^2 + 72.785x^3$ (y is factor for effective λ_D, x is surface potential in V, fitting R is 0.99993)

$$\text{effective } \lambda_D = \lambda_D \ln\left(\tanh\left(\frac{ze\psi_{surface}}{4kT}\right) \Big/ \tanh\left(\frac{ze\psi_{surface}}{4kT\exp(1)}\right)\right)$$

Equation 4-6.

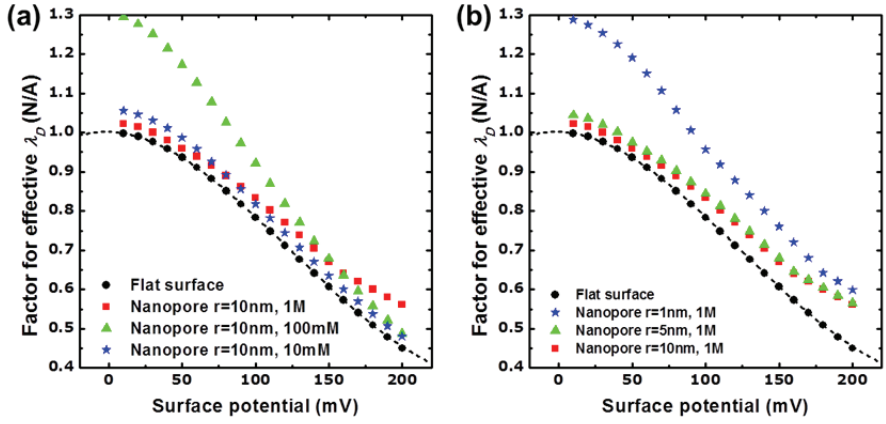

Figure 4-4. Factor for effective λ_D (effective λ_D / calculated λ_D) as a function of surface potential with **a)** different electrolyte strength with 10 nm radius, and **b)** different radius at 1 M. Black dot was calculated in flat surface and black dashed line was fitting line from Figure 4-3b.

If one simply deduces the effect of surface charge density from the effective λ_D, the surface charge effect will be enhanced at smaller radius nanopore, lower electrolyte strength, and lower surface charge potential nanopore. However, this assumption is against the general concepts; surface charge effect will be improved at higher surface charged nanopore. This discrepancy happened by the proportionally determined property of the effective λ_D. Therefore, the effective λ_D as well as equation derived λ_D was not suitable as the determine factor for the evaluation of surface charge effect.

4.3.3. Simulated ionic conductance of nanopore with effect of surface charge

In order to properly evaluate the effect of surface charge in nanofluidic system, we introduce the concept of relative ionic conductance which is defined as an ionic conductance with respect to that at zero surface charge. Relative ionic conductance thus describes the improved ratio of ionic conductance with respect to the surface potential. To calculation relative ionic conductance, an ionic conductance with each condition was calculated using followed equation.

$$G = \sum_{i}^{z=const.} \frac{A_{cell,i}}{h_{cell,i}} n_i z_i q_i \mu_i \qquad \textbf{Equation 4-7.}$$

In the above equation, G is the conductance of nanopore, A_{cell}, h_{cell} is the area and height of cell in FEM simulator, n, z, q, μ are concentration of ion, charge valence, unit charge, and electric mobility, respectively. And, the Equation 4-7 can be simplified to followed equation in KCl electrolyte.

$$G = \frac{\sigma_{1M\,KCl}}{2N_A} \sum_{i}^{z=const.} V_{cell,i} \left(n_{K^+,i} + n_{Cl^-,i} \right) \qquad \textbf{Equation 4-8.}$$

In this equation, $\sigma_{1M\,KCl}$ is the conductivity of 1 M KCl, N_A is the Avogadro number, V_{cell} is the volume of the cell, n_{K^+}, n_{Cl^-} are the concentration of K^+ and Cl^- ion.

Figure 4-5a-c shows the variation of relative ionic conductance at different surface potentials in different size of nanopores; (a) 10 nm, (b) 5 nm, and (c) 1 nm. All the results clearly demonstrate that the relative ionic conductance is increased by the increase of surface potential. Moreover, the result also shows that surface charge effect is more significant at low electrolyte strength, and at smaller diameter nanopores. For instance, while 3 times enhanced ionic conductance is obtained at 10 nm radius, 1 M KCl, and 150 mV as compared zero surface charge condition, the ionic conductance was increased by 5 times to 20 times as the pore size is reduced to 5 nm to 1 nm radius.

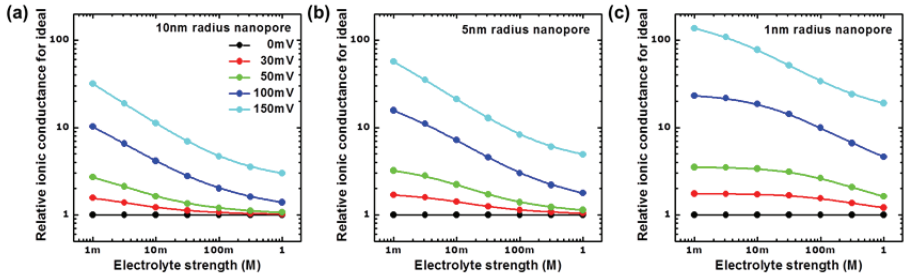

Figure 4-5. Simulated relative ionic conductance of nanopore as compared to ideal ionic conductance (only dependent on electrolyte strength and nanopore radius, $\sigma = \pi r^2 \sigma_{KCl}(M)$). Each plot was represented **a)** 10 nm radius, **b)** 5 nm radius, and **c)** 1 nm radius nanopore.

Distinctive point is that a plateau region exists in low electrolyte strength condition with 1 nm radius nanopore and low surface charge potential (30~50 mV). This means that accumulation of the counter ion was not enough to screen the surface charge, so, the most of potential didn't consume inside of nanopore. More detailed data is shown in Figure 4-6a-c, and each figure shows the relative ionic conductance as a function of : surface potential – electrolyte strength at 5nm radius nanopore (Figure 4-6a), radius – electrolyte strength with 100 mV surface potential (Figure 4-6b), and surface potential – radius with 1 M electrolyte strength (Figure 4-6c).

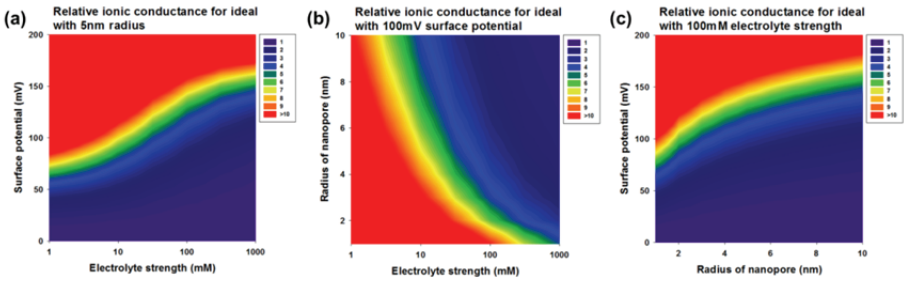

Figure 4-6. Simulated relative ionic conductance of nanopore as compared to ideal ionic conductance as a function of **a)** surface potential – electrolyte strength with 5 nm radius, **b)** radius of nanopore – electrolyte strength with 100 mV surface potential, and **c)** surface potential – radius of nanopore with 1 M KCl.

Interesting things are the changes of ionic conductance with respect to the radius of nanopore at the same electrolyte strength and surface potential. Figure 4-7a-b shows the conductance with unit length of nanopore as a function of its size and surface potential. The conductance with unit length is directly converted to ionic conductance by multiplying length of nanopore. Referring Figure 4-7a (1 M KCl case), ionic conductance appears to be proportional to the square of its radius below 100 mV surface potential. However, when the surface potential is increased to 150 mV, ionic conductance shows more linear dependency and is quite linear in 10 mM KCl with 50 mV surface potential as is shown in Figure 4-7b (other condition with different electrolyte strength from 1 M to 1 mM was shown in Figure 4-8). This is due to surface charge effect in high surface charged or low electrolyte strength.

From this observation, we tried to fit the ionic conductance as a function of radius with given surface potential and electrolyte conductivity by following allometric equation.

$$\sigma = \pi\sigma_{KCl}\sigma_0 r^n \qquad \textbf{Equation 4-9.}$$

σ is ionic conductance of nanopore, σ_{KCl} is ionic conductivity of given electrolyte, r is radius of nanopore. σ_0 and n are surface charge effected ionic conductivity and geometry factor, and determined by surface potential in Figure 4-7c,d. σ_0 is exponentially increased with surface potential, however, the increasing was early started in lower electrolyte strength. Also, n is decreased from 2 to 1 as the surface potential is increased. Particularly, n is more rapidly reached to 1 with 10 mM condition, but, n is again increased below 10 mM. The reason of this trend is that the counter ions are not enough to screening the surface potential at the high surface potential and low electrolyte strength. Also, most of overall charge, contributed on conductance, was concentrated at surface in high surface potentials case, therefore, the conductance has linearity to diameter.

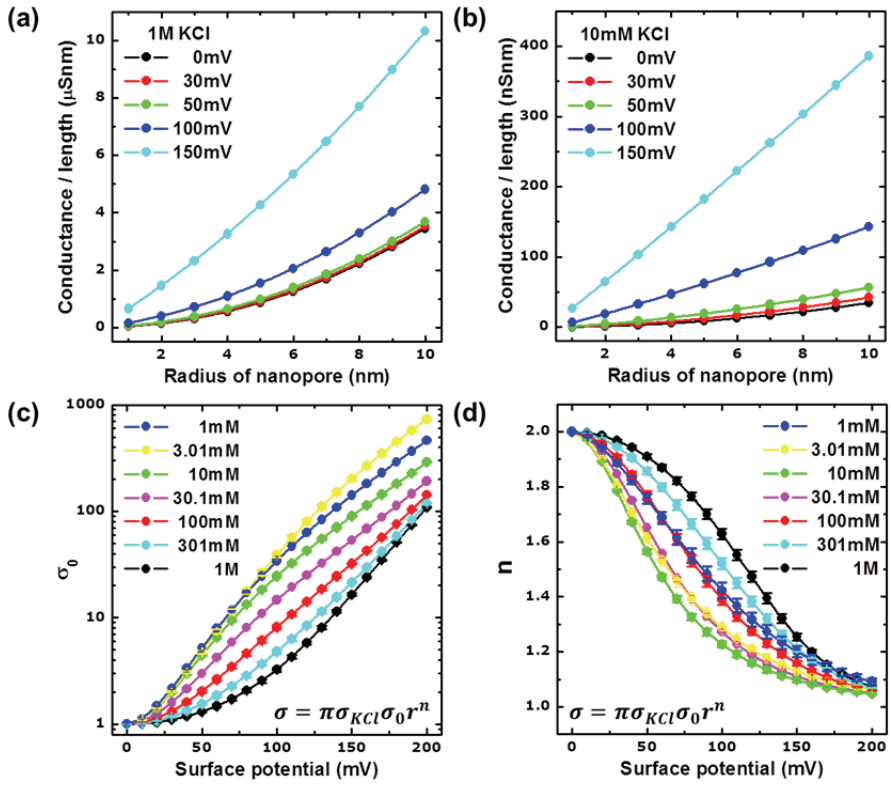

Figure 4-7. Conductance per nanopore length was considered the radius nanopore, surface potential, and electrolyte strength **a)** 1 M, **b)** 10 mM. Fitting parameter **c)** σ_0, **d)** n for ionic conductance calculation using allometric relation ($\sigma = \pi\sigma_{KCl}\sigma_0 r^n$). σ_0 means the enhanced ionic conductance and n is geometry factor for its diameter.

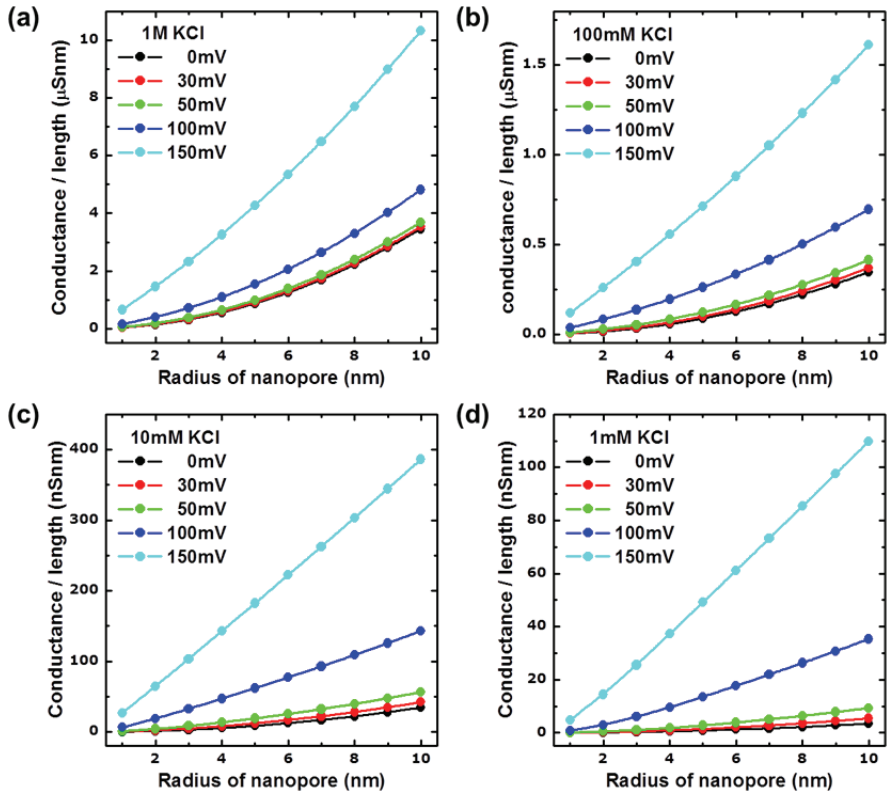

Figure 4-8. Conductance per nanopore length was considered the radius nanopore, surface potential, and electrolyte strength **a)** 1 M, **b)** 100 mM, **c)** 10 mM, **d)** 1 mM.

4.3.4. Measurement and comparison of ionic conductance as a function of surface charge density

To investigate the effect of surface charge, we used the bi-layer structured nanopore with different materials with different point of zero charge (p.z.c.). Chosen materials is a-C, Al_2O_3, and Si_3N_4, and the p.z.c. of each materials have 3 ~ 3.8 pH, 8.3 ~ 9.2 pH, and 6.5 pH, respectively.[19-21] Also, p.z.c. pH number can be converted to surface potential using the following equation.

$$\psi_0 = \frac{kT}{e} \ln\left(\frac{[H^+]}{[H^+]_{p.z.c.}} \right) \qquad \textbf{Equation 4-10.}$$

Conversed surface potential were -236 ~ -189 mV, 76.7 ~ 130 mV, -29.5 mV, respectively.

All materials was deposited on 20-nm-thick Si_3N_4 membrane and perforated by focused electron beam with different diameters from 5 nm to 15 nm. Figure 4-9a shows the 5-nm-diameter nanopore with each material. Si_3N_4 coated membrane was well drilled with circular shape, but a-C coated membrane has triangle shape after the electron beam shape. Also, crystallization by electron beam was observed during the perforation in case

of Al_2O_3 coated membrane, so we expected that around of nanopore is γ-Al_2O_3 (8.3 pH) not α-Al_2O_3 (9.2 pH).

Ionic conductance was measured on each fabricated nanopores with Ag/AgCl electrode at different KCl conentrations. The ionic conductance was converted from 100 mV bias and range of 1 mM ~ 1M KCl condition. Lower than 1 mM KCl condition was not used because of a pA resolution of used patch clamp amplifier system (Axopatch 200B, Axon). The measured ionic conductance was shown in Figure 4-9b. In the case of Si_3N_4, the ionic conductance was almost linearly decreased with electrolyte strength. On the contrary, Al_2O_3 and a-C coated nanopores were not followed linear relation to electrolyte strength, but, more increased than expected.

In order to compare the measured ionic conductance with those of simulated results, the measured value was converted to relative ionic conductance and is shown in Figure 4-9c. The surface charge effect was clearly shown and the same materials were converged similar curve. Case of Si_3N_4 and Al_2O_3, relative ionic conductance has plateau region at > 10 mM KCl. Then, relative ionic conductance was increased as ~5 times from 10 mM to 1 mM KCl and it was happed by surface charge effect as expected from calculation. And the surface charge effect is more clearly shown in a-C coated nanopore. The relative ionic conductance of a-C coated nanopore was continuously increased. Also, the relative ionic conductance in same diameter

and electrolyte strength was improved by high surface potential, a-C, Al_2O_3, Si_3N_4, sequentially.

Discrepancies to the calculated data were that (1) the nanopore size effect was not clearly shown and (2) the improved relative ionic conductance was lower than expected. Former was understood by access resistance of nanopore.[14] When the nanopore radius increased, access resistance was improved in same nanopore length. As a result, electric field at inside of the nanopore was decreased in smaller nanopore with same bias. Latter may happened by slip effect of ion around of surface.[30] The counter ion was accumulated at near surface, therefore the slip effect was easily affected to reduction of ionic conductance.

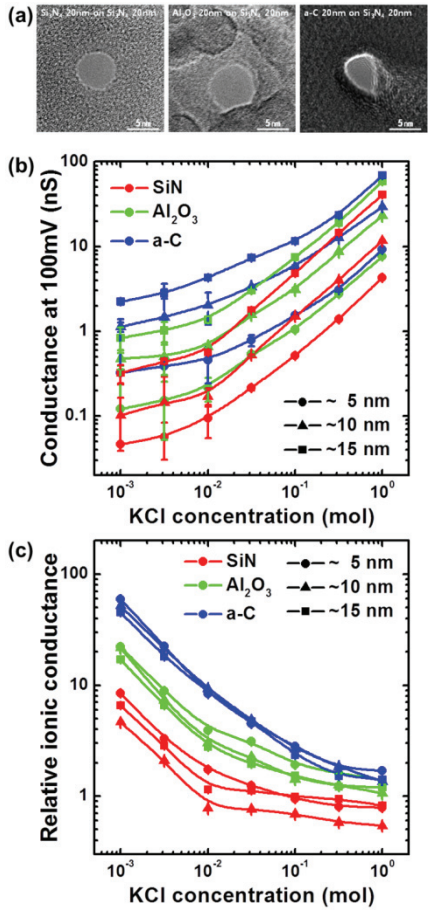

Figure 4-9. **a)** TEM image of different surface charged nanopore modified by Si_3N_4 40 nm, 20 nm Al_2O_3 on Si_3N_4 20 nm, and a-C 20 nm on Si_3N_4 20 nm. In each image, the nanopore has 5 nm diameter. **b)** Ionic conductance as a function of electrolyte strength at 100 mV with different nanopore structure and material represented from a). **c)** Relative ionic conductance calculated from b) and ideal conductance of cylindrical nanopore.

4.4. Summary and Conclusions

In present work, electrical potential distribution in cylindrical cavity was studied with effect of surface charge. Effective λ_D was extracted by 1/e ratio of its surface potential and tried to use as a criterion of surface charge effect. However, effective λ_D showed the ambiguous result as a function of surface potential and radius of nanopore. Accordingly, we introduced the relative ionic conductance for the ideal and it clearly showed the surface charge effect. Commonly, surface charge effect was not expected when the radius of nanopore was larger than λ_D. However, calculated relative ionic conductance was increased by 5 times in 5 nm radius and 10 times in 1 nm radius with 150 mV surface potential even 1M KCl.

This expectation was assessed using surface charge modified nanopore using a-C, Al_2O_3, and Si_3N_4. In cased of a-C coated nanopore, the ionic conductance was improved than zero surface charge case and the other material coated nanopore. As a result, we expected that the DNA blockage area is same to other size nanopore, however, blocked ionic conductance will be improved and the signal-to-noise ratio will be enhanced in smaller and higher surface charge nanopore. Also, the exact the ionic conductance of nanofluidic system has to be considered with access resistance, surface charge governed conductance, and slip resistance of surface.

References

[1] B. M. Venkatesan, R. Bashir, 2011, *Nat. Nanotechnol.* **6**, 615

[2] D. Branton, D. W. Deamer, A. Marziali, H. Bayley, S. A. Benner, T. Butler, M. Di Ventra, S. Garaj, A. Hibbs, X. Huang, *et al.,* 2008, *Nat. Biotechnol.* **26**, 1146

[3] C. Dekker, 2007, *Nat. Nanotechnol.* **2**, 209

[4] H. Craighead, 2006, *Nature* **442**, 387

[5] J. J. Kasianowicz, E. Brandin, D. Branton, D. W. Deamer, 1996, *Proc. Natl. Acad. Sci. U. S. A.* **93**, 13770

[6] A. Meller, L. Nivon, E. Brandin, J. Golovchenko, D. Branton, 2000, *Proc. Natl. Acad. Sci. U. S. A.* **97**, 1079

[7] M. Zwolak, M. Di Ventra, 2008, *Rev. Mod. Phys.* **80**, 141

[8] J. Clarke, H.-C. Wu, L. Jayasinghe, A. Patel, S. Reid, H. Bayley, 2009, *Nat. Nanotechnol.* **4**, 265

[9] S.-W. Nam, M. J. Rooks, K.-B. Kim, S. M. Rossnagel, 2009, *Nano Lett.* **9**, 2044

[10] R. B. Schoch, P. Renaud, 2005, *Appl. Phys. Lett.* **86**, 253111

[11] A. Plecis, R. B. Schoch, P. Renaud, 2005, *Nano Lett.* **5**, 1147

[12] F. Tessier, G. W. Slater, 2006, *Electrophoresis* **27**, 686

[13] G. F. Schneider, S. W. Kowalczyk, V. E. Calado, G. Pandraud, H. W. Zandbergen, L. M. K. Vandersypen, C. Dekker, 2010, *Nano Lett.* **10**, 3163

[14] S. W. Kowalczyk, A. Y. Grosberg, Y. Rabin, C. Dekker, 2011, *Nanotechnology* **22**, 315101

[15] S. Garaj, W. Hubbard, A. Reina, J. Kong, D. Branton, J. A. Golovchenko, 2011, *Nature* **467**, 190

[16] W.-J. Lan, D. A. Holden, H. S. White, 2011, *J. Am. Chem. Soc.* **133**, 13300

[17] H. Liu, J. He, J. Tang, H. Liu, P. Pang, D. Cao, P. Krstic, S. Joseph, S. Lindsay, C. Nuckolls, 2010, *Science* **327**, 64

[18] C. Duan, A. Majumdar, 2010, *Nat. Nanotechnol.* **5**, 848

[19] J. Sonnefeld, 1996, *Colloid Surfaces A: Physicochem. Eng. Aspects* **108**, 27

[20] M. Kosmulski, 2006, *J. Colloid Interface Sci.* **298**, 730

[21] G. A. Parks, 1965, *Chem. Rev.* **65**, 177

[22] B. M. Venkatesan, A. B. Shah, J.-M. Zuo, R. Bashir, 2010, *Adv. Funct. Mater.* **20**, 1

[23] R. Kox, S. Deheryan, C. Chen, N. Arjmandi, L. Lagae, G. Borghs, 2010, *Nanotechnology* **21**, 335703

[24] P. Chen, T. Mitsui, D. B. Farmer, J. Golovchenko, R. G. Gordon, D. Branton, 2004, *Nano Lett.* **4**, 1333

[25] H. Chang, F. Kosari, G. Andreadakis, M. A. Alam, G. Vasmatzis, R. Bashir, 2004, *Nano Lett.* 4, 1551

[26] Y. Astier, L. Datas, R. Carney, F. Stellacci, F. Gentile, E. Difabrizio, 2011, *Small* **7**, 455

[27] J. Xue, Y. Xie, Y. Yan, J. Ke, Y. Wang, 2009, *Biomicrofluidics* **3**, 022408

[28] R. E. Rice, F. H. Horne, 1985, *J. Colloid Interface Sci.* **105**, 172

[29] J. E. Curry, S. E. Feller, D. A. McQuarrie, 1991, *J. Colloid Interface Sci.* **143**, 527

[30] U. Vermesh, J. W. Choi, O. Vermesh, J. Nagarah, J. R. Heath, 2009, *Nano Lett.* **9**, 1315

CHAPTER 5.

Summary and Conclusions

In summary, the following contributions were made through this dissertation;

In chapter 2, by measuring the ionic leakage current using a parameter analyzer, we find that there is a high level of leakage current in the Si-based solid-state nanopore structure. This ionic leakage current is not commonly measured in patch clamp amplifier. Through a judicious experimental plan, we identified that this leakage current occurs as a result of the electrochemical reaction at the water/Si interfaces. Furthermore, we identified that this high leakage current level is closely related with the low frequency noise level in an ionic current. By depositing a thin dielectric layer, we can eliminate the source of leakage current, and therefore, can reduce the low frequency noise level.

In chapter 3, we have developed a novel structure and a fabrication method to dielectric substrate based solid-state nanopore that can be provide us sub-10 pA RMS ionic current noise comparable to protein nanopore. And it was used to make over 100 signal-to-noise ratio with sub-10 nm thickness membrane. Improved signal-to-noise ratio and thinner membrane was useful to detect a small nucleic acids event 40 nt ssDNA. Furthermore, four type of homopolymer consisted with A40, T40, C40, and G40 were discriminated with 1.5 nm diameter and 5 nm thick dielectric substrate based solid-state nanopore. The nanopore has allowed us to distinguish poly A_{40}, poly T_{40}, and

poly C_{40}, roughly. Here some problems for the DNA sequencing were remained that uniform fabrication method for 1~2 nm diameter nanopore, high standard deviation of Gaussian peak of each nucleotide type, and determination of sensing zone in solid-state nanopore. However, the solid-state nanopore will overcome these problems by applying or mimicking of protein nanopore technologies.

In chapter 4, we studied the electrical potential distribution in cylindrical cavity with effect of surface charge. Effective λ_D was extracted by 1/e ratio of its surface potential and tried to use as a criterion of surface charge effect. However, effective λ_D showed the ambiguous result as a function of surface potential and radius of nanopore. Accordingly, we introduced the relative ionic conductance for the ideal and it clearly showed the surface charge effect. Commonly, surface charge effect was not expected when the radius of nanopore was larger than λ_D. However, calculated relative ionic conductance was increased by 5 times in 5 nm radius and 10 times in 1 nm radius with 150 mV surface potential even 1M KCl. This expectation was assessed using surface charge modified nanopore using a-C, Al_2O_3, and Si_3N_4. In cased of a-C coated nanopore, the ionic conductance was improved than zero surface charge case and the other material coated nanopore. As a result, we expected that the DNA blockage area is same to other size nanopore, however, blocked ionic conductance will be improved and the signal-to-noise ratio will be

enhanced in smaller and higher surface charge nanopore. Also, the exact the ionic conductance of nanofluidic system has to be considered with access resistance, surface charge governed conductance, and slip resistance of surface.

Abstract (in Korean)

본 dissertation에서는 3세대 DNA sequencing 기술의 하나인 nanopore를 이용한 DNA sequencing 기술에 대해 다루고자 한다. 특히 기계적 내구성, 다양한 크기의 nanopore 제작 가능성, 외부 전기시스템과의 접합 등과 같이 다양한 장점을 가지고 있는 solid-state nanopore에 대해 다루고자 하였다. 먼저 solid-state nanopore의 문제점을 파악하였다. 첫째, DNA가 protein nanopore를 지나가는 경우에는 초당 100 nucleotides가 통과하나, solid-state nanopore에서는 이에 비해 1000 배정도 빠른 초당 100,000 nucleotides가 지나간다. 둘째, silicon nitride를 기반으로 하는 solid-state nanopore의 경우 안정적인 박막형성을 위하여 20 nm 두께 이상의 silicon nitride membrane을 사용한다. 하지만 이는 solid-state nanopore 내부에 항상 수십개의 nucleotide가 존재하게 하여 DNA sequencing을 하기 위한 resolution을 확보할 수가 없다. 셋째, solid-state nanopore의 경우 nanopore를 통과하는 ionic current에서 수십~수백 pA RMS 정도의 noise를 보여주고 있지만, 이와 달리 protein nanopore에서는 10 pA RMS 이하의 noise를 가지고 있다. 이러한 높은 ionic current noise는 nucleotide 간의 blockade current 차이가 10 pA 이내인 것을 고려하였을 때 solid-state nanopore에서는 nucleotide간의 구별이 불가능하다는 결론을 내릴 수 있다. 이 밖에도 solid-state nanopore에서는 nanopore pore size 및 구조의 재현성과 균일성, 그리고 안정성의 문제가 존재하며, 아직까지 많이 연구되지 않은 DNA와 같은 organic 물질과 solid-state nanopore를 구성하고 있는 inorganic 물질과의 interaction, solid-state nanopore를 구성하고 있는 물질의 surface charge로 인한 ionic conductance 변화 및 DNA 통과 횟수에 대한 영향 등, 많은 문제점 및 밝혀야 할 영역이 존재한다. 이러한 문제점 중, 본 dissertation에서는 solid-state nanopore의 높은

ionic current noise의 원인 및 해결책을 제안하고자 하였다.

첫번째 part에서는 solid-state nanopore의 높은 ionic current noise의 원인을 규명하기에 앞서, 거의 모든 solid-state nanopore의 기반이 되는 Si 기반 solid-state nanopore에서 측정되는 leakage current의 원인 및 이를 효율적으로 감소시킬 수 있는 방안을 제시하였다. Si 기반 solid-state nanopore에서의 leakage current는 대략 1 V에서 5 nA 정도로 나타났으며, 이는 Si 기판의 electrochemical reaction에서 발생하는 400 nA/cm^{2}와 비교하여 nanopore device의 노출된 면적에서 발생하는 leakage current라고 판단할 수 있었다. 이러한 leakage current를 감소시키기 위하여 다양한 방법으로 dielectric 물질을 nanopore device에 증착시켰으며, 20 nm 이상의 두께를 증착하였을 때 100pA 이하의 leakage current를 얻을 수 있었다. 또한 낮아진 leakage current는 nanopore를 통한 ionic current의 noise에도 영향을 주었으며 이를 통해 기존 38 pA RMS의 noise를 28 pA RMS 이하로 낮추는 것이 가능하였다.

이러한 dielectric을 증착하는 것으로 noise가 줄어드는 이유로 Si 기판을 통한 전하 전달을 막는 영향으로 생각되었으며, 이를 통해 두번째 part에서는 insulating 기판을 사용하여 solid-state nanopore를 제작하는 방법을 제시하고 그 특성을 파악하였다. Insulating 기판 기반의 solid-state nanopore에서 silicon nitride membrane을 형성하기 위해서 fishing method를 적용하였으며, 이렇게 제작된 nanopore device의 ionic current noise가 10 pA RMS 이하, 최소 5 pA RMS의 값을 가짐을 보고하였다. 이러한 낮은 noise 특성은 크게 insulating 기판의 높은 저항으로 인하여 기판을 통한 전하 이동이 크게 제한되었고, 낮은 membrane capacitance로 인해 membrane 내의 이동 가능한 전하량이 줄어듦으로 인한 것으로 생각되었다. 제작된 insulating 기판 기반의 solid-state nanopore 소자에서 더 높은 DNA

translocation signal을 얻기 위하여 silicon nitride membrane의 두께를 5 nm 까지 낮추었으며, 이 경우 2 nm 대의 effective thickness를 얻을 수 있었다. 나아가서 높은 current resolution과 얇은 nanopore length를 이용하여 nucleotide의 type, 즉 A, T, C, G의 구별이 가능함을 보여주었다. 이를 위해 A, T, C, G 중 한 종류로만 이루어진 40 nucleotide 길이를 가지는 homopolymer (40 nt ssDNA)가 사용되었으며 1.3 nm의 지름을 가지는 nanopore에서 구별이 가능하였다.

마지막으로 세번째 part에서는 nanopore를 구성하고 있는 물질이 가지고 있는 surface charge 영향을 고려하였으며, 특히 surface charge로 인한 nanopore의 ionic conductance 변화를 simulation과 실험을 통해 고찰하였다. 이를 위해 nanopore와 같이 cylindrical cavity 구조에서의 전기장분포를 예상하였으며 이를 통해 nanopore 내부의 전하의 분포를 계산하였다. Nanopore 내부의 전하의 분포를 다시 nanopore의 ionic conductance로 전환이 가능하였으며 이 결과로 surface charge에 따른 ionic conductance 변화를 예상할 수 있었다. 이러한 예상을 확인하기 위해 silicon nitride, aluminum oxide, amorphous carbon 등으로 이루어진 solid-state nanopore를 제작하였으며 그 특성을 평가하였다. 그 결과 예상과 같이 nanopore를 구성하고 있는 물질의 surface charge가 ionic conductance에 영향을 끼침을 규명하였으며, 이는 surface charge가 높거나, electrolyte strength가 낮을 때, 또는 nanopore의 지름이 작을수록 그 효과가 큼을 확인하였다.

주요어: Nanopore, solid-state nanopore, ionic field effect transistor, DNA sensing, dielectric substrate, noise reduction method, DNA sequencing

학번: 2006-20864